INVESTIGATIONS   OF   THE   PRIMARY   COSMIC

RAY   ELECTRONS   AT   HIGH   GEOMAGNETIC   LATITUDE

A THESIS

submitted by

TREVOR ROBERT SANDERSON

For the Degree of

DOCTOR OF PHILOSOPHY

in the

UNIVERSITY OF LONDON

January 1970

ABSTRACT

Measurements have been made of the electron component of the cosmic rays at balloon altitudes with a detector using the range-energy method of separating electrons from the cosmic ray beam. A total of five flights have been made, each to altitudes of $\sim$ 5 gm/cm^2 of residual atmosphere. The two flights from Cardington, Bedfordshire in 1966 and 1967 were used to determine the effects of re-entrant albedo and atmospheric secondary electrons. Three flights from Kiruna, Sweden in 1967 and 1968 have been used to look at the primary electrons. The detector measures electrons in the energy range $\sim$ 25-1000 Mev at the top of the atmosphere. The response of the detector was determined in the electron beam of the electron-synchrotron at D.E.S.Y., Hamburg, and in the proton beam of the proton-synchrotron, NIMROD.

The 1967 flight from Kiruna was made when the sun was inactive, and fluxes of 0.52 and 0.047 p/m^2 sec. ster. Mev in the range 23-280 and 280-900 Mev were measured. A class 3B solar flare occurred before the 1968 flights. The first flight took place during the Forbush Decrease following the flare. In the low energy channel the flux was $\sim$ 7 times the 1967 flux. In the high energy channel it was $\sim$ 50% of

the 1967 flux.   The low energy flux increase in interpreted

as solar electrons, and the high energy flux depression due to

the Forbush Decrease.   The second flight of 1968, towards the

end of the Forbush Decrease showed flux levels similar to the

1967 levels..

The implications of solar electrons and solar modulation

are discussed.   The relation between the electrons in the

galaxy and the production of cosmic ray photons is examined.

ACKNOWLEDGEMENTS

CONTENTS

CHAPTER I

INTRODUCTION

1.1 General Introduction

The measurement of the electron component of the primary cosmic rays has made tremendous progress in the past decade. The development and use of polythene balloons around 1960 enabled small detectors to reach altitudes of ~ 5 gm/cm^2 of residual atmosphere. Subsequent developments have enabled detectors weighing several hundred pounds to reach atmospheric depths of ~ 2 gm/cm^2. With the resulting decrease of matter above the detector, and the possibility of flying detectors with large counting rates, the accuracy of the necessary secondary corrections have been increased. Using the effects of the night-time lowering of the geomagnetic cut-off at high latitudes, measurements can now be made down to a few tens of Mev, whilst development of new detection methods have pushed the upper limit of measurements up to ~ 300 Gev. The use of detectors on board satellites has brought the lower energy limit down below 1 Mev, and enabled measurements to be made free of any terrestrial effects.

Progress on the theoretical interpretation of the electron measurements has been equally rapid. Comparisons of the electron spectrum in the Galaxy, derived from synchrotron radio noise, with that measured at the earth give useful indications on the conditions existing in the Galaxy. Measurement of the relative modulation is at present only in its infancy, but when sufficient data is available, the information will supplement the proton modulation data and determine the modulation processes taking place. Already the data on solar electron emission gives good indications on the type of propagation processes present in interplanetary space and the mechanism of solar electron production.

1.2 Electron Measurements

The first attempts to measure the primary electron component were made between 1940 and 1960 by various groups (Schein, Jesse and Wollan, 1941; Hultsizer and Rossi, 1948; Critchfield, Ney and Oleksa, 1952) using balloon borne detectors. None of the experiments gave a finite flux value but upper limits were set at approximately 1% of the total cosmic radiation. They all suffered from

effects of the secondary electrons produced in the atmosphere above the detectors, these being flown to altitudes of $\sim$ 20 gm/cm^2 of residual atmosphere. The problem of atmospheric secondary contamination still remains one of the major problems of measuring primary electrons at balloon altitudes especially at energies around 100 Mev. The absence of any measurable flux of electrons was in agreement with the idea put forward by Feenberg and Primakoff (1948), that electrons are eliminated by inverse compton collisions with starlight.

The first successful measurements of the primary electrons were made in 1960, simultaneously by Earl (1961), and by Meyer and Vogt (1961). Their balloon borne experiments reached altitudes of approximately 5 gm/cm^2 of residual atmosphere, and claimed finite flux values over and above the atmospheric secondary flux. Earl used a cloud chamber with random exposure. Meyer and Vogt used a range-energy loss detector.

The early measurements were in the region 25-3000 Mev. Extension of the energy range has been performed by many experimenters using a variety of techniques. Bleeker et al (1965), extended the energy limit up to 30 Gev. Similar measurements have been made by Danjo et al (1967); Webber

and Chotkowski (1967): and L'Heureux and Meyer (1965),

using lead glass absorption spectrometers. Nuclear emul-

sions have been used by Freier and Waddington (1965), and

also by Daniel and Stephens (1965), who have made measure-

ments up to 300 Gev. Spark chambers have been used by

Agrinier et al (1964), and cloud chambers by Schmoker and

Earl (1965). Detectors using lead-scintillator sandwiches

have been used by Neely (1968); Verma (1967a); Rubstov

(1967), and on the present experiment.

Experiments to look at the low energy end of the spectrum

are made more difficult by atmospheric and geomagnetic

effects, and so allowance for this must be made in any meas-

urements on balloon borne detectors. For this reason, most

low energy experiments have been performed on satellites.

The first of these was the IMP-I satellite (Cline,

Ludwig and McDonald, 1964) which measured electrons in the

energy range 3-12 Mev. Further measurements have been

made on later IMP satellites covering the range 3-40 Mev

(Fan et al, 1967; Simnett and McDonald, 1968), and on the

OGO-5 satellite, covering the range 10-200 Mev and 0.5 to

10 Gev. (Datlowe, L'Heureux and Meyer, 1969; Bleeker et

al, 1969b). Similar experiments have been performed on

ESRO II (Marsden et al, 1969) and HEOS-A1 (Bland et al, 1969).

Further experiments on OGO-1, 3 and 5 have attempted
to measure the positron flux below 10 Mev (Cline and Hones,
1967; Cline and Porreca, 1969). All of these experiments
except the ESRO-II experiment were performed on highly
eccentric orbiting satellites which make measurements out-
side the magnetosphere, and so are free from terrestrial
effects. As well as deriving spectra, the experiments
continually monitor the flux, so enabling measurements to
be made of solar modulation and activity.

1.3 Terrestrial Effects

Measurements at low energies have been made at balloon
altitudes(Beedle and Webber, 1967; Jokipii, L'Heureux
and Meyer, 1967; Israel and Vogt, 1968; Rockstroh and
Webber, 1969). Such measurements must be corrected for
contamination by atmospheric secondaries-and re-entrant
albedo. Various estimates have been made of the secondary
contributions (Okuda and Yamamoto, 1965; Perola and Scarsi
1966; Verma, 1967b). The processes involved begin with
nuclear collisions between a nucleon of the primary cosmic
radiation and an atmospheric nucleus. The products of
this collision are charged and neutral π-mesons which
decay into μ-mesons or gamma-rays. The μ-mesons then

decay into electrons, whilst the gamma-rays can materialize

into an electron-positron pair, thus:

$$p + p \longrightarrow p + p + a\pi^0 + b(\pi^+ + \pi^-)$$

$$\pi^{\pm} \longrightarrow \mu^{\pm} + \nu, \qquad \mu^{\pm} \longrightarrow e^{\pm} + 2\nu$$

$$\pi^0 \longrightarrow 2\gamma, \qquad \gamma \longrightarrow e^{\pm} + e^-$$
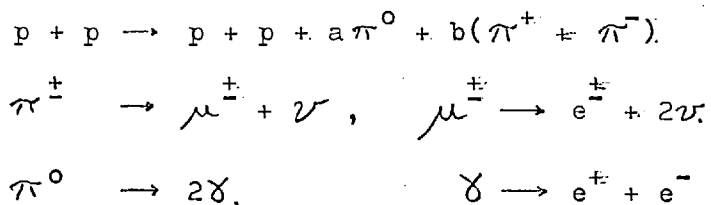
The calculations use meson production rates derived either

from cosmic ray studies or accelerator data. The work of

Verma also includes angular distributions of the π -mesons

in the collisions. The decay lifetimes are then used to

give the μ -meson production spectrum, and hence the electron

spectrum for various atmospheric depths. From this can be

derived growth curves appropriate to any detector, which

can then be used to correct the measured altitude dependence

of the electron flux.

As well as contamination by atmospheric secondaries,

the measurements may also contain contamination from re-entrant

albedo. Simple geomagnetic theory gives a well defined

rigidity cut-off for any point on the earth. A particle

with rigidity less than this cannot appear in the primary

radiation, whilst particles with rigidities above this can

appear as primaries. Electrons with rigidities less than
the cut-off can appear at the top of the atmosphere, but
in this case they are re-entrant, i.e. produced in nuclear
collisions in the southern hemisphere and guided back to
the northern hemisphere along the earths magnetic field
lines. Modifications to this simple theory are due to
the presence of the solid earth, and deviations of the
earths field from a true dipole. The exact value of the
cut-off is clearly important in separating primary and
re-entrant electrons.

To make measurements of high energy ($\sim$ 10 Gev) elect-
rons, it is possible to use balloon borne detectors at
low latitudes, but to look at low energies ($<$ 500 Mev) it
is essential to go to high latitudes, where the cut-off
is lowest. The situation at high latitudes is complicated
by the presence of the magnetosphere and its effect upon
the geomagnetic field. At latitudes between 65° and 70°
(geomagnetic latitude) a boundary exists between closed and
open field lines. The closed lines connect the northern
to the southern hemisphere. The open field lines are con-
nected directly to the interplanetary field via the tail
of the magnetosphere. Inside the closed field lines, the
cut-off is well defined by the normal Stoermer theory.

Where open field lines exist, low energy electrons have access from interplanetary regions via the tail of the magnetosphere (Michel, 1965; Reid and Sauer, 1967), In this case the cut-off is determined by the effects of the converging field lines in the tail.

A further effect of the magnetosphere is the diurnal variation of the cut-off in the transition region from open to closed field lines. The distortion of the earth's magnetic field caused by the solar wind moves the transition region to higher latitudes on the daylight side of the earth, and lower latitudes on the night side. In the region $65^{\circ}-70^{\circ}$, the cut-off is high during the day because the field lines are closed, and low during the night because the field lines are open. Confirmation of this effect comes from satellite measurements, both on the boundary of trapped particles (O'Brien, 1963; McDiarmid and Burrows, 1964), and the cut-off for low energy protons (Stone, 1964). The effect is also observable in the day-time recovery of PCA events (Leinback, 1962) and in direct measurement of low energy electrons at balloon altitudes (Jokipii, L'Heureux and Meyer, 1967; Rockstroh and Webber, 1969; Webber, 1968b; and Israel and Vogt, 1969).

In the measurements of the low energy electrons in

the region 65°-70°, the diurnal variation of the electrons
show an increased counting rate during the daytime, due to
a large flux of re-entrant albedo.   During the night,
the very low cut-off prevents the albedo from appearing,
and allows only the primaries access to the top of the
atmosphere.   In this way, electrons with rigidities much
less than the internal cut-off have been observed.

The cut-off at Kiruna has been investigated (Gall,
Jimenez and Camacho, 1968), using a simple model of the
magnetosphere (Williams and Mead, 1965), and is found to
vary from $\sim$ 500 Mv during the daytime down to $\sim$ 50 Mv
at night.   The exact value of the night time cut-off
depends critically upon the parameters assumed for the tail
of the magnetosphere.

1.4   The Electron Spectrum

The current measurements of the electron spectrum
span the range from a few Mev up to a few hundred Gev.
The more prominent measurements are shown in Fig.6.2.
The data shows a slope which varies over different parts
of the spectrum, and distinct kinks are observable.   The
low energy region is covered exclusively by satellite

measurements, made outside of the magnetosphere. Above

10 Mev, there is some overlap between balloon and satellite

measurements, but at these energies, the balloon results

are somewhat uncertain due to the contributions from

re-entrant electrons and atmospheric secondaries, both of

which are not accurately known. The balloon measurements

up to 200 Mev utilize the depression of the cut-off to

allow the electrons access to the earth. Above a few

hundred Mev, the measurements are taken above the cut-off

at the location of the balloon flights, and so these results

are relatively free from geomagnetic effects. Satellite

measurements are available up to 10 Gev, whilst balloon

results extend the spectrum up to $\sim$ 300 Gev.

The best fit to the slope of the spectrum is $\sim$ 1.5 in

the region 300 Mev to 3 Gev and $\sim$ 2.5 in the region 3-300 Gev.

1.5 The Electron Source

Concurrent with the early electron experiments, meas-

urements were being made of the galactic radio noise, the

source of which was explained as relativistic electrons..

Alven and Herlofson (1950) were the first to apply the

theory of radiation from accelerated electrons in magnetic

fields, whilst Kiepenheuer (1950) showed that the emission
was a by-product of cosmic rays in the galactic magnetic
fields. This type of radiation had been investigated
previously in connection with particle accelerators
(Schwinger, 1949) and was later applied to cosmic rays
(Ginzburg and Syrovatskii, 1964). The source of this non-
thermal radio noise was explained as synchrotron radiation
from electrons spiralling in the galactic magnetic fields.

Whereas a non-relativistic electron in a magnetic
field radiates as a classical dipole, a relativistic electron
emits radiation in a narrow cone in the direction of the
instantaneous velocity. When the electron spirals in a
magnetic field, an observer sees a pulse of radiation each
time the electron is moving towards him, which appears as
a collection of harmonics of the frequency of rotation,
with a maximum frequency corresponding to the width of the
pulse. Whilst the non-relativistic electron produces a
single frequency, the relativistic electron produces a con-
tinuum of radiation. A single relativistic electron,
with total energy E, produces an intensity proportional to
$E^2 H_\perp^2$ and a frequency distribution proportional to $E^2 H_\perp$,
where $H_\perp$ is the component of the magnetic field perpendicular
to the line of sight from the observer to the electron.

For the distribution of electrons described by a power law $n(E) = n_o E^{-\gamma}$ dE, the intensity of the radiation is given by:

$$I_\nu \approx 4.8 \times 10^{-20}(4.9 \times 10^2)^{3-\gamma} n_o.R.H^{\frac{1+\gamma}{2}} \nu^{\frac{1-\gamma}{2}}$$

in units of watts m^{-2} ster.$^{-1}$ cycles sec.$^{-1}$, where n_o and γ describe the electron distribution, R is the path length of the radiating region in light years, H is the average field in microgauss, and ν is the frequency in megahertz. The intensity is thus proportional to $H^{\frac{1+\gamma}{2}}$ and $\nu^{\frac{1-\gamma}{2}}$ so that measurement of the frequency distribution of the intensity enables the distribution of electrons producing the radiation to be calculated. This approach has been used by many workers (Woltjer, 1961; Felten, 1966; Sironi, 1965; Pollack and Fazio, 1965; Baldwin, 1961) to compare the radio noise to the electron spectrum.

It was pointed out by Ginzburg (1958) and by Hayakawa (1961) that the products of proton-proton collisions of the primary cosmic radiation with the galactic gas should contain positrons and electrons, with a majority of positrons at energies around the π-threshold. The products of any direct acceleration should be negative

electrons only. The determination of the positron

fraction ($e^+/e^+ + e^-$) should then give the relative

contribution from collision sources and other acceler-

ation mechanisms. The measurements of De Shong (1964)

using a balloon borne magnet and spark chamber to meas-

ure the positron fraction, showed that there were in-

sufficient positrons to account for a collision source

alone.

The production of electrons from collisions was

investigated thoroughly by Ramaty and Lingenfelter (1966a)

who considered the primary protons and helium nuclei

colliding with molecules of the galactic gas, producing

π -mesons and neutrons, which decay into electrons. Using

the cross sections, multiplicities, spectra of helium

nuclei and protons, and the density of the galactic gas

enables the pion and neutron spectra to be found. The

decay of these then gives the electron source spectra.

The more important loss mechanisms, leakage from the gal-

axy, synchrotron radiation, inverse compton collisions

and bremsstrahlung then modify the spectrum to give the

equilibrium spectrum. The same analysis also gives the

positron fraction, $e^+/e^+ + e^-$.

More comprehensive measurements of the positron

fraction (Hartman, 1967) using techniques similar to those

of De Shong have established more precisely the positron

fraction.   The expected value is 0.5 at high energies

(> 10 Gev) rising to $\sim$ 1.0 at low energies around the

π -threshold (Ramaty and Lingenfelter).   Measurements

reveal a flux of positrons which is much less than the

negative electron flux, suggesting a source other than

collisions for the majority of the primary flux.   The

measurements of Agrinier et al (1964), and Daniel and

Stephens (1965) have used the difference in the geomagnetic

cut-offs in the east and west directions as a measure

of the charge ratio of the particle, and hence measured

the positron fraction.   The measurements of Agrinier et

al are in good agreement with those of Hartman, but those

of Daniel and Stephens contradict them, but in view of the

poor statistics, their results cannot be taken too seriously.

The source of electrons which can account for the

measured flux is direct acceleration, the electrons coming

mainly from supernovae outbursts and also outbursts of

galactic nuclei.   Radio noise measurements of supernovae

such as Cassiopeia-A and Taurus-A (the crab) have shown

that a strongly polarized non-thermal component is present,

which can only be explained in terms of synchrotron radiation

from relativistic electrons within their envelopes.   From

the intensity of the radio noise, and the frequency depend-

ence, the spectra of the electrons have been found.   For

Cassiopeia-A, $\delta \simeq 3$ and for Taurus-A, $\delta \simeq 1.5$.   Moreover,

the energy output is sufficient to explain the observed

energy density of the cosmic ray electrons.

The electrons produced in any source in the galaxy

or in the extragalactic regions have their source spectra

modified by the various loss mechanisms which act upon them.

Consideration of these effects suggest that a simple power

spectrum will have its slope changed.   These losses are:

$$- \frac{dE}{dt} = A + BE + CE^2$$

where A represents ionisation losses, B represents brem-

sstrahlung, and C synchrotron and inverse compton losses.

For a non time dependent case, the continuity equation:

$$\frac{\partial}{\partial E} \left(\frac{dE}{dt} \times N(E) \right) + \frac{N(E)}{T} = n(E)$$

gives the equilibrium spectrum $N(E)$, where $n(E)$ is the

source spectrum, and the term $\frac{N(E)}{T}$ represents leakage

out of the galaxy.   The solution to this is:

$$N(E)\,dE \propto \frac{E^{-\gamma}\,dE}{\frac{A}{E} + B + CE}$$

At low energies, where the A term dominates, the spectrum
flattens by one power.   At intermediate energies, B domin-
ates, and the slope of the spectrum is preserved.   At high
energies, where C dominates, the spectrum steepens by one
power.   The spectral breaks produce corresponding breaks
of half a power in the synchrotron and inverse compton
spectra.   The positions of the spectral breaks are related
to the energies at which adjacent loss terms have equal
significance.   The positions of these breaks give an ind-
ication of conditions existing in the galaxy.

The presence of a universal 3°K radiation, discovered
by Penzias and Wilson (1965) make the effects of inverse
compton scattering more important (Hoyle, 1965; Gould,
1965).   The position of the spectral break at high energies
depends on whether or not allowance is made for this rad-
iation (Felten and Morrison, 1966).   The presence of the
3°K radiation makes the existence of the electrons in
intergalactic regions extremely unlikely due to the energy

losses they would incurr (Fazio, Stecker and Wright, 1966;
Hoyle, 1965; Ginzburg and Syrovatskii, 1967).

The galactic theory of origin of electrons assumes
that the electrons are produced in sources inside the
galaxy (supernovae and galactic nuclei) and confined in
either the disc or the halo. The disc model requires more
energy than can be reasonably expected from the sources
present (Burbidge, 1969) and suggests a knee at $\sim$ 50 Gev
(Tanaka, 1967), which is not, as yet, observed. The
halo model predicts a knee at $\sim$ 2-5 Gev (Felten and
Morrison; Tanaka) which fits the observational data well.
With a knee at this energy, the measured slope of $\sim$ 2.5
in the spectrum above the knee suggests a slope of $\sim$ 1.5
below the knee, and an injection mechanism with $\gamma = -1.5$.

The theoretical works of Anand et al (1968b), and
Webber (1968a) have shown in greater detail the relation
between the radio noise and the electron spectrum. The
electron spectrum derived from the radio noise from the
galactic anti-centre can explain the electron flux meas-
ured at the earth, especially at energies where modulation
is unimportant. This spectrum is consistent with the radio
noise observed in other directions (i.e. the galactic halo

and the galactic ridge).   This is a good indication that
similar electron spectra exist in different parts of the
galaxy, as would be expected from a halo model.

1.6 Modulation of Electrons

Very little data is available on the modulation of
the electron component. Although experiments began in
1960, only one group (L'Heureux, Meyer, Verma and Vogt,
1967) have made measurements continually since then.   Of
the available data, there is little agreement about the
amount of modulation present.   The results of L'Heureux
et al indicate that in the period from 1960 to 1964/5,
i.e. from solar maximum to solar minimum the ratio of the
fluxes measured was 1.0 ± 0.4 in the energy range 250-1000
Mev.   During the time from 1965 to 1968 (solar minimum
to solar maximum) the measurements of Rockstroh and Webber
(1969) indicate a ratio of $\sim$ 0.15 at an energy of $\sim$ 200
Mev.   The measurements of Bleeker et al (1969a), in the
energy range 500-5000 Mev show that from 1966 to 1968,
the ratio was $\sim$ 0.6.

Theoretical predictions are still uncertain as to the
amount of modulation.   Recent measurements of the

interplanetary field (Ness, 1965) show that it is an archimedes spiral, with superimposed upon it a continuous distribution of magnetic irregularities, essentially fixed in the solar plasma. Measurements of the power spectra (Sari and Ness, 1969; Siscoe et al, 1968; Coleman, 1966) of these irregularities suggest a function of the form $M(f) \sim \frac{r}{f^{\alpha}}$, where $M(f)$ is the mean square deviation of the magnetic field per unit interval of frequency, at a given frequency f. The magnetic field and the solar wind are assumed to stop at around 50 A.u. from the sun. In the diffusion convection model (Parker, 1967), the cosmic rays outside this region, the solar cavity, diffuse along the field lines and are subjected to a random walk by scattering in the field irregularities. Parker predicts the intensity of cosmic rays at the earth at a given kinetic energy as:

$$J_E(T) = J_\infty (T) \exp \left(- \int_{1\ A.u.}^{L} \frac{V_w}{D_{\shortparallel}} \right) dr$$

where j is the intensity outside the solar cavity, L

is the radius of the cavity, V_w is the velocity of the
solar wind, $D_{||}$ the diffusion coefficient, and r, the
distance from the sun. For a power spectrum, $1/f^{\alpha}$, the
diffusion coefficient is determined by the value of α ,
such that D is proportional to $2\alpha(\alpha + 2)$ Jokipii, (1966).
Hence the intensity at the earth is:

$$j_E(T) = j_\infty (T) \quad \exp \frac{\eta}{\beta R^{2-\alpha}}$$

where η is a constant independent of R and β , R and β
being the particle rigidity and velocity. The relative
modulation is thus:

$$\ln(j_1/j_2) = \frac{\eta'}{\beta R^{2-\alpha}}$$

Results from Pioneer 6 (Sari and Ness) indicate a value
of α between 3/2 and 1 at low frequencies becoming 2 at
higher frequencies. From their power spectrum, they expect
a modulation varying as $1/\beta$ below 0.4 Gv, and becoming
$1/\beta R^{\frac{1}{2}}$ to $1/\beta R$ above this rigidity. The measurements of
Rockstroh and Webber give a value of η = 0.7 Gv, and show
a $1/\beta R$ dependence above 1 Gv, with some flattening below

1 Gv, but because of the severe atmospheric secondary corrections below 1 Gv, the exact function cannot be determined.

The variation of the modulation with rigidity as measured by Rockstroh and Webber is well explained by the diffusion convection model. However, the ratio of the relative proton and electron modulation is in disagreement. The ratio,

$$\frac{(dj_1 / dj_2)_p}{(dj_1 / dj_2)_e}$$

is predicted to be $\sim$ 1.0 at high rigidities, rising to higher values at low rigidities. The measurements of Webber (1967), however, indicate a mean value of $\sim$ 1.0 independent of rigidity. This can be explained to some extent by allowing some energy loss to be present. The effect of inverse Fermi deceleration due to expansion of the scattering centres can account for a reduction in the ratio of the relative proton and electron modulation.

Estimates have also been made of the residual modulation present, using either information on the galactic flux derived from radio noise and the measured electron spectrum (Anand et al, 1968a; Webber, 1968a) or by comparison of

the calculated positron flux from collisions in the galaxy
with the measured flux of positrons derived from the total
electron flux and the positron fraction (Ramaty and
Lingenfelter, 1968). Each of the methods have given
reasonably consistent results. Anand et al find that
the formula:

$$J_E(T) = j_\infty(T) \exp\left(\frac{-\eta}{R\beta}\right)$$

where $\eta = 0.65$, is valid for energies above 500 Mev, and
has a constant (i.e. $1/\beta$) dependence at energies below
500 Mev. Ramaty and Lingenfelter (1968) find a value of
$\eta = 0.4$, with the same changeover at 500 Mev, whilst
Webber (1968a) finds a value of 0.75 Gv.

In view of the agreement of these theoretical estim-
ates of the residual modulation, it is difficult to explain
the lack of modulation measured by L'Heureux et al, and
the large amount of modulation measured by Rockstroh and
Webber seems the most plausible.

1.7 Solar Electrons

The only reported measurement of solar electrons at
balloon altitudes is by Meyer and Vogt(1962), who detected

high energy electrons above 100 Mev, following two class 3 flares, occurring on July 18th and 20th, 1961. Their first balloon flight, two days later, detected a flux of ~ 0.4 p/cm^2 sec. ster. above the background flux of ~ 0.02 p/cm^2 sec. ster. measured on flights later that year. The spectrum of the solar electrons had a form of E^{-2}.

In 1965 electrons with much lower energies (> 40 Kev) were detected following solar flare activity (Van Allen and Krimigis, 1965; Anderson and Lin, 1966) on board the satellites Mariner 4 and IMP I and II. The fluxes observed were of the order of 100-1000 p/cm^2 sec. ster. against a background of 5-10 p/cm^2 sec. ster. These and subsequent measurements (Lin and Anderson, 1967; Anderson, 1969) have shown that low energy electrons are closely associated with solar flares of class 1 and above, and with radio noise and X-ray emission. They are observed ~ 30-60 minutes after the maximum development of the flare, with a long decay time, and display a high anisotropy, even late in the event. Some of the solar electrons exist in long lived streams, which last for several days, in which transverse diffusion appears to play a negligible part.

The experiments of Cline and McDonald (1968) on the
IMP series of satellites enabled measurements to be made
continuously from November 1963 to May 1967.   The early
results showed no solar events, and led to the conclusion
that the background fluxes are due to galactic origin.
The first solar event was on the 7th July, 1966 and subse-
quently, other solar flares of importance 2 or more were
seen to be producing solar electrons, with fluxes ~ 3 p/cm^2
sec. ster. above the background level of $\sim$ 0.2 p/cm^2 sec.
ster.   These electrons were created simultaneously with
the X-ray and microwave bursts observed on the earth, and
stored near the sun before being released.

The mechanism of production of these electrons is at
present unclear.   It is possible that protons are stored
in some trapping field for a considerable time, and are
released suddenly, rather than being accelerated during the
flare by rapid conversion of magnetic energy.   The first
process (Elliot, 1969) assumes a slow build up of energy
with a sudden release caused by dumping in the lower
chromosphere and photosphere of the stored protons, prod-
ucing an upward jet of material.   Energetic electrons pro-
duced in collisions will betray their presence in the form
of X-rays and synchrotron radiation.   Those which escape

from the trapping region will leave the sun's atmosphere and possibly reach the earth.

The alternative to this mechanism is the rapid transfer of magnetic energy directly to the electrons, using either the Fermi effect; or the Betatron effect. In the Fermi process, particles are accelerated by interactions with magnetic regions, such as shock fronts and moving magnetic fields, whereas the Betatron process requires increasing magnetic fields to accelerate the particles. In both cases, the particle energy must be supplied from the magnetic energy in the order of 30 minutes.

Observations have shown that in many complex solar flares, some diffusion takes place in the solar corona before the electrons are released into interplanetary space (Lin and Anderson, 1967). It is during this time, between the start of the flare and release of the electrons, that the X-ray and microwave emission takes place, often covering substantial fractions of the solar disc. Upon release of the electrons they then propagate along the field lines with little scattering, hence their anisotropy.

CHAPTER II

THE DETECTOR

2.1   General Requirements

The experiment is designed to measure the flux of
primary electrons at the top of the atmosphere at Kiruna,
Sweden.   However, at the height to which the detector
can be taken with a balloon, there are present as well as
the primary electron flux, a relatively intense flux of
protons, which by interaction with the remaining atmosphere
above the detector produce secondary electrons.   These,
of course, are indistinguishable from the primary electrons
of the same energy.

The detector must be capable of measuring these
electrons without contamination from the proton flux, and
must be able to give energy and time information about the
electrons.

The flux of protons at the top of the atmosphere is
well known, and the spectrum of these protons is shown in
Fig. 2.1, together with the various heavier nuclei.   These
primary particles are absorbed in the atmosphere, and so
their flux decreases with atmospheric depth.   The differential

spectrum of the secondary electrons is shown in Fig. 2.2,
at different depths of the atmosphere, and is compared with
the primary proton flux.   It can be seen that the balloon
altitude is crucial in getting a low background from second-
aries.

2.2   Design of the Detector

The detector used in this series of balloon flights
is a simple range measuring detector, using a lead-scint-
illator sandwich.   A three element cerenkov telescope is
used to define the acceptance angle and the threshold for
particle detection.   Beneath this, and within the telescope
geometry is a two layer lead-scintillator sandwich which
measures the range of the particles.   An electron can be
measured if its energy is sufficient to pass through the
matter in the telescope (approximately 15 Mev or above),
and, if the electron energy is below $\sim$ 800 Mev it can be
stopped in one or other of the lead blocks in the sandwich.
A proton must have an energy greater than 600 Mev for det-
ection, and at this energy and above it will pass through
the lead blocks.   Hence the two different particles can be
separated.   The layout of the detector is shown in Fig. 2.3.

2.3　　Individual Detector Elements

Before discussing the relative performance of cerenkov and scintillator materials, it is necessary to examine the means by which their light output will be measured, namely the photomultiplier tube, since the response of this can considerably modify their performance.

The photomultipliers used are E.M.I. types, 6097, 9524, 9530, all selected for low noise and high gain, with typical sensitivities of $\sim$ 50 μA/Lumen, and dark currents of $\sim$ 1 nA.　The photocathode response is shown in Fig. 2.4. The maximum quantum efficiency is 16% at λ = 4000 A.u. It is the combination of this response and the light output of the elements in the wavelength interval around 4000 A.u. which determines the electrical output of the photomultiplier.

The charge collected on the anode of the photomultiplier is amplified and then used to trigger a discriminator. The pulses from the discriminators are then used to activate the logic circuits.

The limitation in the sensitivity of the photomultiplier tube is the dark current, which is produced by thermal electrons emitted from the photocathode.　These electrons can be emitted in bunches of up to $\sim$ 8 at a time (Birks, 1964)

so that the noise level due to them can appear as a signal, unless the signals produce many more photoelectrons from the photocathode.

2.4   The Cerenkov Elements

The cerenkov light output from a medium of refractive index n is given by:

$$\frac{dN}{d\ell} = \frac{2\pi\,Z^2}{137}\left(1 - \frac{1}{\beta^2 n^2}\right)\int \frac{d\lambda}{\lambda^2}$$

where $\frac{dN}{d\ell}$ is the number of photons emitted per unit path length, β is the velocity of the particle, λ is the wavelength of the emitted light, and Z the atomic number of incident particle. The light output is mainly in the visible and near visible regions (Jelley, 1958). It is important that this light output is matched to the spectral response of the photomultiplier tube. When a photomultiplier is used with a cerenkov radiator, the measure of its effectiveness as a particle detector is given by the number of photoelectrons liberated at the photocathode since this brings into account the spectrum of the emission, and the response of the photomultiplier. The number of photoelectrons emitted is given by:

$$\frac{dN_e}{d\ell} = \frac{2 \pi Z^2}{137} \left(1 - \frac{1}{\beta^2 n^2} \right) \int_0 \frac{S(\lambda) d\lambda}{\lambda^2}$$

Here, $\frac{dN_e}{d\ell}$. is the number of photoelectrons liberated per

unit path length of the particle in the absorber, and

$S(\lambda)$ is the quantum efficiency of the photocathode as a

function of wavelength.

The cerenkov light has the following characteristics:

(i)   Velocity threshold for detection is $\beta = \frac{1}{n}$.

(ii)   Light output is in a cone, maximum angle is

$\theta = \cos^{-1}(\frac{1}{n})$.

(iii) Radiation is emitted in visible and near visible

regions.

(iv)   Light output is proportional to Z^2.

The light output for a $\frac{1}{2}$" element of perspex, as

used in the detector, can easily be calculated. For the

photomultiplier tubes used, the integration of $\int_0 \frac{S(\lambda) d\lambda}{\lambda_0^2}$

gives a value of 1.7×10^3 between 3000 A.u. and 7000 A.u.

For $\beta = 1$ and n = 1.5 the number of photons emitted is

~ 5000, whereas the number of photoelectrons liberated

is approximately 100 if all the available photons are

collected by the photocathode. The collection efficiency

is more realistically 10% so that the number of photoelectrons

coming from the photocathode is $\sim$ 10. This is comparable with the noise level due to thermal emission at the photocathode, and so some means of eliminating the noise is necessary. This is discussed further in section 2.6.

The three elements used in the telescope are all of the cerenkov type. The top element is a $4\frac{1}{2}$" diameter disc of perspex, $\frac{1}{2}$" thick. The top and bottom and the edges are coated with white TiO_2 diffuse reflecting paint, and the disc is viewed from the edge with a 2" photomultiplier, optically coupled to the disc with a flexible perspex cement.

The centre element, a $4\frac{1}{2}$" diameter disc of $\frac{1}{2}$" thickness is viewed from beneath with a 5" photomultiplier. A downward moving relativistic particle produces a cone of light which is transmitted directly into the photocathode. To the top of the disc is cemented a disc of black perspex to absorb light from upward going particles, and so eliminate these from the detector response.

The third element in the telescope is an FC-75 (manufactured by Minnesota Mining & Manufacturing Co.) liquid cerenkov element. The FC-75 was chosen because of its low refractive index (n = 1.27) to give a high threshold for detection of particles, so improving the proton rejection.

The threshold for detection in perspex is 320 Mev, whereas in FC-75 it is 650 Mev. The liquid is contained in a vacuum tight brass box, coated inside with reflecting paint, and viewed from the edge by a 2" photomultiplier, looking in through a perpex window.

The light output of the two types of elements are shown in Fig. 2.5 for 100% collection efficiencies. The actual efficiencies are $\sim$ 10%.

The three detector elements are operated in triple coincidence to initiate all the events which the detector measures.

2.5   The Scintillator Elements

The energy loss by ionisation from a charged part-icle, of charge ze, in a medium of N atoms/cc and atomic number Z, is given by:

$$\frac{dE}{d\ell} = \frac{4\pi e^4 z^2}{m_o v^2} \; NZ \left(\ell n \frac{2m_o v^2}{I} - \ell n(1 - \beta^2) - \beta^2 \right)$$

where $v = \beta c$ is the particle velocity, m_o its mass and I an emirical constant for a given medium. The ionisation loss is essentially the same for all particles with the same charge and velocity. At low velocities it is proportional

to $1/v^2$ and reaches a minimum at relativistic velocities.
In a scintillator material, some percentage of this energy
loss is converted into light. The efficiency for this is
of the order of 1 - 10%, and the amount of light given out
is proportional to the energy lost by ionisation, hence
follows the same function as energy loss vs energy.

The light output of the scintillator material used
in the detector can easily be calculated. The minimum
energy that will be lost by a particle going through the
scintillator is ~ 1 Mev/gm cm^{-2}. For the thickness of
scintillator used in the detector, 600 kev will be lost.
If the conversion efficiency is 10%, then approximately
60 kev will be converted into useful light, and if the mean
photon energy is 3 eV, then there will be 20,000 photons
produced. Allowing a further 10% for the light collection
efficiency, and 10% for the quantum efficiency of the
photomultiplier means that 200 photo-electrons will be
produced from the photocathode. This is well above the
noise level of the photomultiplier.

The scintillators used in the detectors are required
to determine the presence of particles in the lead scint-
illator sandwich. It is necessary to be able to detect
the presence of particles over a wide range of energies,

and so the scintillator is to be prefered in this applic-
ation, as the detection threshold is very much lower than
the cerenkov threshold.

The scintillators used are 7" and 9" in diameter,
both $\frac{1}{4}$" thick, viewed from the edge via a tapering light
guide by a 1" photomultiplier tube.   Light collection
is assisted by silver foil placed around the scintillator
and the light guide.

2.6   Coincidence Operation of Telescope

It is necessary to use at least two elements in
coincidence to define the opening angle of the telescope.
The use of the photomultiplier tubes in coincidence reduces
the contribution to the counting rate from the individual
tube noise.   For the cerenkov elements, the noise from
the tube is comparable with the signal, so the 2-fold
coincidence is insufficient to eliminate all the counts due
to noise, and so a third element in coincidence must be
introduced.   This brings the chance coincidence rate down
to negligible proportions.

The counting rate due to noise coincidences is given
by:

$$N = 3 N_1 N_2 N_3 \tau^2$$

where N is the noise coincidence rate, N_1, N_2 and N_3 the

individual counting rates of the cerenkov elements, and τ

the resolving time of the coincidence circuit. The res-

olving time of the coincidence unit is less that $1\,\mu$s

and with this the chance rate is ~ 1 per day even if the

photomultipliers are operating at rates of ~ 10,000

counts/minute. In practice the photomultipliers operate

at ~ 300 - 3000 counts/minute.

When the three elements are placed in coincidence,

they define an opening angle. The charged particle count-

ing rate of the detector depends upon the geometrical factor,

a quantity which takes into account the area of the elements

as well as the opening angle of the telescope. The geo-

metrical factor of the telescope was calculated using the

method of Heristchi (1967), and has a value of 11.8 cm^2 ster.

As well as defining the geometrical factor and the

opening angle, the telescope defines the threshold for

detection for the various particles encountered.

2.7 Response of Telescope to Various Particles

(i) Protons

The telescope response is governed by the cerenkov

elements used in it, their responses being shown in Fig. 2.5.

The criterion for detection is that the pulse height from the photomultiplier is sufficient to trigger the discriminator, and so a certain light output will correspond to this threshold. Because of the fluctuations in light output, collection and quantum efficiencies, the threshold energy will not be well defined. The measured response to a beam of mono-energetic protons from the NIMROD accelerator at Harwell is shown in Fig. 2.6, from which it can be seen that the threshold corresponds to approximately 75% of the maximum light output.

(ii)   Electrons

The energy threshold for the electrons is not determined by the cerenkov threshold, since electrons at that energy cannot penetrate the matter in the telescope. The electrons at the detector threshold energy must have sufficient energy to penetrate all the material in the telescope and still be relativistic in the FC-75 to give a light pulse there. The threshold for electrons is thus 15 ± 2 Mev.

(iii)   Mesons

Because of their penetrating nature, the π and μ mesons behave in a similar way to the protons, and protons and mesons of the same velocity will give the same light

output in the cerenkov elements.   In Fig. 2.6 is shown
the theoretical meson response, derived from the measured
proton response, with allowance made for the ionisation
losses of the mesons in the telescope.

(iv)   Heavy Particles

The detection threshold for heavy particles is
similar to the threshold for protons.   Since the particles
must be relativistic to be detected, the detection thresh-
old for α -particles is 3 Gev, and is correspondingly
higher for heavier particles.

2.8   Telescope Efficiency

The above discussion on response is in terms of
normalised response, i.e. when the maximum of light out-
put is obtained from the cerenkov elements the efficiency
is taken as unity.   Because of the nature of the light
collection the detector is not 100% efficient.   The term
telescope efficiency is the measure of the detector eff-
iciency for relativistic particles.   This quantity was
determined by using a 2-fold telescope to define a beam
through the 3-fold telescope, and measuring the fraction
of the 2-fold events which trigger the telescope.   This
fraction is the telescope efficiency, and is $\sim$ 50%.

2.9.   Range Method of Electron Separation

In the discussion so far, only the telescope has been discussed.   A particle, having registered in the telescope then encounters the lead scintillator sandwich. Its behaviour in the sandwich is important in separating the electrons from other particles.   For the sandwich to be effective, it must stop the electrons whilst transmitting the protons and other particles.

The lead scintillator sandwich is made up of two lead blocks, placed beneath the liquid cerenkov element, each block having a scintillator beneath it, as in Fig. 2.3. The lead and the scintillators are suitably shaped to ensure that the sandwich overlaps the geometry of the tele-scope.   The first block is 5 radiation length thick, and the second one makes a total of 11.

2.10   Interactions of Particles in the Sandwich

The particles considered are those which are detected in the telescope, and their corresponding energies, as it is the telescope coincidence which is used to initiate all the measurements.   Since the lead scintillator depends upon stopping particles for its operation, it is necessary

to consider the various means of energy loss for the
particles in the absorber.   The main energy loss mech-
anisms which are important are:

(i)   Ionisation

(ii).   Bremsstrahlung

(iii)   Nuclear interactions

Electrons lose their energy by ionisation at low energies
and at higher energies by bremsstrahlung.   The energy loss
is different for different media, and a measure of the
effectiveness of the media for bremsstrahlung is the radi-
ation length.   The energy where ionisation and bremsstrah—
lung effects are equal is termed the critical energy.

Protons and heavier nuclei have strong nuclear int-
eractions which are dominant before the minimum in the
ionisation curve is reached, whereas for mesons, ionisation
loss is dominant over all energies.   The relative energy
losses for these particles are shown as a function of energy
in Fig. 2.7.   Ionisation and bremsstrahlung energy losses
are shown for the electrons, whereas only the ionisation
losses are shown for the protons and mesons.

In the choice of the absorber, the requirement is
that electrons must be stopped whilst all other particles
are passed.   Electrons will lose most of their energy by

bremsstrahlung, and so the absorber must be effective at
doing this.   The absorber should have a suitably short
radiation length.   It is also necessary to be able to
transmit the protons with minimum loss.   Since the proton
energy under consideration is above 650 Mev, the most
important loss mechanism is due to nuclear interactions.
The most suitable material will be one with a small radiation
length and a long collision length.   Of the readily avail-
able materials, the most suitable is lead, as can be seen
from the table of radiation lengths and collision lengths,
table 2.1.

2.11   Response of Sandwich to Various Particles

(i)   Electrons

Various theoretical works exist on the topic of
cascade showers in lead.   Notable ones are the Monte-
Carlo calculations of Nagel, (1965), Crawford and Messel,
(1962) and Wilson, (1952), and the calculations of Rossi (1952).
Nagel gives the probability of a given number of electrons
appearing at a given depth in the absorber.   For the lead
scintillator sandwich it is the probability of zero electrons
which is required.   The other calculations give the average
number of electrons at a given depth, and from this it is

possible, using Poisson statistics to find the probability
of zero electrons at that depth.   The response of the
detector using some of these calculations is shown in Fig. 2.8
and 2.9.

The response of the detector to electrons was deter-
mined experimentally using the electron synchrotron at
D.E.S.Y., Hamburg..   The electrons in the synchrotron were
used to produce gamma rays in a target in the machine.
These gamma rays were then converted in a lead target into
an electron-positron pair, which were then momentum analysed
in a magnetic field.   To ensure that only electrons were
being detected, an extra scintillator element was used to
detect the positron as well as the electron, and only coin-
cidences of the two were accepted.   Electrons from 50 Mev
up to 2000 Mev were used to calibrate the detector.   The
results show excellent agreement with those of Nagel.
The response shown in Figs 2.8 and 2.9 is the response of
the lead-scintillator sandwich with the telescope material
in front of it, and is thus the response of the whole detector
to electrons.

(ii)   Protons

Any proton which triggers the coincidence unit, but
because of interactions in the absorber fails to register

in either the lower scintillator, or both, behaves in the
same way as an electron.. Such a proton cannot be disting-
uished from an electron. Although the fraction of protons
which interact in this way is small, the contribution to
the electron counting rate is significant, due to the rel-
atively large flux of protons present at balloon altitudes..

Using proton interaction lengths given by various
authors (e.g. Shaw and references therein), the probability
of a collision in the absorber can easily be calculated,
but to find the fraction of protons not detected by the
scintillators requires information about the angular dist-
ribution at various energies. A direct measurement was
thus made, using the proton synchrotron, NIMROD, at the
Rutherford Laboratory. The proton beam from the synchrotron
included many other particles such as electrons and mesons.
The protons were separated from the rest using time of
flight techniques. The particle beam was first momentum
analysed using a series of magnets, and then particles
with the appropriate time of flight were used to gate the
detector, so ensuring that only protons of the required
energy were detected. The response of the sandwich to
protons is shown in Fig. 2.10. The curve A represents
the response of the telescope alone, curve C gives the

fraction of protons which do not go through the first

scintillator, and curve B the fraction which miss the

second scintillator. These two curves show the contam-

inations of the electron channels due to the protons,

and are corrected for in each flight.

(iii) Mesons

Almost all the mesons detected by the telescope

have sufficient energy to penetrate the lead absorber,

and so appear in the proton channel. Since the lead

absorber is 11 r.l. thick, only π mesons with energy less

than 135 Mev and μ mesons with less than 130 Mev will

stop in the lead. Since the threshold for detection

by the telescope is 95 Mev for π mesons, and 75 Mev for

μ mesons, all those detected will pass through the 5 r.l.

of the first block, so that none will contaminate the low

energy channel. The only contamination will be in the

high energy channel, due to those mesons between the thresh-

old energies and $\sim$ 130 Mev. The detection efficiencies

for these mesons is shown in Fig. 2.6. The contribution

from mesons behaves in a similar way to the secondary

electrons, and so are included in the corrections for the

secondary electrons.

(iv)   Helium Nuclei and Heavier Particles

Since the threshold for these particles is much
higher than for protons, it follows that in any interactions
in the lead, the products will be collimated more in the
forward direction than for protons, and so the chance of
being missed by the scintillators is much less than for
protons.

2.12   The Electronics

All the information from the detector must be trans-
mitted back to a ground station from the balloon since
retrieval of the payload cannot be relied upon.   The elect-
ronics is used to process the signals from the photomultiplier
tubes, and put them into a suitable form for transmission
on the telemetry link, together with pressure and temperature
information.   The electronics must operate reliably in the
environment encountered, i.e. from one atmosphere down to
zero pressure, from +40 to $-20^{\circ}C$, and for periods of up to
12 hours or more at altitude.

(i)   Balloon Electronics

The information about each cosmic ray event appears
as a signal from the photomultiplier tubes.   The signal

from each photomultiplier is first amplified with a charge

amplifier, and then used to trigger a discriminator.   The

discriminator pulses from the three cerenkov elements in

the telescope are together applied to a coincidence circuit,

which provides a coincidence pulse which initiates all

measurements.   The discriminator pulses from the scintill-

ators are fed into a store, via gates which are opened by

the coincidence pulse.   The information in the store is

then used to set the state of a binary counter.   The coin-

cidence pulse starts the 3 khz subcarrier oscillator, which

is fed directly into the counter.   If no information has

come from the scintillators, the subcarrier completes 64

cycles before being switched off.   If a particle is det-

ected in either of the scintillators, then the subcarrier

oscillator is switched off after less than 64 cycles.

In effect, each scintillator pulse, if coincident with the

telescope coincidence, subtracts its own number from the

64 cycles: the upper scintillator subtracts 16, and the

lower one 32.   The subcarrier can thus be switched on for

anything between 16 and 64 cycles, in multiples of 16.

The subcarrier word is transmitted to the ground each time

a cosmic ray particle triggers the telescope.

Pressure and temperature information are measured on

an Olland cycle, a commercial device using aneroid capsules and a bi-metallic strip to measure pressure in the range 0-20 and 0-1000 mb, and temperature from -40 to + 60.$^{\circ}$C. The device puts the information into morse code, which is used to modulate a 400 Hz subcarrier oscillator.

The information is sent back to ground using a 180 mw transistorized F.M. transmitter, operating at 136.5 mhz.. The signals are radiated from an aerial which combines the properties of a turnstile and an inverted ground plane, to give a suitable response for transmission to the ground.

The power to the electronics is provided from a 2000 mA/hr nickel cadmium battery, giving a total operation time of $\sim$ 12 hours. To compensate for changing battery voltage, a L.T. convertor is used to provide stable +5 and -15 volt lines, despite changes from 13 to 8 volts in the battery. E.h.t. supplies come from a separate convertor, which provides 1500 volts. All leads and components carrying e.h.t. are potted in silastomer to prevent corona discharge at low pressures..

A cut-down receiver is included in the detector, so that it can be released from the balloon if necessary. A clock and a pressure operated switch are included as safeguards against failure of the cut-down receiver. Range

measurements are made possible by measuring the time
delay for a signal to be sent to the balloon and back to
the ground station.

(ii)   The Ground Station

During a balloon flight, the signals are received
by a twin 7 element yagi aerial. A low noise aerial
amplifier is used to feed the signals to an Eddystone
V.H.F. receiver. A range of 400 miles is possible with
this arrangement. The signals are recorded on a Tandberg
stereo tape recorder, one channel recording the receiver
output, and the other the data signal after being passed
through a band pass filter. The data signals are simult-
aneously punched onto paper tape, ready for computer anal-
ysis. If there is any interference in the radio link,
the number of cycles punched onto the paper tape may vary
slightly. The redundancy in the number of cycles used
ensures that adjacent channels can be distinguished.

The balloon electronics and the ground station are
shown schematically in Fig. 2.11 and 2.12.

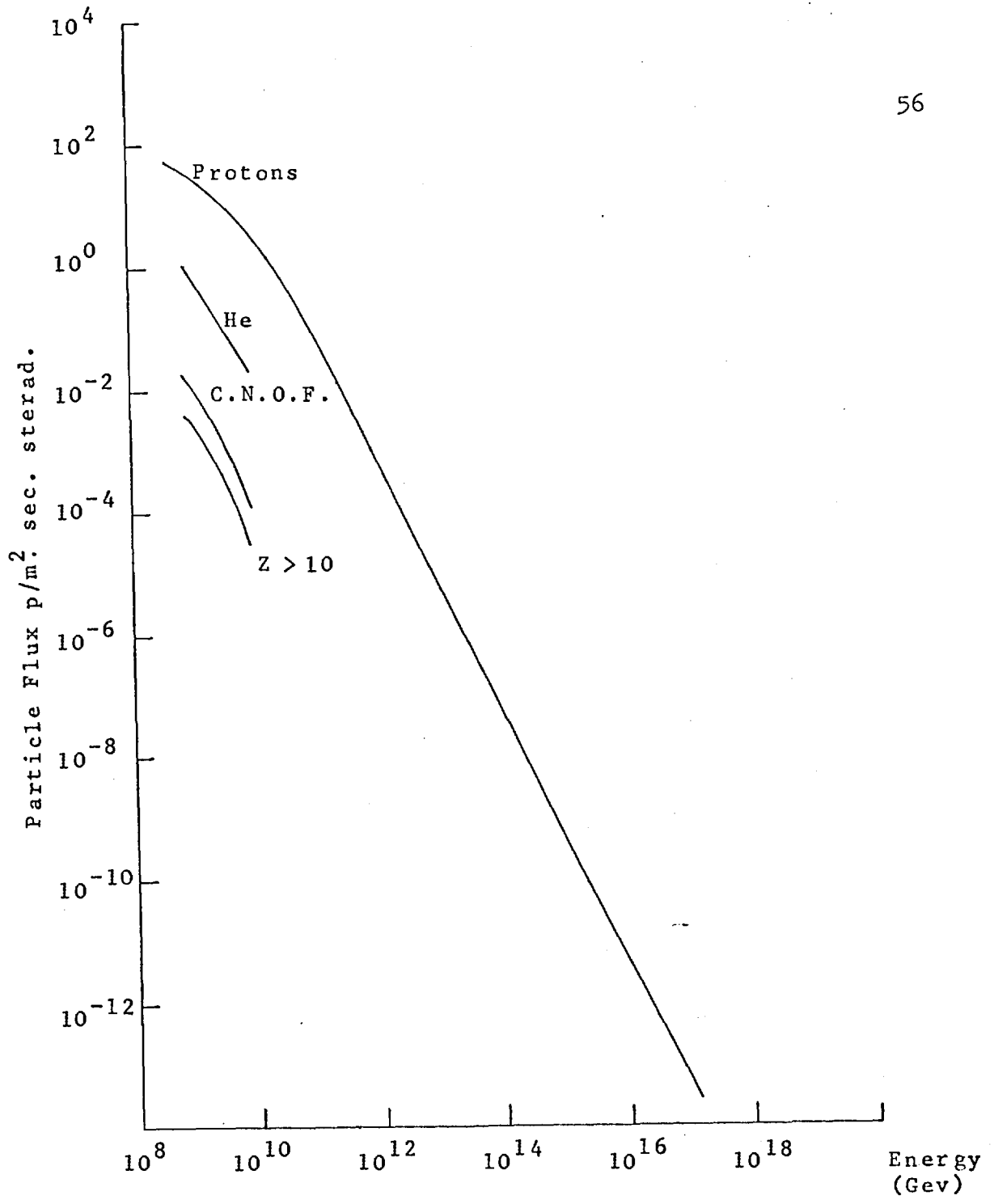| Material	Radiation length X_o (gm/cm^2)	Collision length (gm/cm^2)
Carbon	44.6	76.2
Aluminium	24.5	99.6
Iron	14.1	127.0
Copper	12.1	133.0
Lead	6.5	197.0

Table 2.1. Radiation lengths and collision lengths.
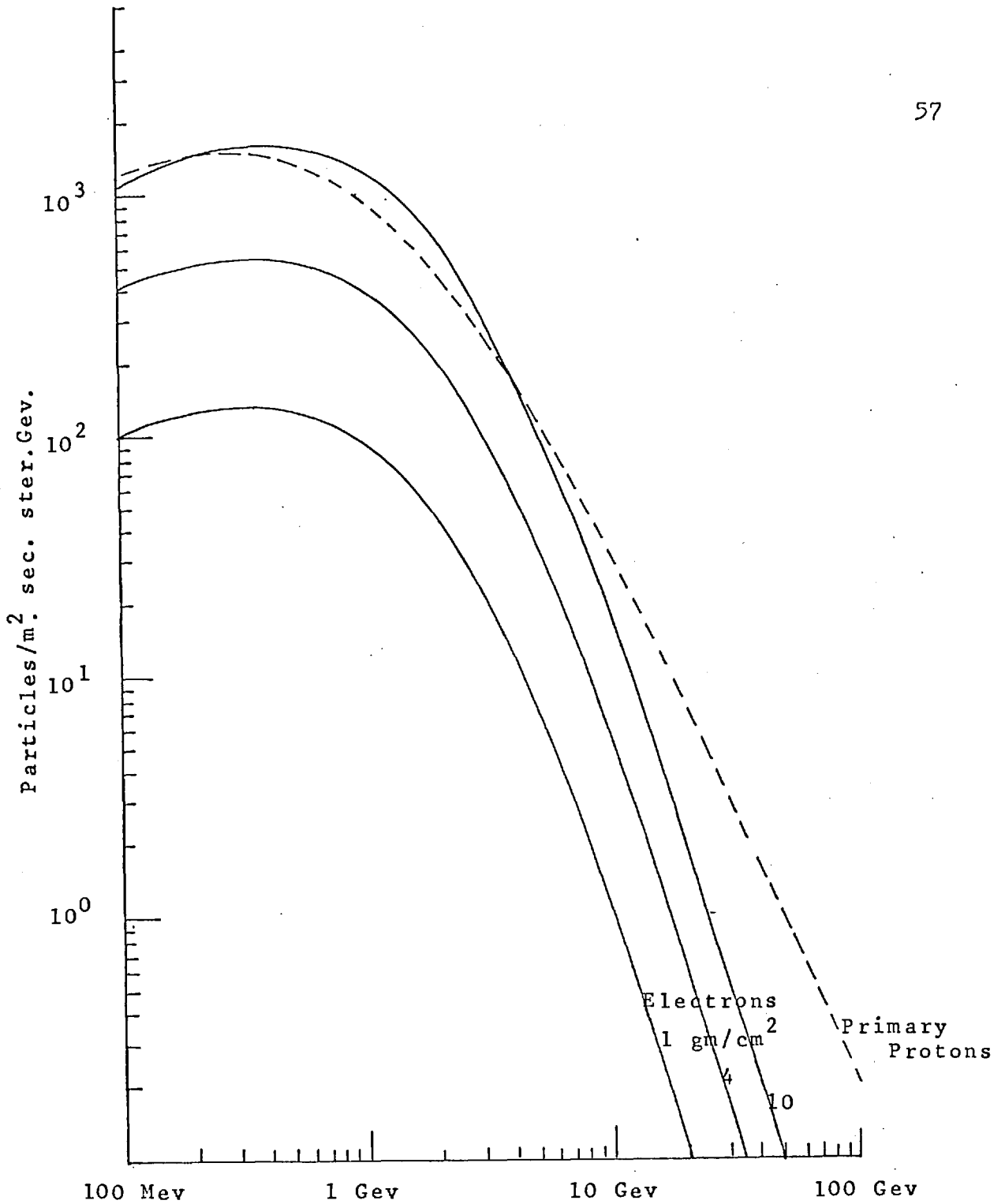
Fig. 2.1.   Integral Spectrum of Primary Particles.

Fig. 2.2.   Differential Flux of Secondary Electrons
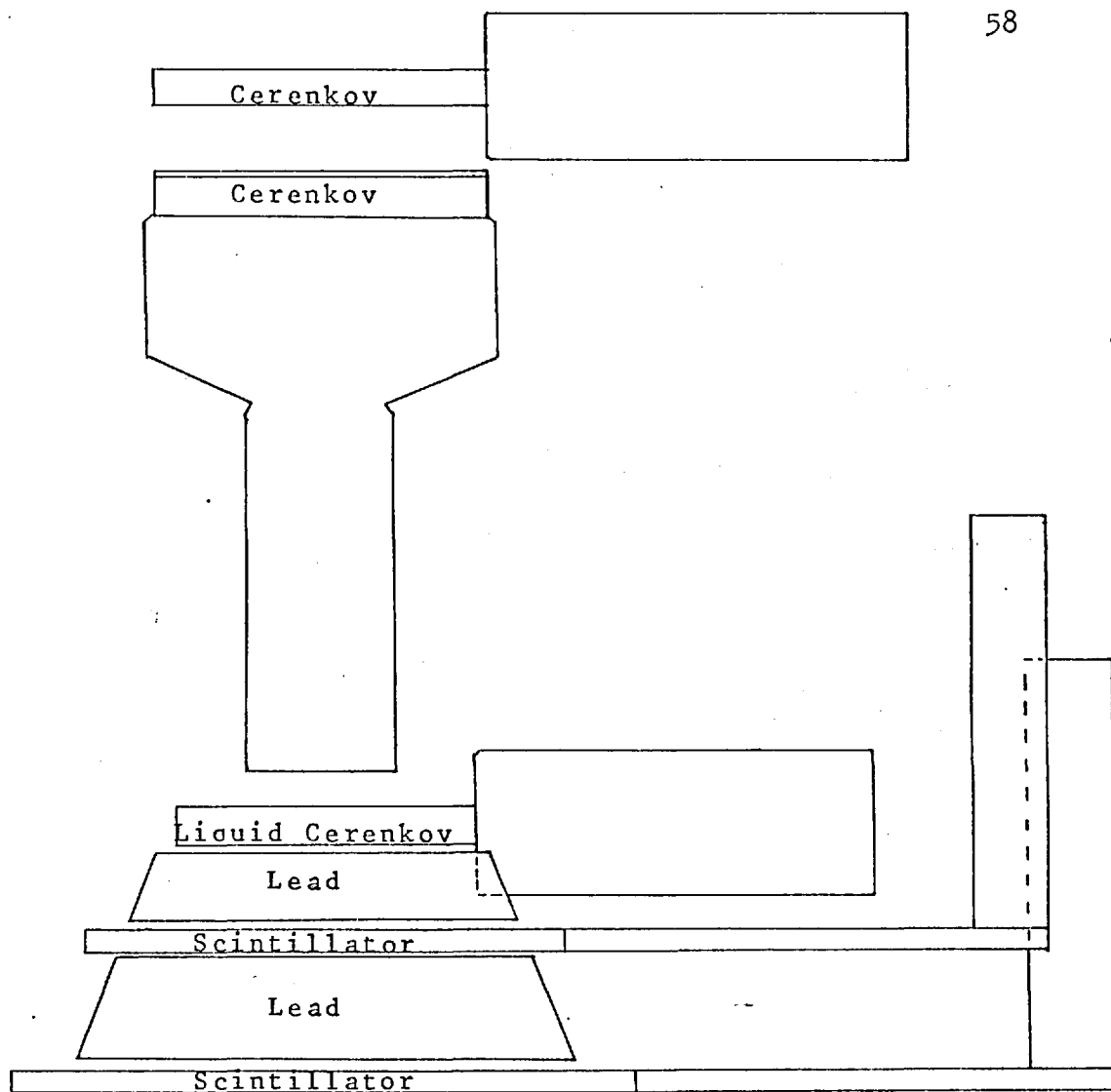and Primary Protons.

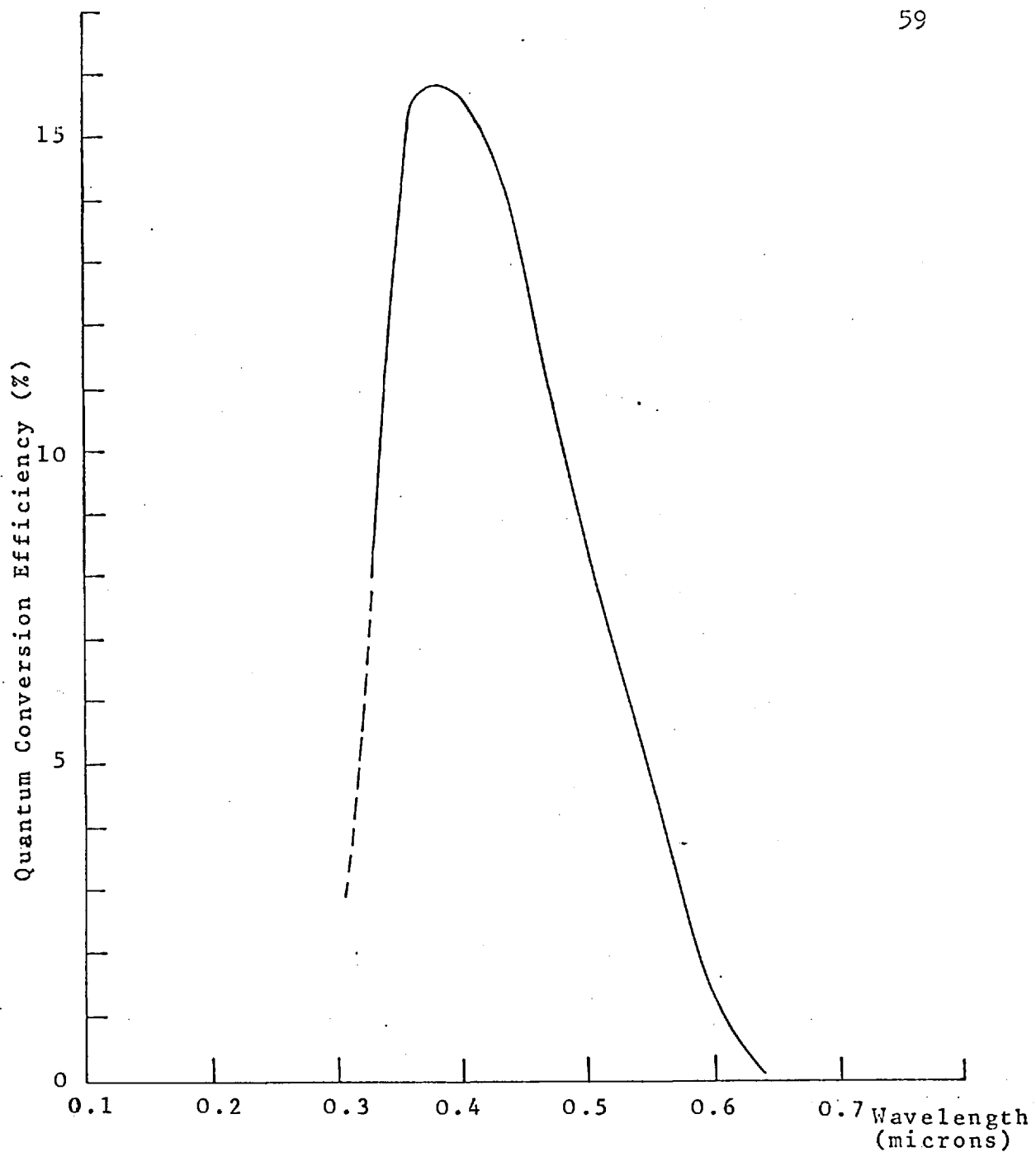Fig. 2.3.   Layout of Detector.

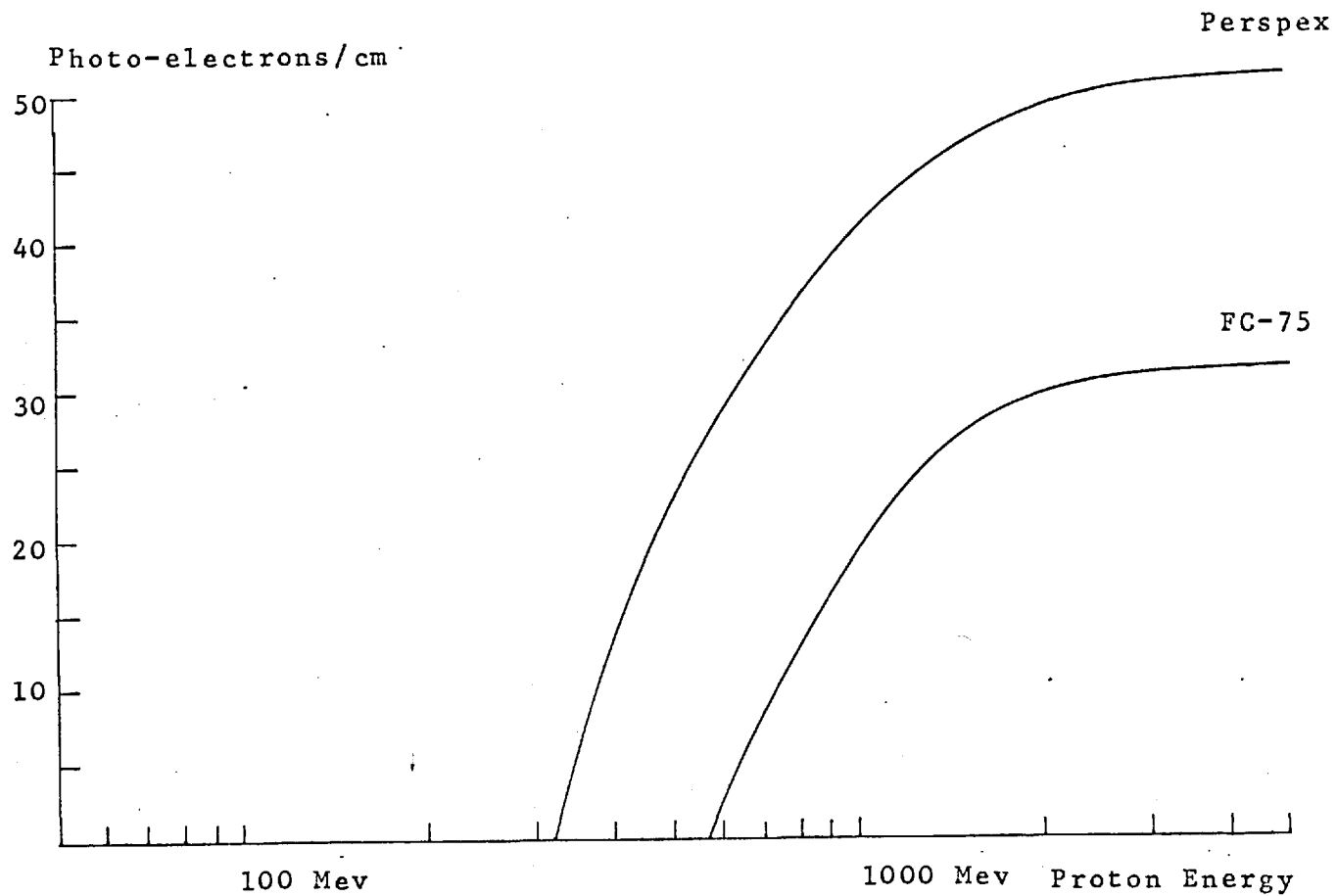Fig. 2.4. Quantum Efficiency of Photomultiplier Tubes.

Fig. 2.5   Light Output of a Cerenkov Radiator - number of Photo-Electrons per cm of Path Length, emitted by Photocathode for 100% Collection Efficiency.
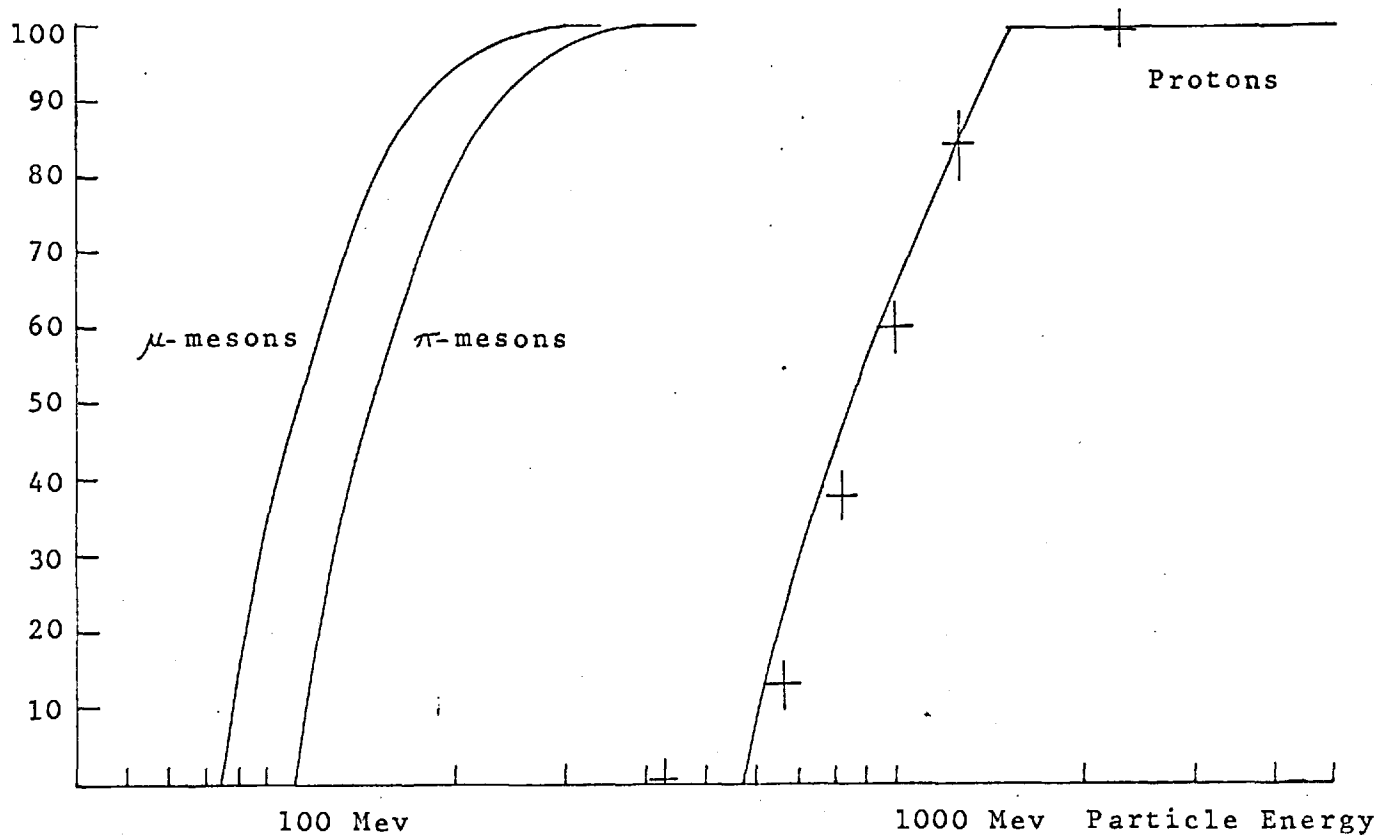
Detection Efficiency
(%)

Fig. 2.6. Detection Efficiency of Telescope for Various Particles.
Proton Measurements from NIMROD. Meson Curves are Derived
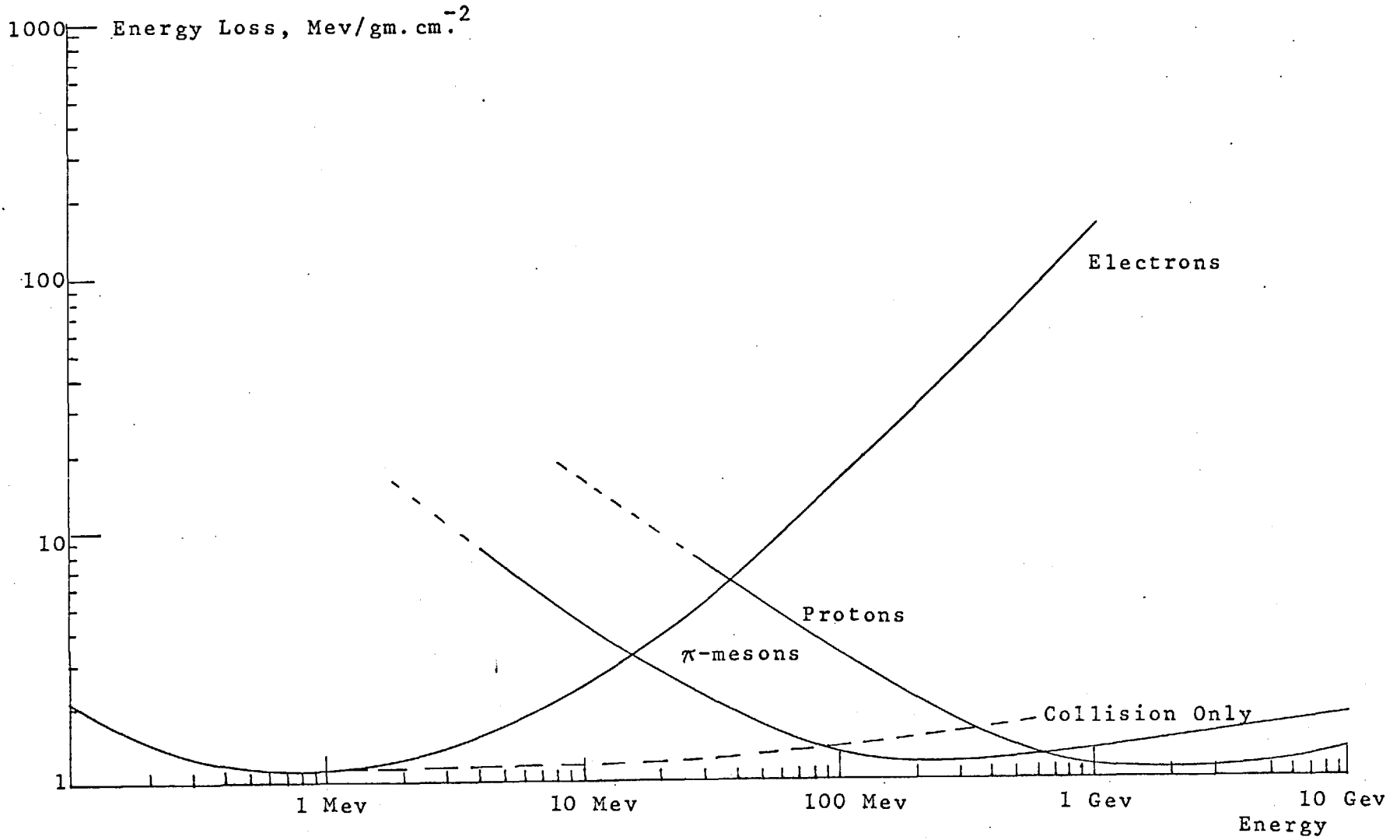from Proton Measurements.

Fig. 2.7. Energy Losses of Charged Particles due to Ionisation and Bremsstrahlung.
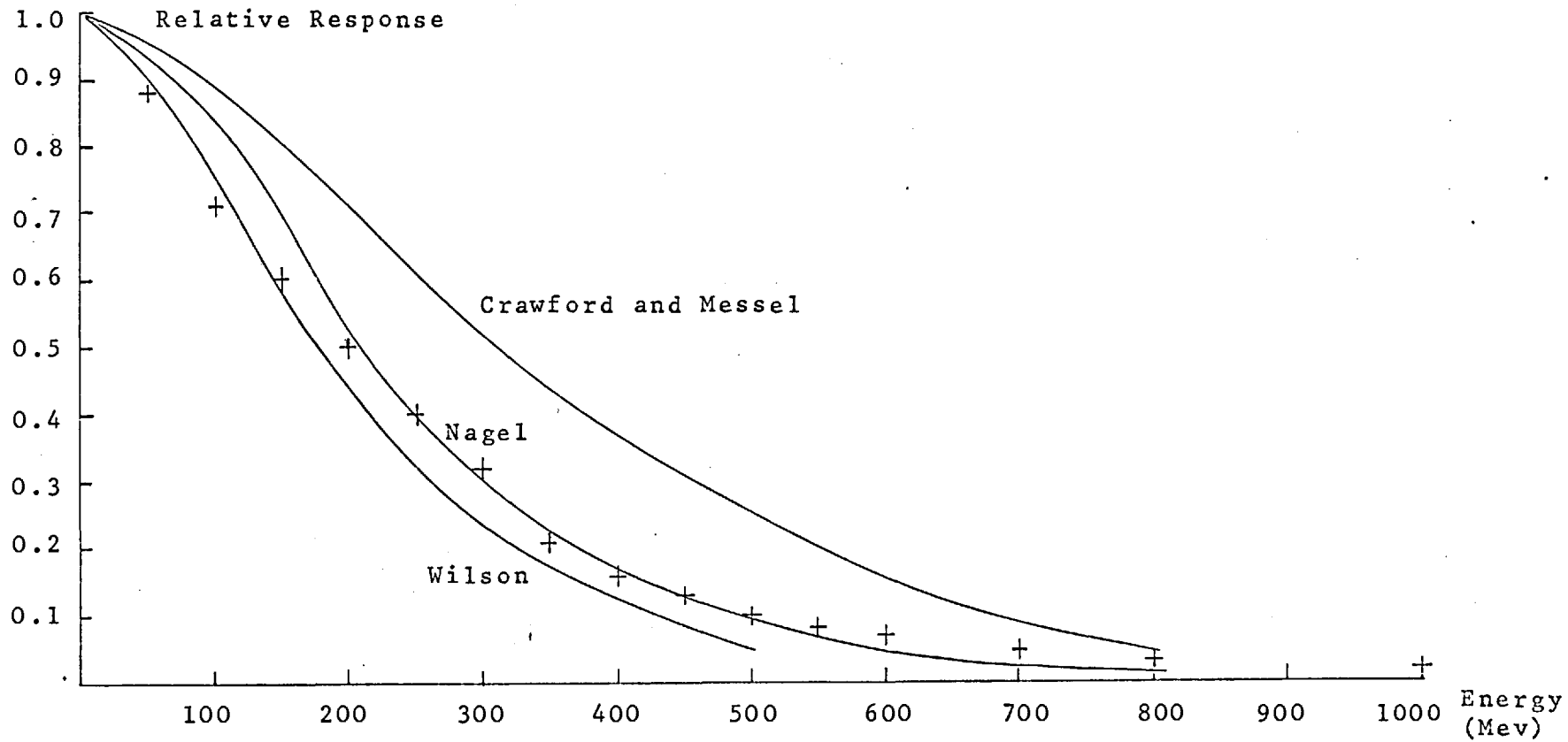
Fig. 2.8   Electron Response.   Low Energy Channel;   Measured and Theoretical.
Measurements taken from D.E.S.Y.
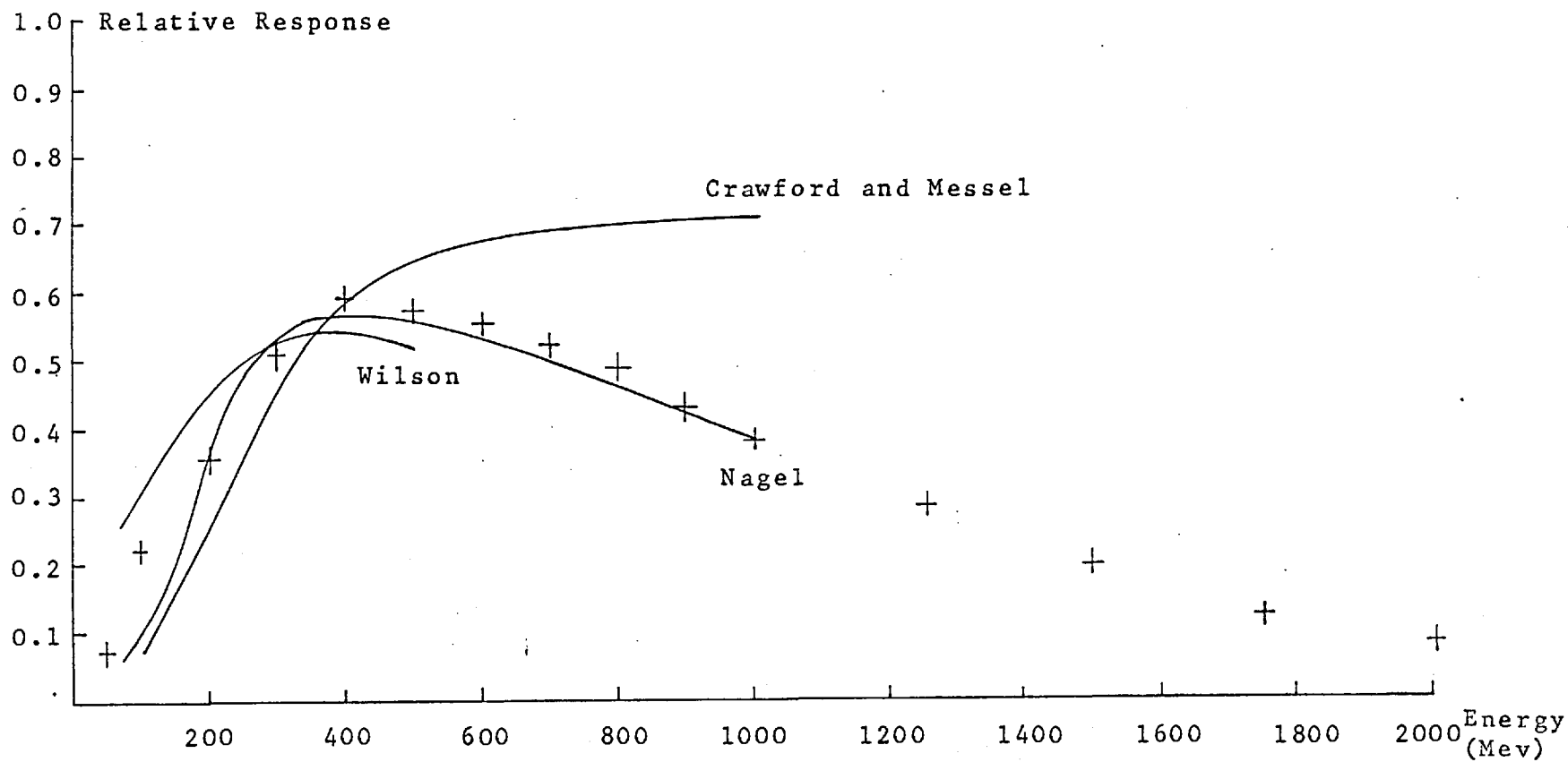
Fig. 2.9.   Electron Response, High Energy Channel;   Measured and Theoretical.
Measurements taken from D.E.S.Y.
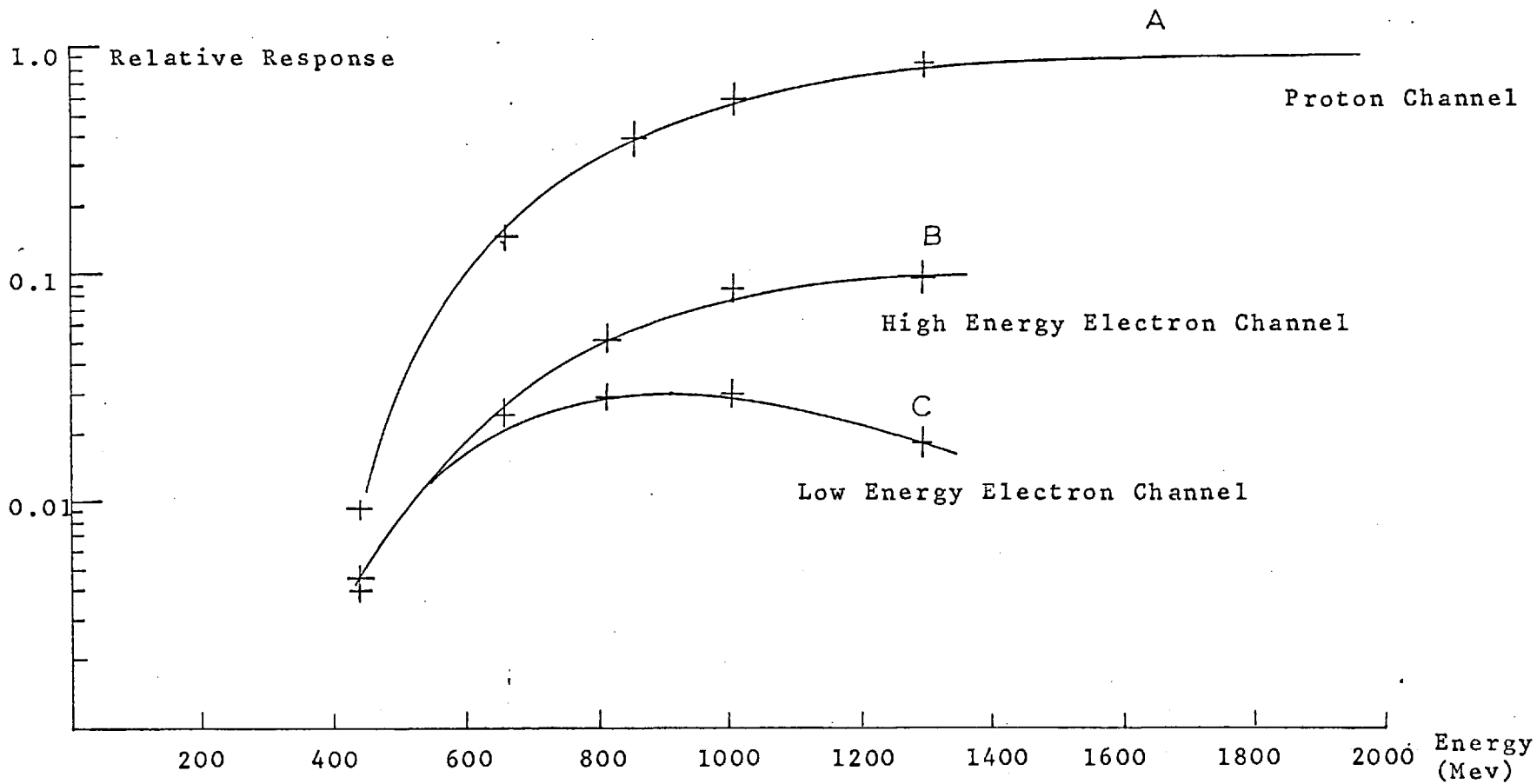
Fig. 2.10   Response of Detector to Protons, showing Contamination in Electron
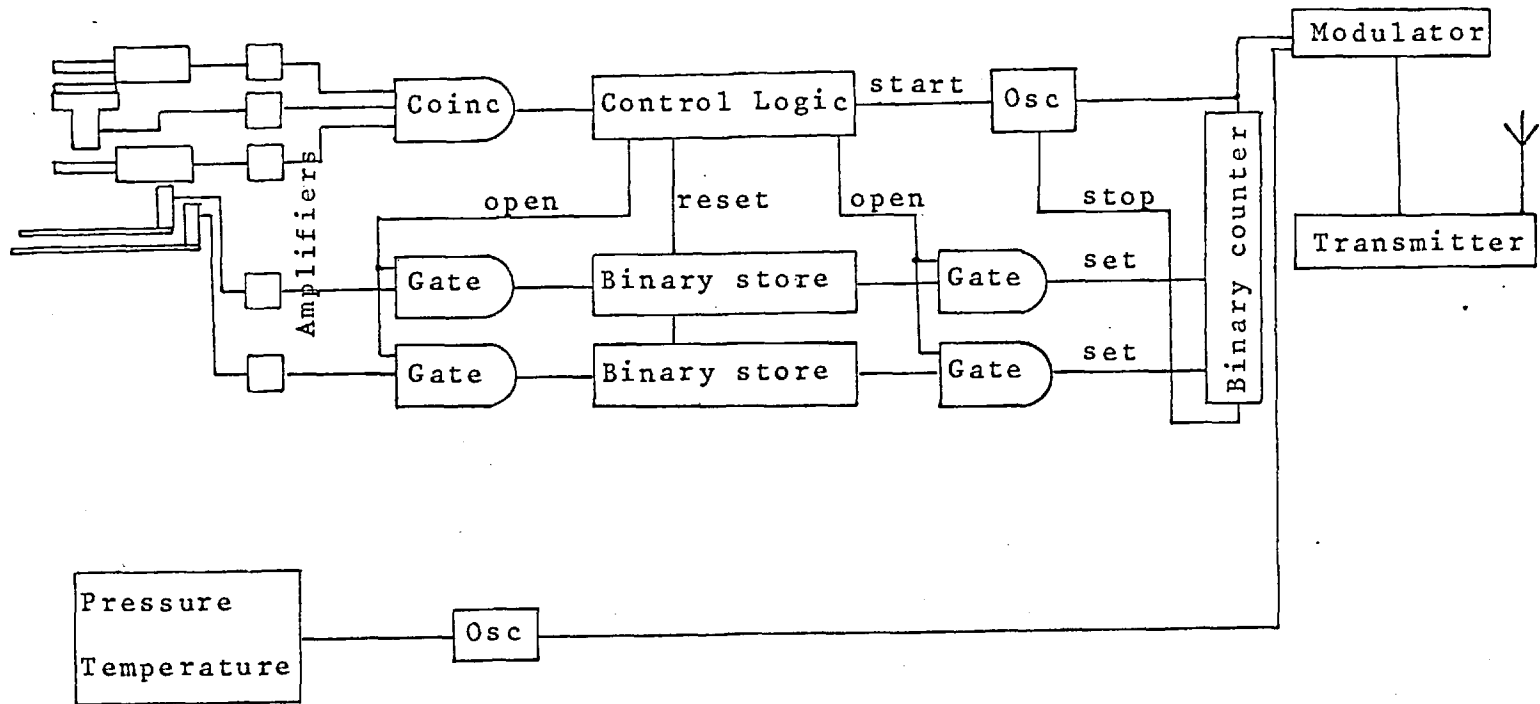Channels.
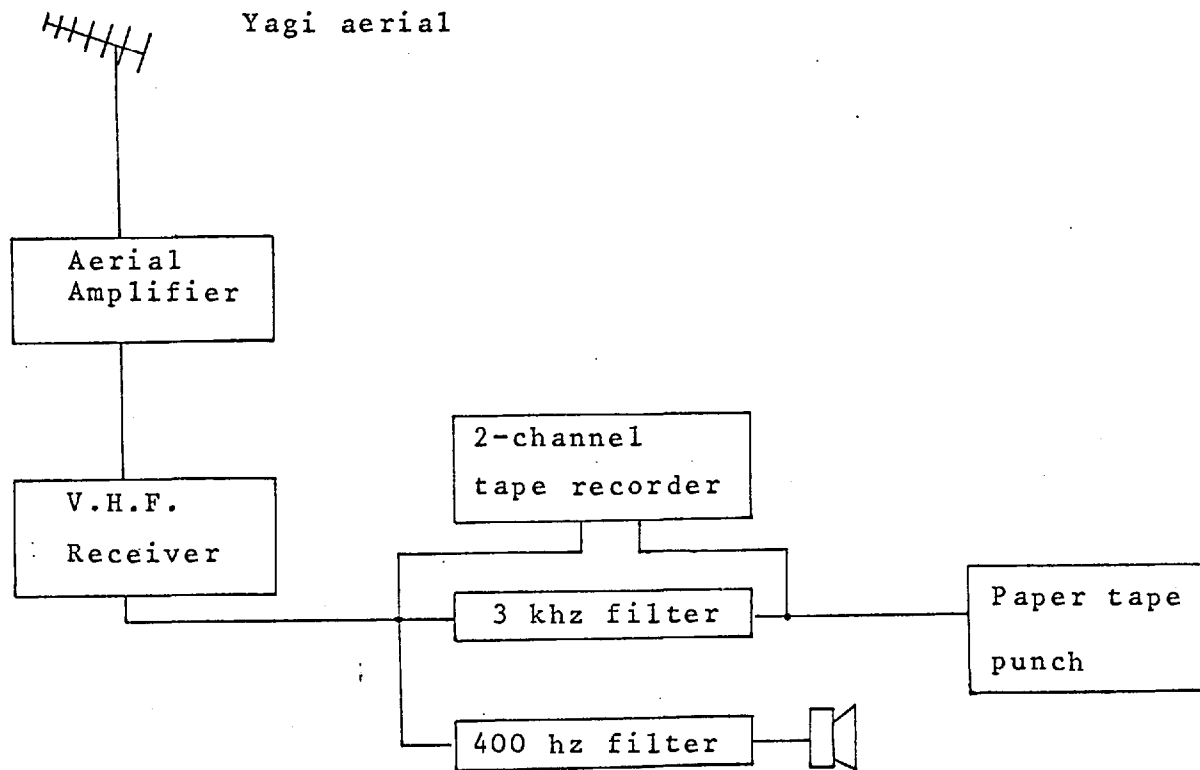
Fig. 2.11.   Balloon Electronics

Yagi aerial

Aerial
Amplifier

V.H.F.
Receiver

2-channel
tape recorder

3 khz filter

Paper tape
punch

400 hz filter

Fig. 2.12   Ground Station

CHAPTER III

THE BALLOON FLIGHTS

Five balloon flights have been made using the design of detector described in the previous chapter. The flights were made from two locations, Cardington, in Bedfordshire, and Kiruna, in Northern Sweden. The balloons used were American polythene ones, inflated with hydrogen. Two types were used, 360,000 cu. ft volume balloons, manufactured by Raven Industries, and 450,000 cu. ft volume ones, made by Winzen Inc. The total flight weight, i.e. balloon plus detector was approximately 150 lbs, which could reach an altitude of $\sim$ 130,000 ft - 3 to 4 mb of residual atmosphere.

Each flight carried as well as the detector, a parachute, radar reflector and a radio controlled cut-down device, as well as associated aerials. A clock and a pressure trip for the cut-down device were carried as precautions against failure of the radio. The detectors were housed in insulating boxes made out of polystyrene. The early flights used 1" expanded polystyrene, whilst later ones used 2" thick Sytrofoam. The long time constant for heat loss through the insulation keeps the

detector temperature within a few degrees of its initial temperature during ascent. At altitude, the temperature gradually rises due to the influx of heat absorbed by the blackening on the box. The temperature profiles for the flights are shown in Fig. 3.1.

The duration of the balloon flight is determined by the time it is illuminated by the sun. When the temperature of the hydrogen falls, the contraction causes the balloon to descend. In Kiruna, during summer time, the midnight sun keeps the balloon illuminated throughout the night, and so the balloon can stay aloft for many days. The usefulness of the flight is then determined by the battery life and the telemetry range. For balloon flights in England, the Air Traffic Control regulations require the payload to be on the ground half an hour on the daylight side of sunrise and sunset.

When at altitude, the upper atmosphere winds determine how long the balloon stays in range of the telemetry link. During the flights from Kiruna, the maximum wind speed encountered was $\sim$ 40 m.p.h. giving a flight time of $\sim$ 10 hrs. For one of the flights, which drifted towards the west, it was possible to obtain further tracking from the SPARMO receiving station at Andennes in Norway, giving a flight

time of $\sim$ 20 hrs. Winds of up to 100 m.p.h. have been encountered in flights from Cardington. Under these conditions the SPARMO station at Lindau, W. Germany, has been used to increase the flight time, and enable the full daylight hours to be utilized. When the winds were not so violent, the flight times have been determined by the preset cut-down clock.

The height of the balloon was measured using an Olland cycle. Ascent curves for the flights are shown in Fig. 3.2. The balloons rise at $\sim$ 1,000 ft/min, taking approximately 2 hours to reach altitude, where they remain for the rest of the day. When too much hydrogen is used, the balloon rises too quickly, overshoots the ceiling altitude, venting some of the gas, and so descends slowly. In three of the flights, the pressure device failed before the end of the flights, but in each case, it was after the balloon had reached altitude.

The first balloon flight was made in 1966, the detector being flown inverted to measure upward going particles. The balloon was launched from Cardington, and reached an altitude of 3.2 mb. After 8 hours, the clock cut-down released the detector, which was subsequently recovered from Holland.

The next flight, in 1967 was from Kiruna, and reached an altitude of 3.2 mb, staying aloft for 8 hours before going out of range. The second flight in 1967 was made from Cardington, and reached an altitude of 4.3 mb. The balloon moved off at approximately 100 m.p.h. and was tracked from both London and Lindau. Contact was lost after 6 hrs.

Two flights were made in 1968, both from Kiruna. The altitudes reached were 4.7 and 4.8 mb, and were tracked for 11 hours and 20 hours respectively. Both drifted west-wards, the second being tracked from Andennes as well as from Kiruna. The detector from this flight was subsequently recovered in Canada.

The flight paths are shown in Fig. 3.3. Only two of the flight paths are accurately known, these being the 1966 flight, for which the recovery point is shown, and the 1967 Cardington flight which was followed optically from Lindau. All other flight directions are deduced from the aerial directions. The relevant details of all the flights are shown in Table 3.1.

Date	23.9.66	8.11.67	11.8.67	18.7.68	24.7.68
Location	Cardington	Cardington	Kiruna	Kiruna	Kiruna
Duration at altitude	8 hours	6 hours	8 hours	9 hours	18 hours
Max. height	3.6 mb.	3.9 mb.	4.3 mb.	4.7 mb.	4.8 mb.
Neutron monitor	2267	2257	2258	2183	2199

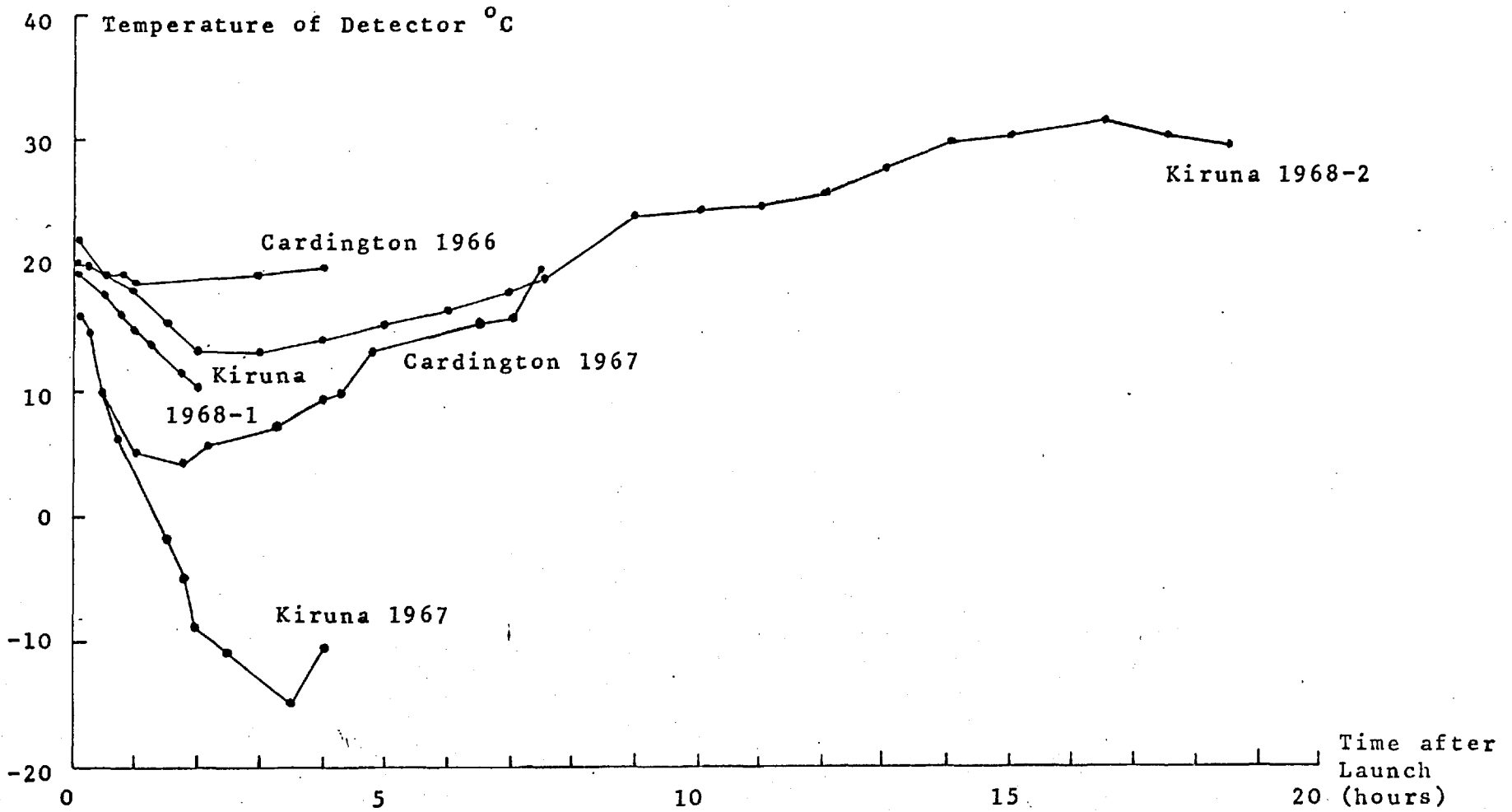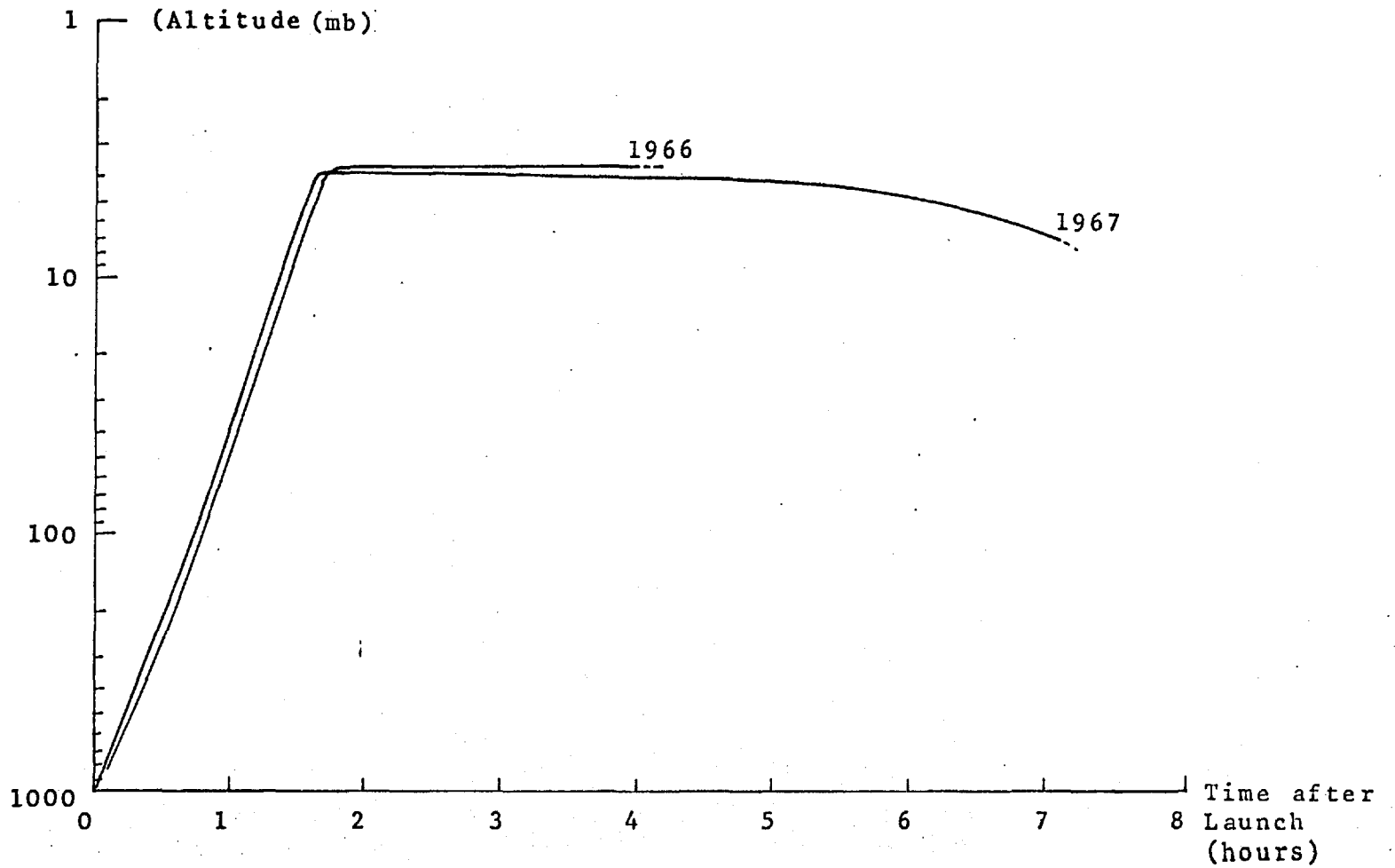Table 3.1. Table of Balloon flights.

Fig. 3.1.   Temperature Profiles for the Balloon Flights.

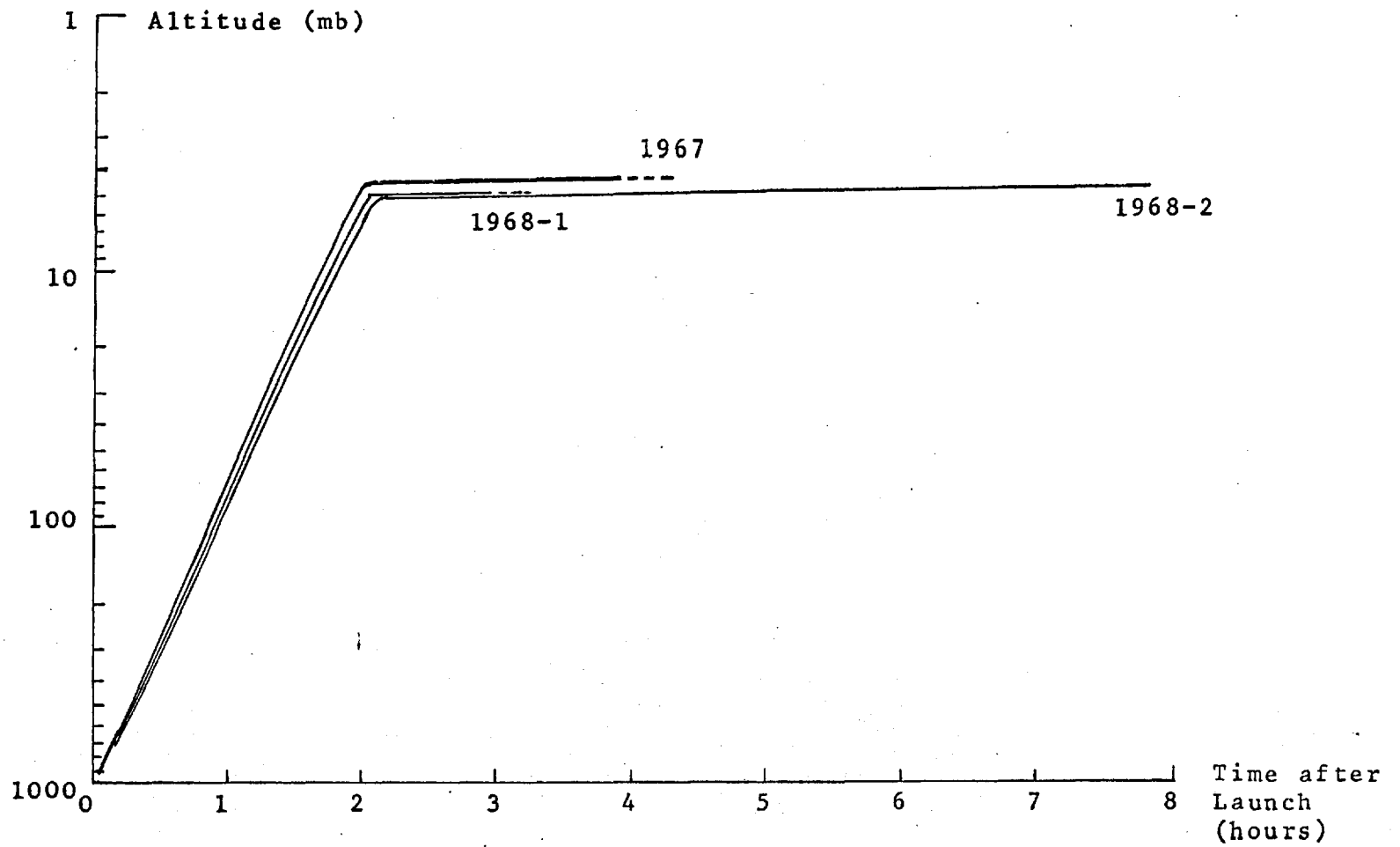Fig. 3.2a. Altitude Profiles for Flights from Cardington.
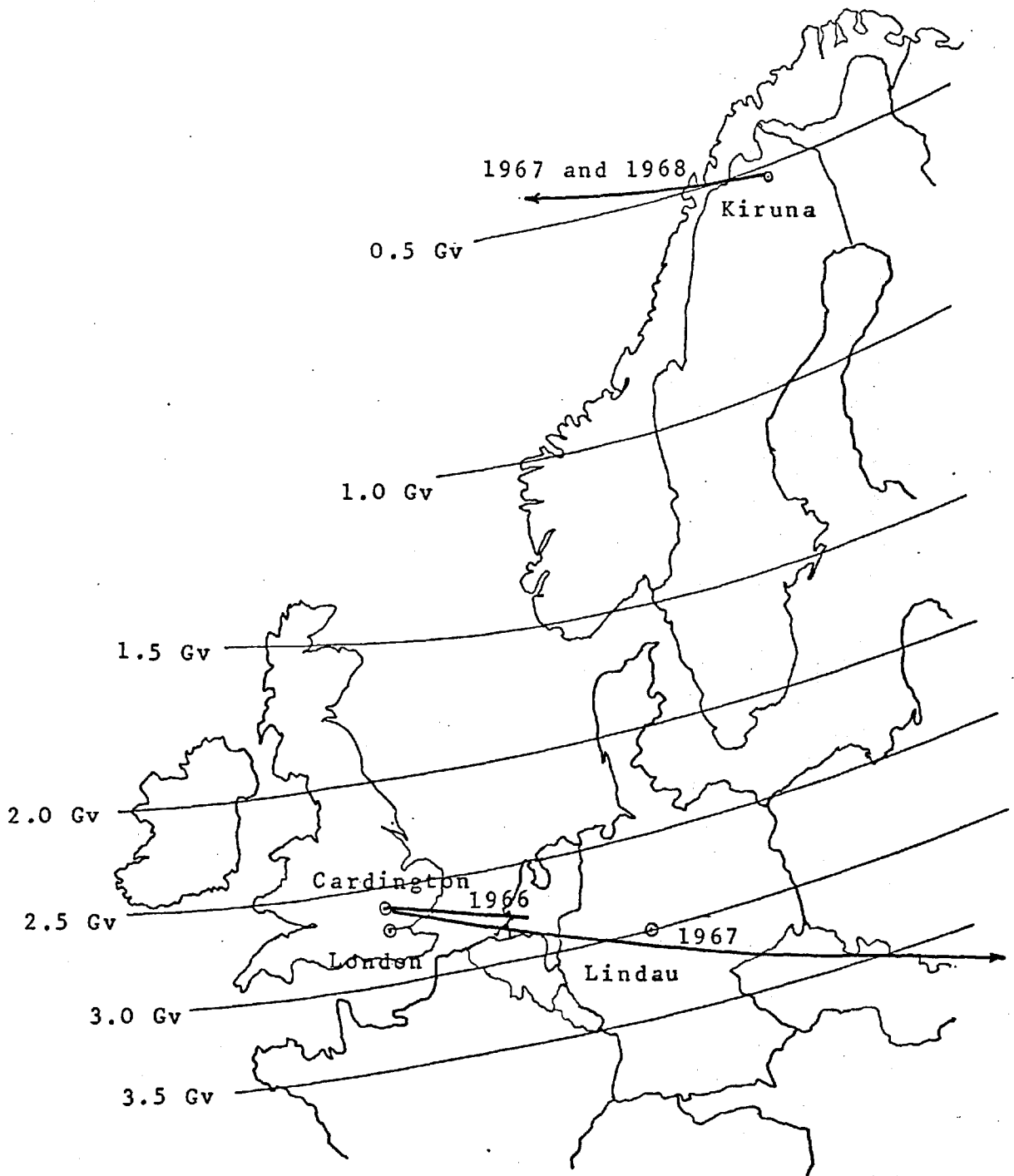
Fig. 3.2b. Altitude Profiles for Flights from Kiruna.

1967 and 1968

0.5 Gv

1.0 Gv

1.5 Gv

2.0 Gv

2.5 Gv

3.0 Gv

3.5 Gv

Kiruna

Cardington

London

1966

1967

Lindau

Fig. 3.3.   Track of Balloon Flights.

CHAPTER IV

PROTON   FLUX

The detector begins to measure protons at 600 Mev
but the full efficiency is not reached until $\sim$ 1500 Mev.
The counting rate in the proton channel is due to particles
which are relativistic in the liquid cerenkov detector,
and have sufficient energy to penetrate the lead absorber.
The majority of these particles are protons with more than
$\sim$ 1000 Mev energy, and helium nuclei with more than 2.8 Gev
total energy.   The contribution from heavier particles is
less than 2% of the counting rate.

When measurements are made at Kiruna, where the int-
ernal cut-off is $\sim$ 500 Mv, the primary proton flux extends
down to below 100 Mev, and the helium flux down to below
150 Mev.   The measured flux is limited by the detector
threshold for these particles.   The fluxes measured at
Cardington, where the cut-off is 2.5 Gv, are limited by the
geomagnetic cut-off and not the detector.   Between the
detector threshold and the cut-off energy are measured a
small contribution from the re-entrant albedo which con-
tributes less than 1% of the total counting rate.   The
cut-off energy at Cardington for protons is 1.7 Gev and for

helium nuclei is 2.5 Gev.   The fluxes measured by the proton

channel at Kiruna and Cardington are shown in Table 4.1.

Corrections are applied to these fluxes to allow for the

helium nuclei encountered.   The proton fluxes are then

corrected for the amount of matter above the detector using

a mean free path for absorption of 250 gm/cm^2.   This differs

from the usual figure of 100-150 gm/cm^2 quoted elsewhere,

since it takes into account the mesons generated in the

atmosphere, which cannot be distinguished from protons.

No corrections have been made for re-entrant or splash pro-

tons, since the high detector threshold ensures that this

flux is less than 1% of the counting rate.

The fluxes measured at Kiruna are shown in a regression

plot of proton flux vs. neutron monitor counting rate in

Fig. 4.1.   Mt. Washington neutron monitor is quoted, which

has a mean response of 15 Gev.   Also shown are other meas-

urements taken at various times in the solar cycle, and

corrected to give the integral flux > 1 Gv.   The flux at

Cardington in 1967 is shown together with the integral flux

greater than 2.5 Gv for various other workers.   The 1966

result cannot be compared directly, as the detector was

flown inverted, with the lead blocks directly above the

telescope.   The nuclear interactions in the lead cause an

increase in the number of particles and so effectively
increase the geometric factor of the telescope, making the
measured flux greater than otherwise expected.

In Fig. 4.2 is shown the counting rate in the proton
channel as a function of atmospheric depth. This measures
a combination of protons, helium nuclei and mesons, the
relative proportions varying with altitude. This flux is
absorbed with an absorption length of $\sim$ 250 gm/cm^2. The
constituents of the total rate are shown, the helium flux
and the proton flux being absorbed with characteristic
lengths of 50 gm/cm^2 and 150 gm/cm^2. The difference bet-
ween the total rate and these two is due mainly to mesons.

On all but one of the flights, the proton counting
rate remained constant whilst at altitude. The detector
flown in 1967 from Cardington was carried off at $\sim$ 100 m.p.h.
due east as shown in Fig. 3.3. Also shown are contours
of constant geomagnetic cut-off. During the flight, the
cut-off changed from 2.5 to 3.5 Gv. The temperature var-
iations were less than 15°C and the pressure altitude only
changed from 3.6 to 3.9 mb in the first 4 hours at altitude.
The change in counting rate during the flight is shown in
Fig. 4.3 and compared with the other flights. During this
time, the proton rate decreased to 60% of its original value.
This change is due solely to the change in cut-off rigidity.

Flight	1967-C	1967-K	1968-K1	1968-K2
Total flux in proton channel	1090	1900	1740	1630
Helium flux at top of atmosphere	65	139	128	131
Helium correction	62	132	122	124
Proton flux at floating altitude	1028	1768	1618	1508
Proton flux at top of atmosphere	1056	1810	1660	1550

Units of p/m^2.sec.ster.

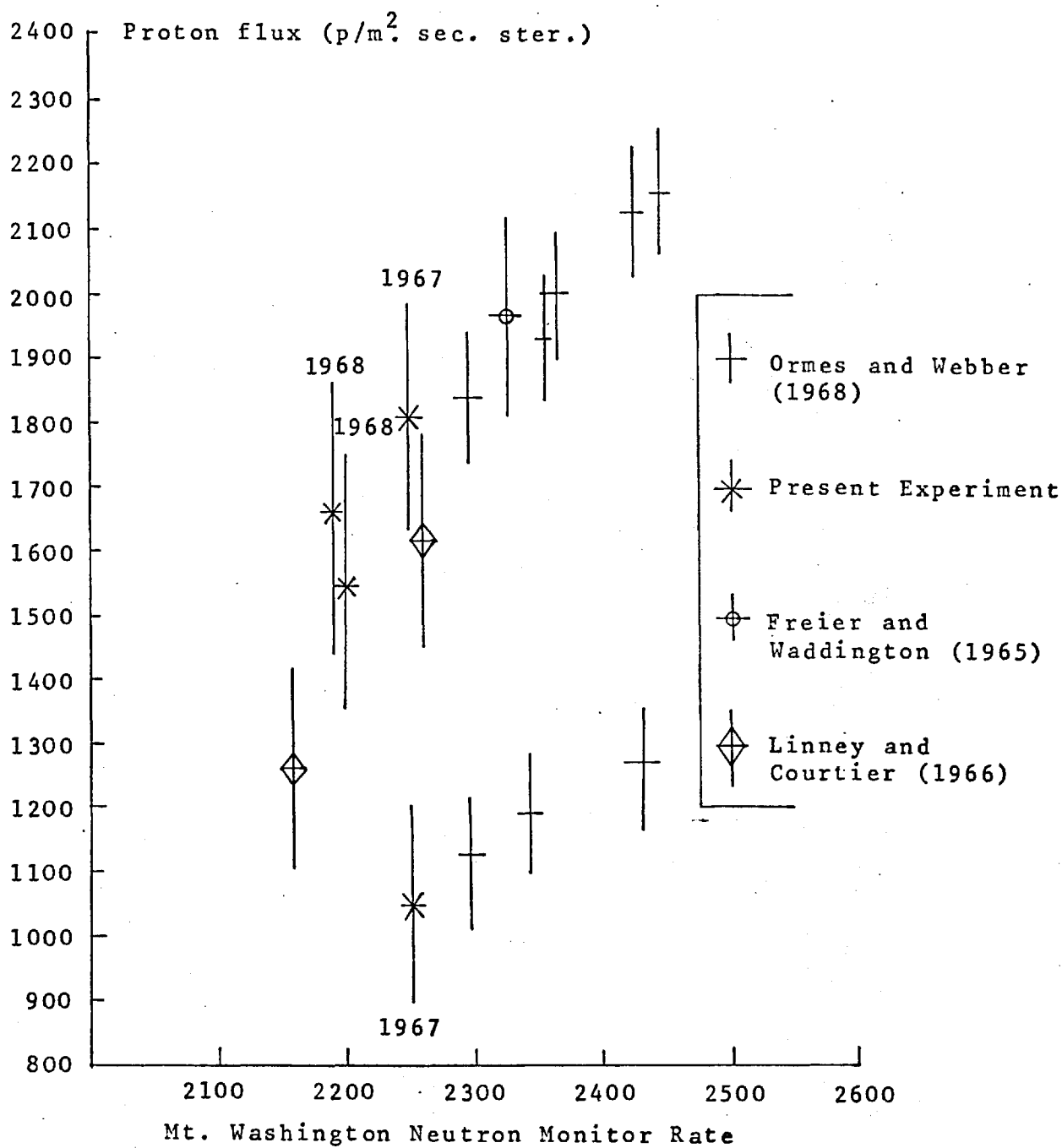Table 4.1. Table of Proton fluxes.

Fig. 4.1.   Regression Plot of Integral Proton Intensity
(>1 Gev) and (>1.7 Gev).
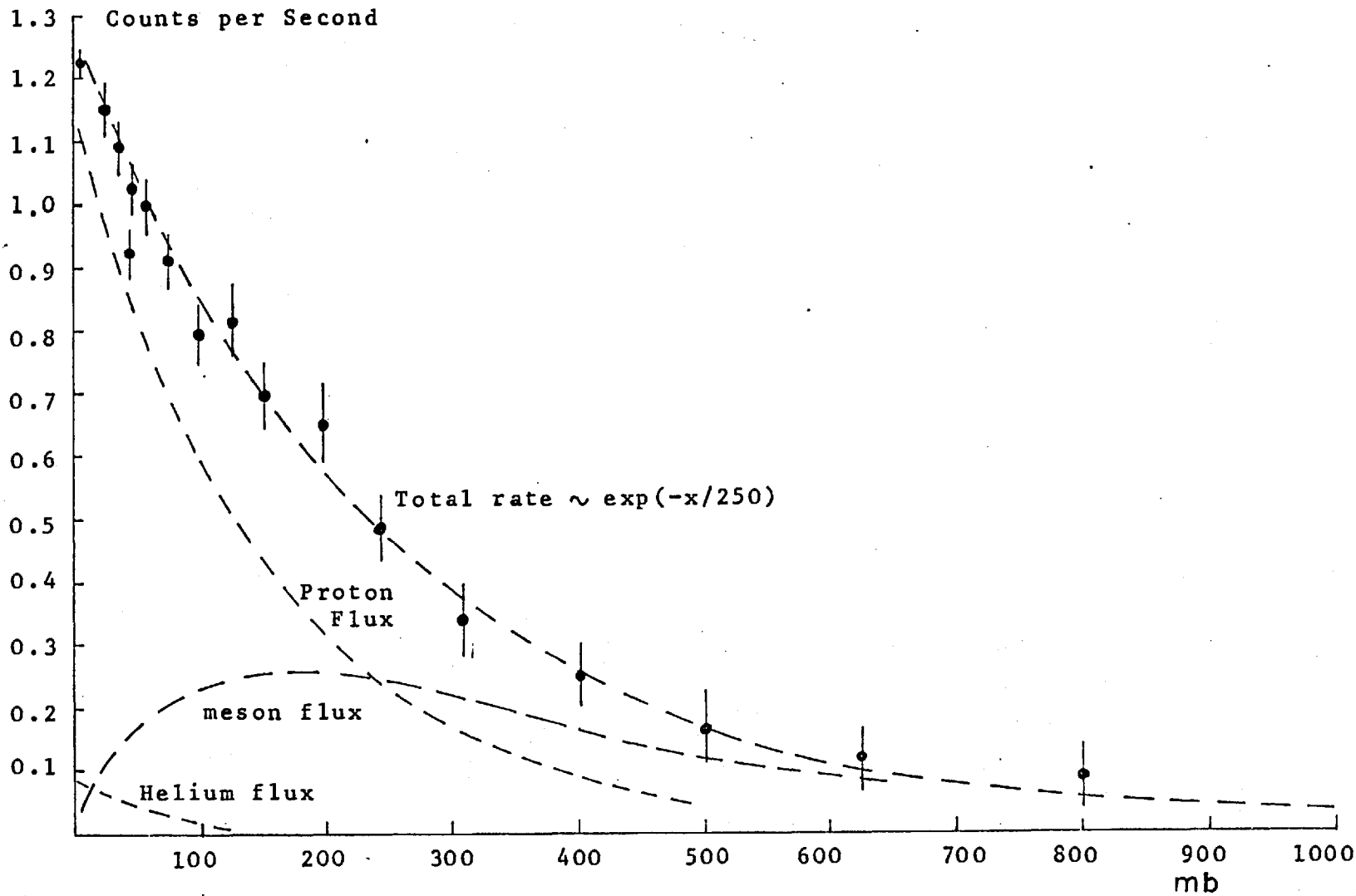
Fig. 4.2.   Proton Channel Counting Rate vs Altitude.
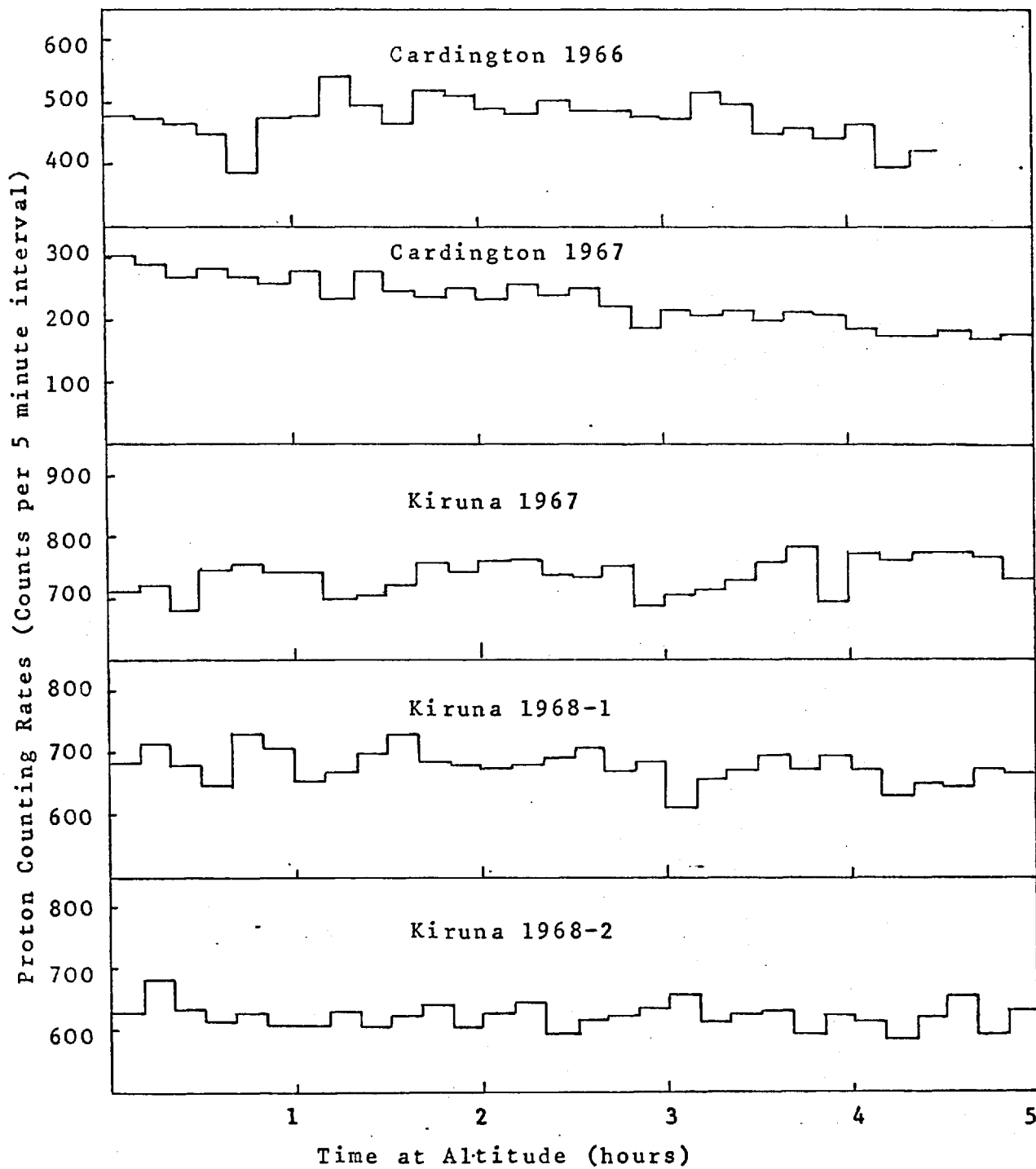
Fig. 4.3.   Proton Counting Rates at Altitude.

CHAPTER V

THE   ELECTRON   MEASUREMENTS

The two electron channels measure the electron flux
at the top of the detector, within an opening angle of 22°,
and with a detection efficiency as shown in Figs 2.8 and
2.9, which takes into account the telescope material as well
as the lead-scintillator sandwich response.   The low energy
channel measures from 15-250 Mev.   The high energy channel
from 250-500 Mev.   Due to the straggling nature of the
electrons, the energy response is poor, and account of this
must be taken in determining the fluxes and spectra.

5.1   Balloon flights from Cardington

(i)   1966 Flight

The purpose of this flight was to measure the upward going
flux of electrons at Cardington.   The detector was flown
inverted, downward moving particles being rejected by
blackening on the surface of the cerenkov disc on the 5"
photomultiplier tube.

Protons and heavier particles, incident upon the top
of the atmosphere at large zenith angles, and with suffic-
iently high energy can produce π -mesons moving in an

upward direction.   The subsequent decay of the mesons,

by the processes:-

$$\pi^{\pm} \longrightarrow \mu^{\pm} + \nu \; , \qquad \mu^{\pm} \longrightarrow e^{\pm} + 2\nu,$$

$$\pi^{0} \longrightarrow 2\gamma \qquad , \qquad \gamma \longrightarrow e^{+} + e^{-}.$$
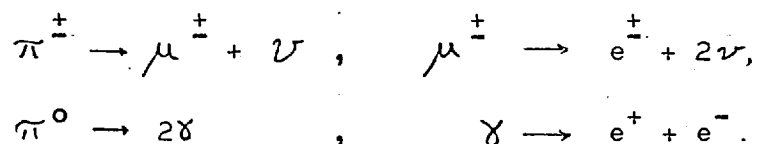
produces high energy electrons in directions which are

substantially the same as the original meson.   The flux

is produced in a large layer of atmosphere below the det-

ector, and will not vary significantly with altitude near

the top of the atmosphere.   The flux of these 'splash'

albedo electrons leaving the atmosphere will be almost

identical to the flux measured at floating altitude.   The

counting rate variations with atmospheric depth are shown

in Fig. 5.1, together with an extrapolation to the top of

the atmosphere.   The measured flux of electrons requires

corrections for interactions of protons in the lead blocks,

amounting to 6.5% and 2.8% of the proton flux for the high

energy and low energy electron channels respectively.

The fluxes of upward going electrons at the top of the

atmosphere are shown in Table 5.1.

(ii) 1967 Flight

The purpose of this flight was to investigate the growth

of the atmospheric secondary electrons in the upper atmosphere

without any contribution from the primary electron flux.
The geomagnetic threshold rigidity at Cardington is 2.5 Gv
which prevents primary electrons in the energy range of the
detector from having access to the top of the atmosphere.
In place of the primary flux is the re-entrant albedo flux,
caused by upward going electrons at the conjugate point to
Cardington (lat. - 45.4°, long. 26.7°)in the Southern hemi-
sphere) with rigidities less than the threshold being guided
via the field lines to re-enter at the top of the atmosphere
at Cardington.

The counting rate of the detector contains the follow-
ing contributions:-

(a) Re-entrant albedo electrons, absorbed in the
atmosphere, with absorption length L_e.

(b) Secondary electrons, produced in the atmosphere
from interactions with protons with a growth
curve described by:-

$$A \times (\text{depth}) + B \times (\text{depth})^2$$

(c) Contributions from interactions in the lead,
which are proportional to the proton flux.
The proton flux is absorbed with an absorption
length L_p.

The measured flux in the electron channels can be described by

$$J = R_e e^{\frac{-x}{L_e}} + Ax + Bx^2 + I.P_o.e^{\frac{-x}{L_p}}$$

where R_e is the re-entrant electron flux at the top of the atmosphere, A and B are constants describing the growth of the secondary electrons, I is the fraction of protons interacting and appearing as electrons, P_o the flux of protons at the top of the atmosphere and x the atmospheric depth. If only the first few gms/cm^2 of atmosphere are considered, then

$$J = (R_e + I.P_o) + (A - \frac{R_e}{L_e} - \frac{I.P}{L_p})x$$

which is a linear function of atmospheric depth, x. Extrapolation to the top of the atmosphere gives the re-entrant flux plus the contribution due to interactions in the lead. The depth curves of the electron fluxes, corrected for the interactions in the lead are shown in Fig. 5.2, together with an extrapolation to the top of the atmosphere. The re-entrant fluxes at the top of the atmosphere are given in Table 5.1.

5.2   Balloon Flights from Kiruna

One flight was made in 1967 and two in 1968 to
investigate the primary electrons at the top of the atmo-
sphere at Kiruna.   The flight in 1967 was made at a time
when the sun was quiet, whilst the 1968 flights were made
following a period of intense solar activity.   Enhanced
electron fluxes were observed in the low energy channels
during both 1968 flights.   The counting rates of the
detector as a function of atmospheric depth are shown in
Fig. 5.3 and 5.4. for the Kiruna flights.   In this case,
the measured flux is given by:

$$J = J_e \, e^{\frac{-x}{L_e}} + Ax + Bx^2 + I.P_o \, e^{\frac{-x}{L_p}}$$

where J_e is the primary electron flux at the top of the
atmosphere.   A linear extrapolation of the curves in the
top few gm/cm^2 of atmosphere give the primary fluxes for
the various flights.   These are given in Table 5.1.

5.3   Derivation of Spectra from Fluxes

Derivation of a spectrum is difficult with the two
channels available, due to the large energy limits.   The
ideal response would have channels sufficiently narrow so

that the magnitude of the differential flux remains con-
stant across each channel.   With wide channels, the count-
ing rate varies with the slope as well as the magnitude of
the differential spectrum.   To investigate how the counting
rate varies with the slope of the differential electron
spectrum, the counting rate of the detector was calculated
for an energy spectrum $\propto E^{-\gamma}$.   The counting rate is
given by:

$$\text{counting rate} = \int_{E_{MIN}}^{E_{MAX}} \eta\,(E) \cdot E^{-\gamma}\ dE$$

where $\eta\,(E)$ is the energy response of the electron channel
as shown in Figs 2.8 and 2.9, E the electron energy and
the slope of the power law spectrum.   From this, the
spectrum $AE^{-\gamma}$ was found which gives a counting rate of
1 p/m^2 sec. ster., for various values of γ , assuming a
100% efficient telescope.   These spectra are shown plotted
in Fig. 5.5 and show a region where the counting
rate is virtually independent of γ .   These points are
taken as the centre of each channel, and occur at 62 Mev,
where a differential flux of $(6.0 \pm 0.5) \times 10^{-3}$ p/m^2 sec. ster.
Mev. gives a counting rate of 1 p/m^2 sec. ster., and at
330 Mev, where the corresponding differential flux is

$(1.92 \pm 0.5) \times 10^{-3}$ p/m^2 sec. ster. Mev.   These values
are used in converting the counting rates of each channel
into differential fluxes, and are independent of the slope
of the spectrum.   Using this method, the primary electron
differential fluxes at Kiruna were derived, and are shown
in Table 5.2.

5.4   Spectra of Splash and Re-Entrant Albedo

The differential fluxes of the splash and albedo
electrons at Cardington were derived using the above method.
In order to compare the two measurements, it is necessary
to investigate the connection between splash and albedo
electrons.   The first assumption is that the upward going
flux at the top of the atmosphere at the conjugate point
is the same as the upward going flux at Cardington.   This
assumption is quite valid, since the upward going electrons
are produced by primaries with energies much greater than
cut-off, and so are not a function of latitude.   The
second assumption is that the upward going electrons in the
southern hemisphere at the conjugate point will return to
Cardington.   For the low energy electrons this assumption
is valid, since then the electrons can follow the field
lines.   The assumption is not valid for the higher energy

electrons since they cannot follow the field times so easily.
However, it is possible for electrons which were upward
going at some other point in the southern hemisphere to
re-enter at Cardington. Energy losses from the top of
the atmosphere and back again are negligible due to the
small amount of matter encountered.

The measurement of the splash and re-entrant flux
shows no significant difference in the high energy channel.
There is a significant difference in the low energy flux,
which is due to the change in energy in extrapolation to
the top of the atmosphere. Due to ionisation and brem-
sstrahlung losses, the upward going 15-250 Mev electrons
become 8-225 Mev at the top of the atmosphere, whilst the
downward going electrons are due to 23-280 Mev electrons.
The differential fluxes are shown in Fig. 5.6, together with
measurements of other workers. The fluxes are also given
in Table 5.2.

5.5   Secondary Corrections

All the electron fluxes at the top of the atmosphere
are derived using the assumption that a linear extrapolation
to the top of the atmosphere is valid. The counting rate
of the electron channel, after correction for interactions

in the lead has the form:

$$J = J_e \, e^{\frac{-x}{L_e}} + Ax + Bx^2$$

$$= J_e \left(1 - \frac{x}{L_e} + \frac{x^2}{L_e} \cdots \right) + Ax + Bx^2$$

Using the values $L_e = 50 \text{ gm/cm}^2$, and $A = 10 \text{ p/m}^2$ sec. ster. $\text{gm}^{-1}\text{cm}^2$, $B = \frac{1}{50} \text{ p/m}^2$ sec. ster. $\text{gm}^{-2}\text{cm}^4$, as in the calculations of Verma (1967b) and using a primary electron flux of 100 p/m^2 sec. ster., a function was derived to represent the electrons in the atmosphere. A linear extrapolation should result in a primary flux of 100 p/m^2 sec. ster. if such an extrapolation is valid. However, due to the curvature of this function, the extrapolation to the top of the atmosphere gives a primary flux of 110 p/m^2 sec. ster. using the first 60 gm/cm^2 of the atmosphere. Thus, if the growth of the secondary electrons is as predicted by Verma, the linear extrapolation of the depth curves gives an error of approximately 10% in the primary flux value.

To see how well the measured growth curves and the theoretical estimates agree, the counting rates of the detector at various depths in the atmosphere were calculated from the theoretical spectra of Verma, and of Perola and Scarsi (1966) using:

$$C = \int_{E_{MIN}}^{E_{MAX}} \eta'(E)\, S(E)\, dE$$

where $\eta'(E)$ is the energy response of the electron
channel, taking into account the telescope efficiency, and
S(E) the secondary electron spectrum, and C the expected
counting rate.

The expected counting rates as a function of depth
are shown in Fig. 5.7. Also shown is an estimate of
secondary electrons measured in 1967, derived by subtract-
ing $J_e\, e^{\frac{-x}{L_e}}$ from the measured depth curve. The discrepancy
between the two calculated secondary counting rates at
floating altitude is sufficient to show that calculation
alone is inadequate for correction of secondary fluxes.

Date	23.9.66	8.11.67	11.8.67	18.7.68	24.7.68
Location	Cardington	Cardington	Kiruna	Kiruna	Kiruna
High energy flux	20.6±6.5	upper limit 13.0	24.4±3.0	11.9±2.5	21.6±3.0
Low energy flux	93.5±8.0	44.0±10.0	86.7±4.0	532.0±10.0	282.0±7.0

Units of p/m^2.sec.ster.

Table 5.1. Table of Electron fluxes

Date	23.9.66	8.11.67	11.8.67	18.7.68	24.7.68
Location	Cardington	Cardington	Kiruna	Kiruna	Kiruna
High energy flux	0.04 ±0.01	upper limit 0.025	0.047 ±.01	0.023 ±.005	0.042 ±.01
Low energy flux	0.56 ±0.05	0.26 ±0.1	0.52 ±.05	3.2 ±0.4	1.69 ±0.2

Units of p/m^2.sec.ster.Mev.

Table 5.2. Table of Differential Electron fluxes.
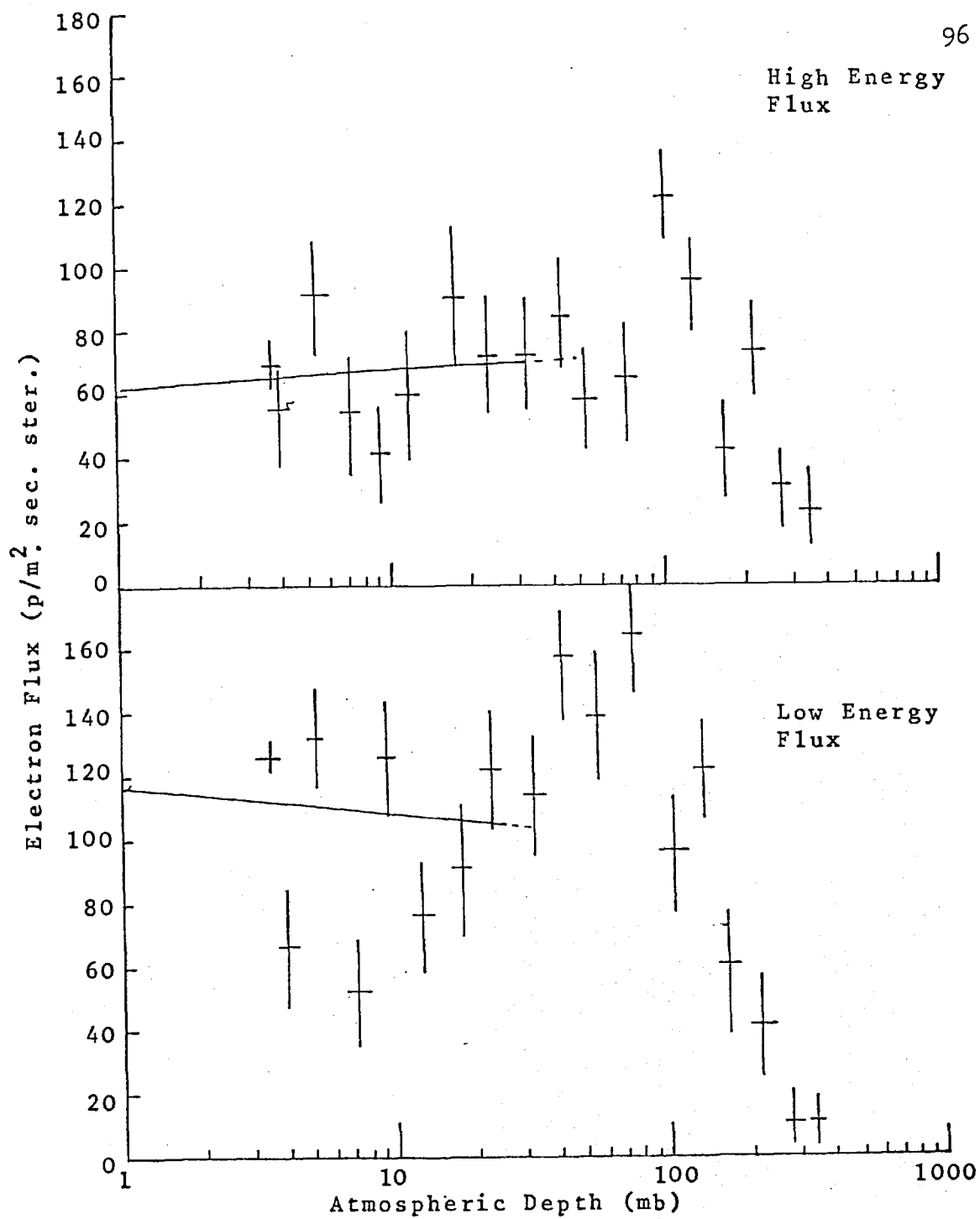
Fig.5.1   1966 Cardington Flight. Counting rate of
Electron channel.   Upward going Electrons
Plus interacting Protons.
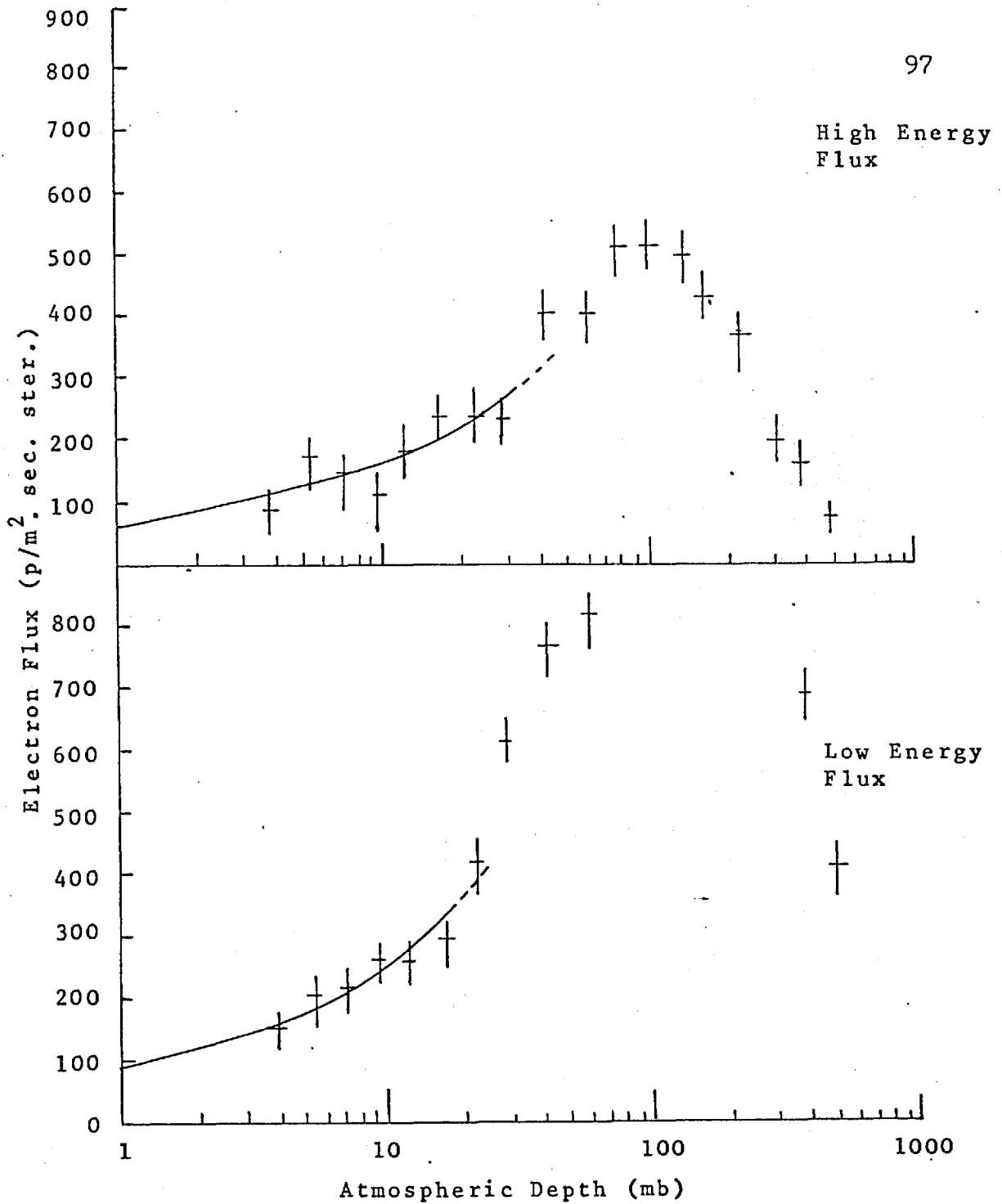
Fig. 5.2. 1967 Cardington Flight.   Downward going
Electrons.   Variation of Electron Flux with
Atmospheric Depth.
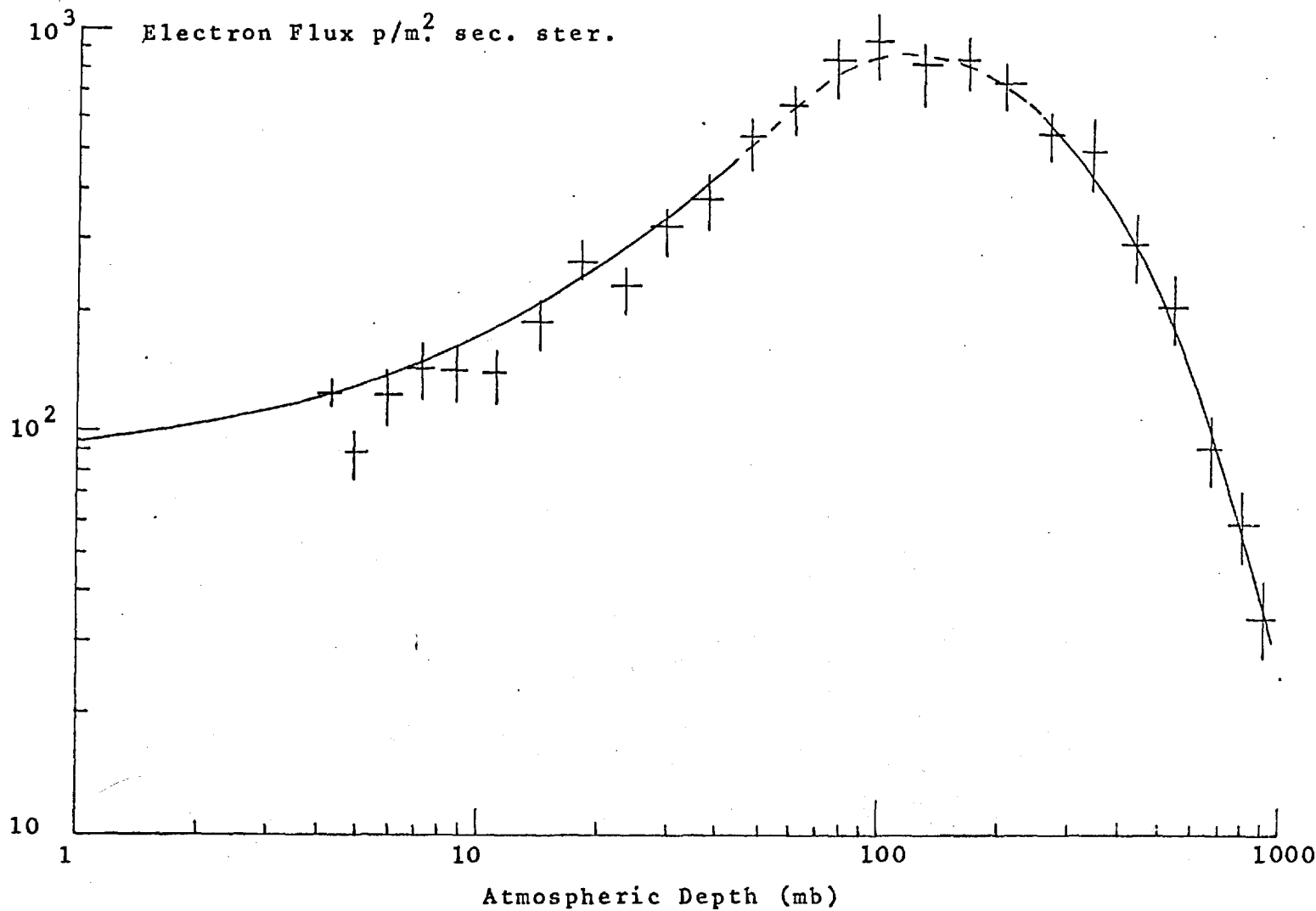
Fig. 5.3a.   1967 Kiruna Flight.   Low Energy Electrons.   Variation of
Electron Flux with Atmospheric Depth.
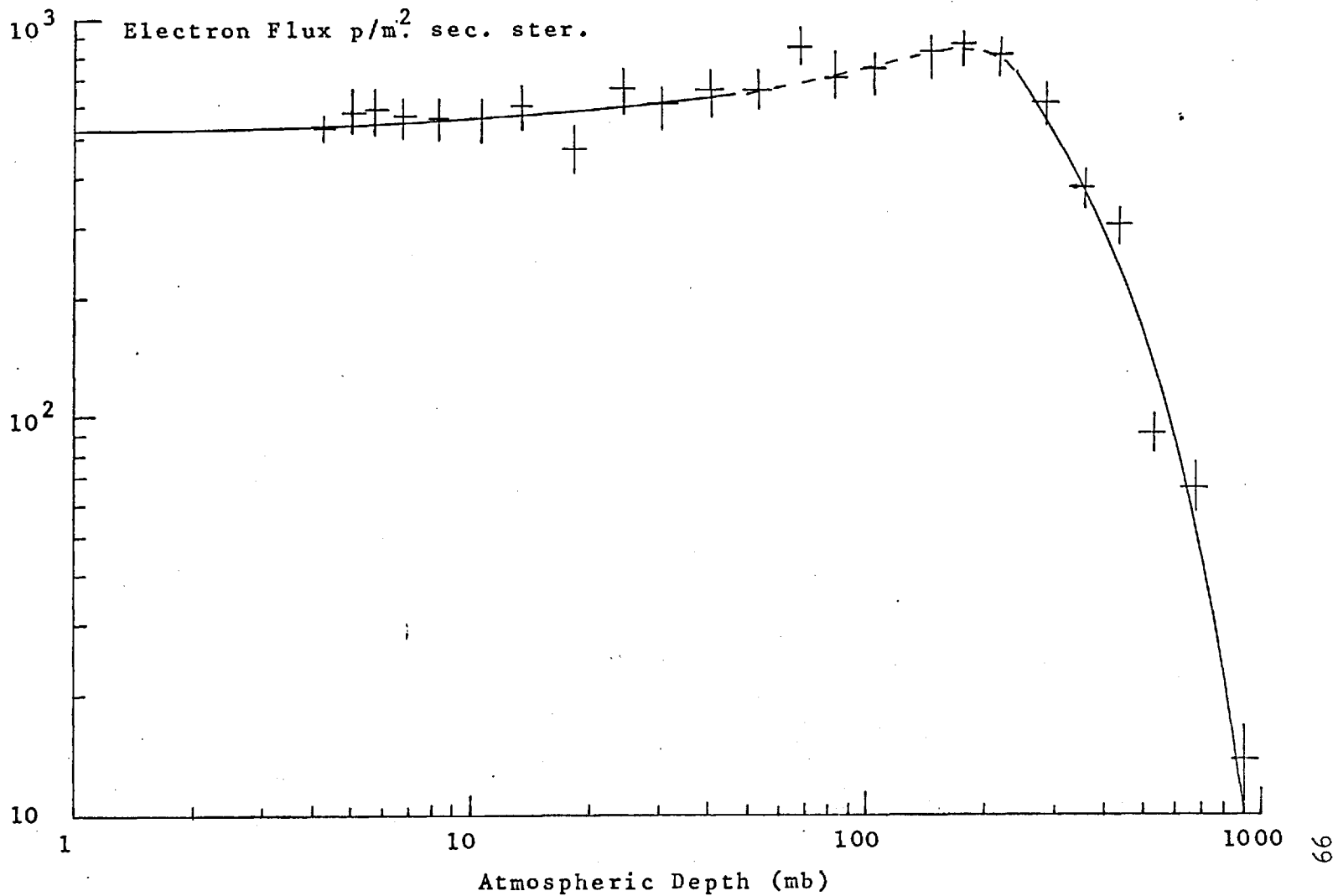
Fig. 5.3b.   1968-1 Kiruna Flight.   Low Energy Electrons.   Variation of
Electron Flux with Atmospheric Depth.
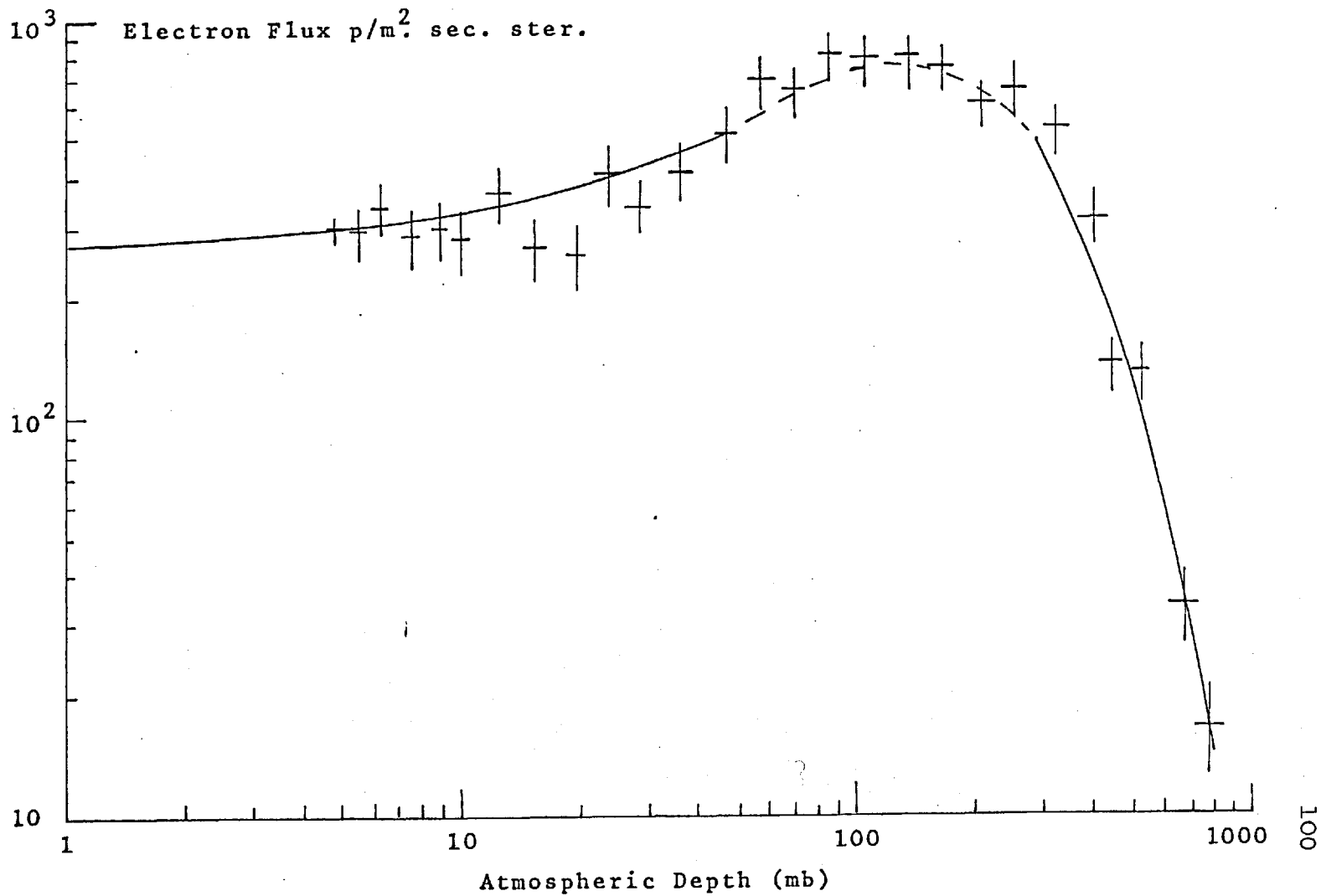
Fig. 5.3c.   1968-2 Kiruna Flight.   Low Energy Electrons   Variation of
Electron Flux with Atmospheric Depth,
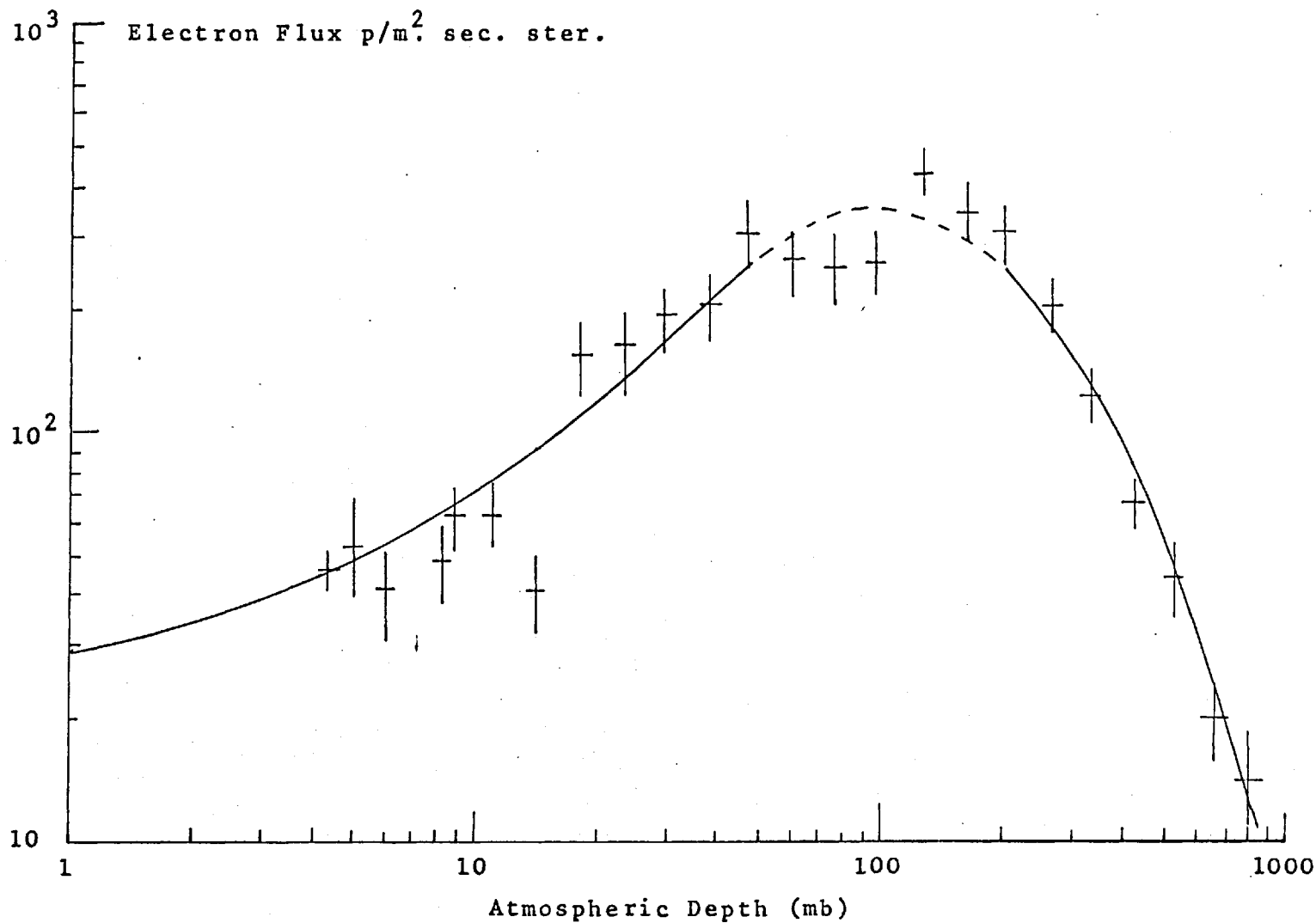
Fig. 5.4a.   1967 Kiruna Flight.   High Energy Electrons.   Variation of
Electron Flux with Atmospheric Depth.
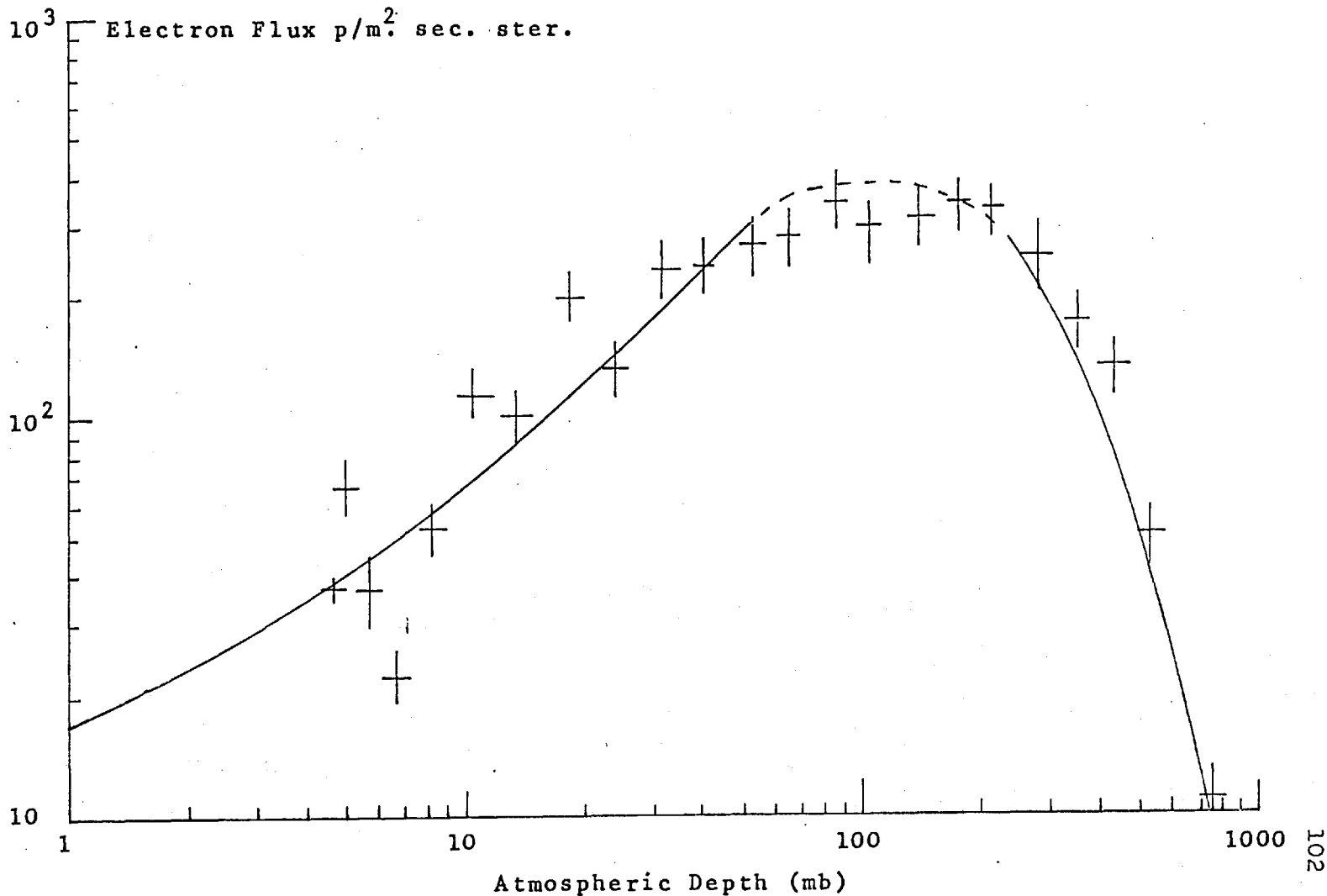
Fig. 5.4b.   1968-1 Kiruna Flight.   High Energy Electrons.   Variation of
Electron Flux with Atmospheric Depth.
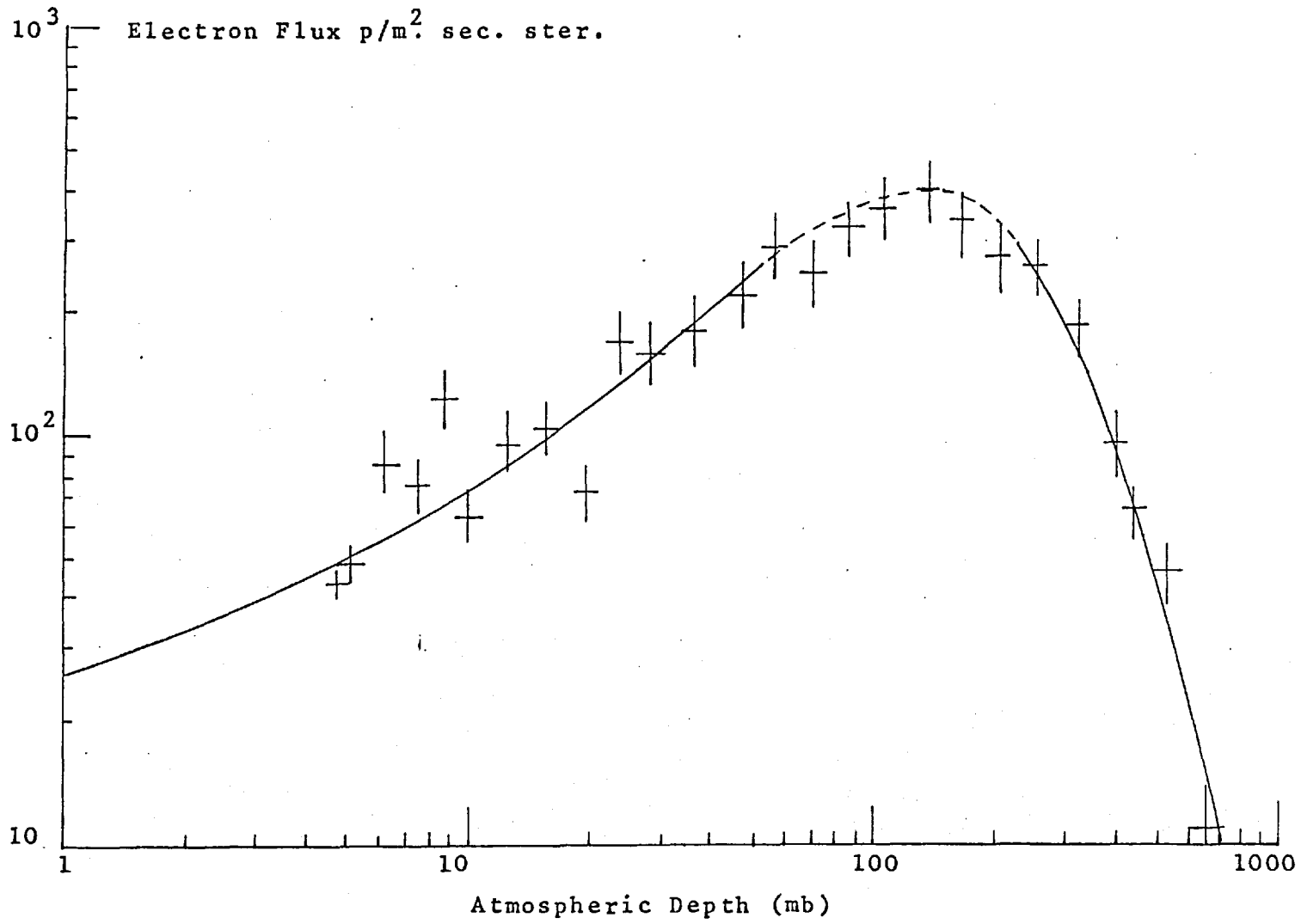
Fig. 5.4c.   1968-2 Kiruna Flight.   High Energy Electrons.   Variation of
Electron Flux with Atmospheric Depth.
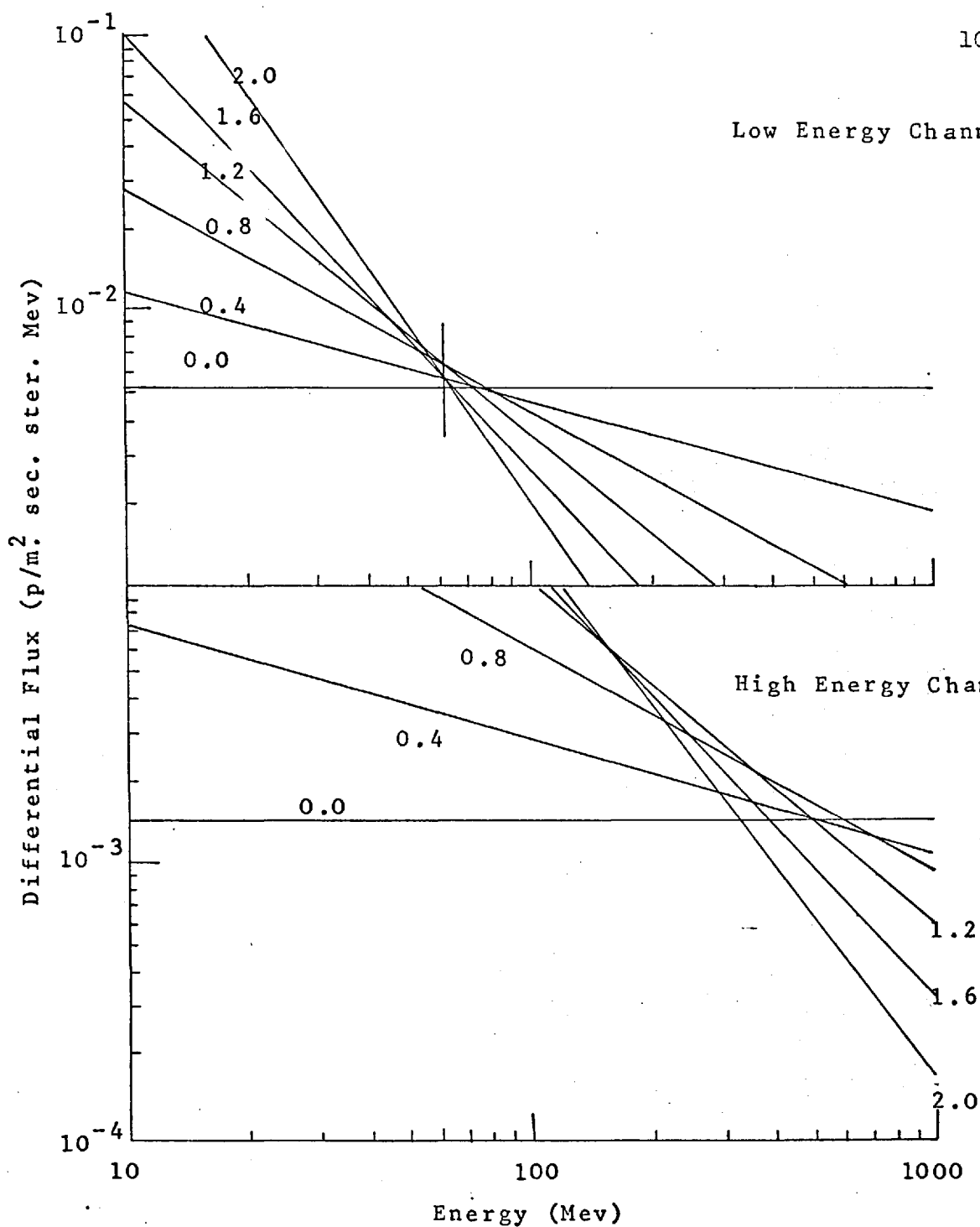
Fig. 5.5.   Spectra which give a Counting Rate of
1 p/m² sec. ster. in Electron Channels
for various values of γ.
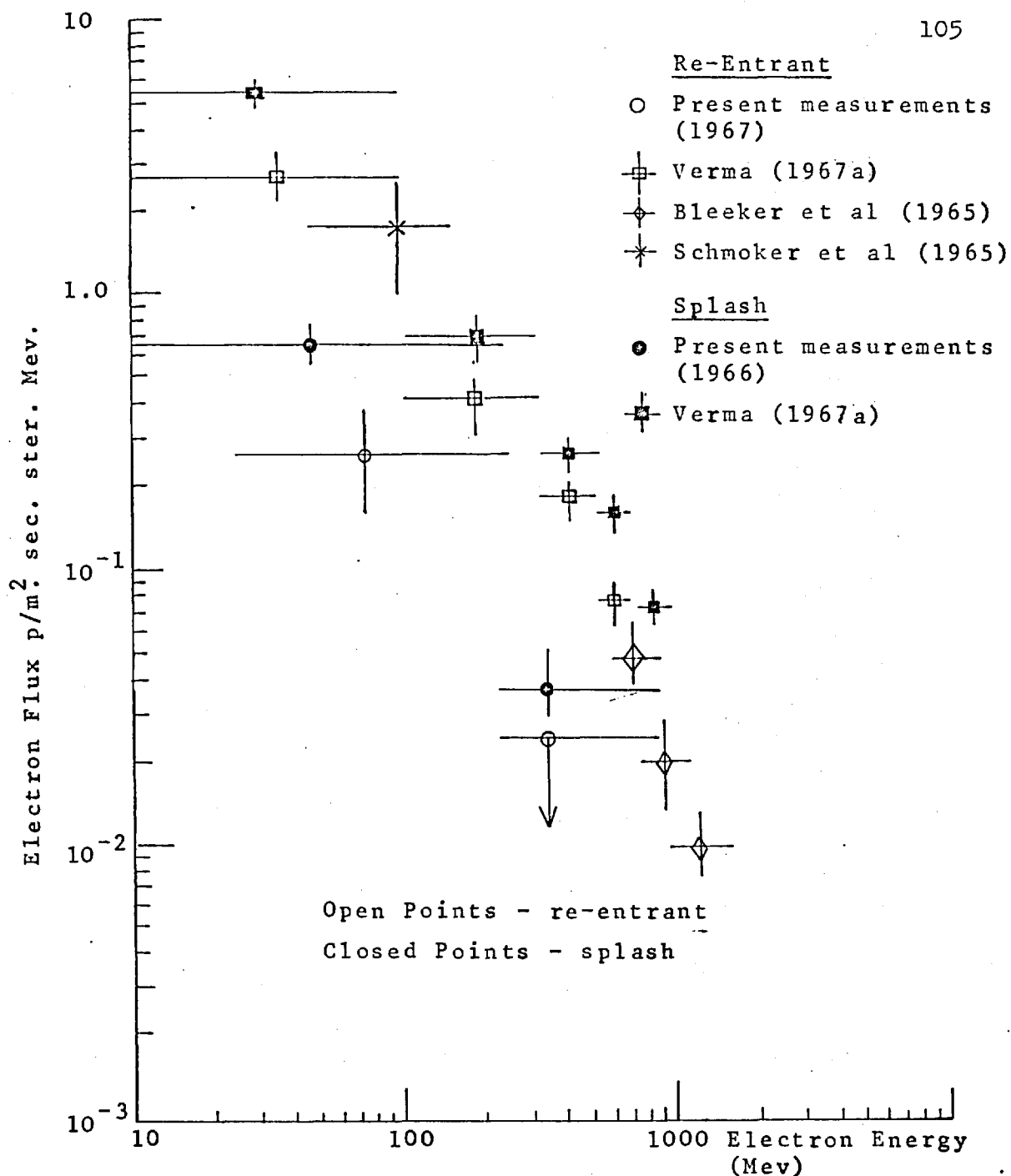
Fig. 5.6.   Re-Entrant and Splash Albedo Electron Spectra.
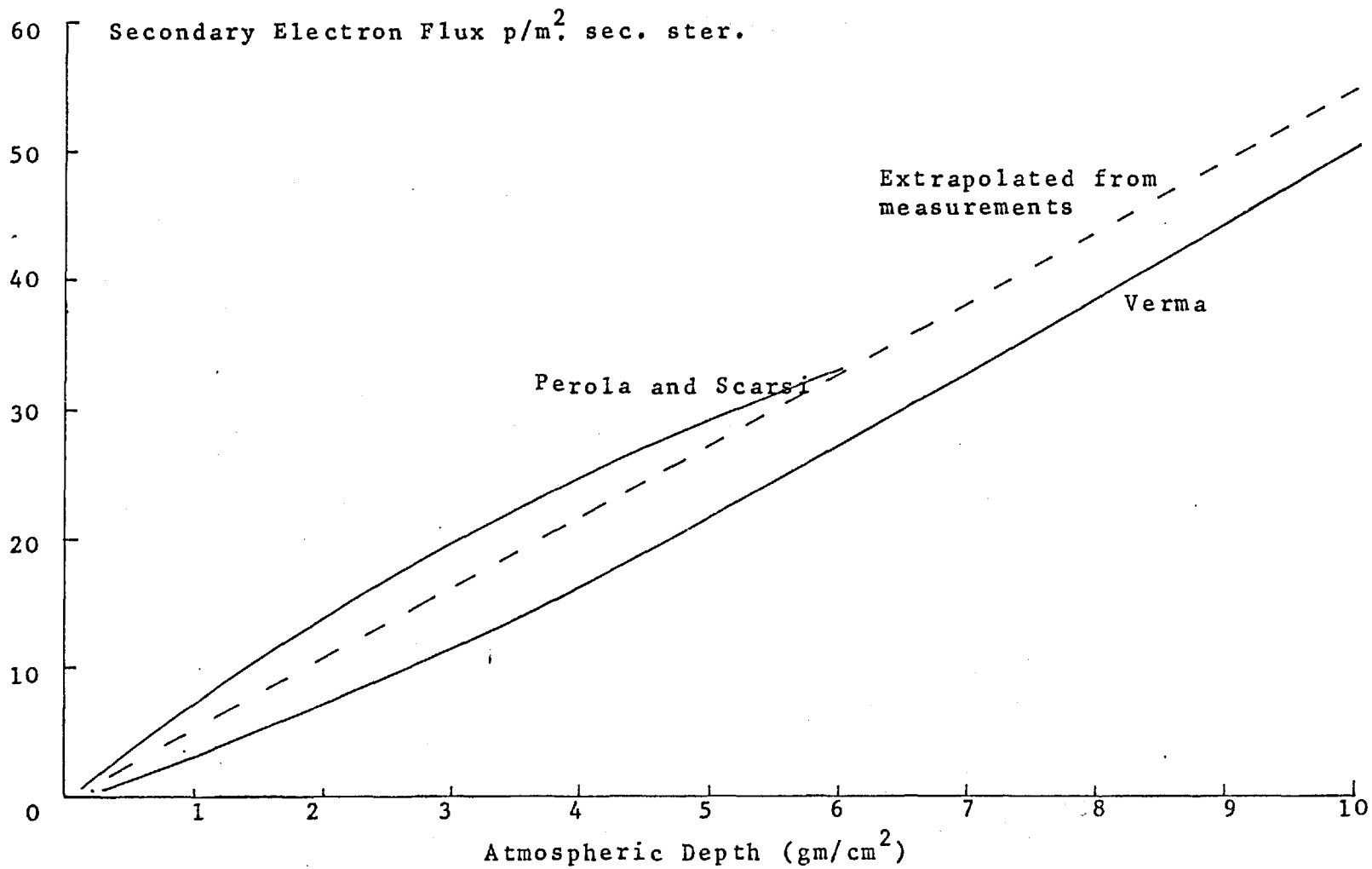
Fig. 5.7. Comparison of Extrapolated Secondary Flux with Calculated Secondary Flux (Verma, Perola and Scarsi) in High Energy Channel.

CHAPTER VI

DISCUSSION

6.1 Solar Electrons

The measurements taken in 1968 were affected by intense
solar activity in the few days before the flights.   The
flights were made on the 18th and the 24th of July, and
class 2B flares were observed on the 6th, 9th and the 12th,
and a class 3B flare on the 8th.   X-ray emissions were
observed on most of the days from the 6th until the 14th,
the two largest X-ray events coinciding with the 2B flare
on the 6th and the 3B flare on the 8th.   Associated with
each of these were solar protons, which were monitored
approximately 5-7 hours later on Pioneer 34.   Type IV
radio emission accompanied these two events, and also the
event of the 12th July.   The solar flares were produced
from a complex sunspot group which appeared on the east
limb on the 5th July, and disappeared on the west limb on
the 18th.   The solar proton flux was enhanced throughout
the period from the 6th until the 17th, and as well as the
two events correlated with the solar flares, an increase
in proton flux was observed on the 13th July, when the
sunspot group was at approximately W20.   A large Forbush
decrease began on the 11th, and was enhanced by a further

decrease on the 13th. The relevant data are summarized
in Fig. 6.1.

Together with all this activity, low energy electrons
were observed on both flights, with fluxes 8 times and 3
times the background level for the 1st and 2nd flights
respectively. In the high energy channel, the flux during
the first flight was depressed to approximately 50% of the
flux measured in 1967, and during the second flight it was
essentially the same as in 1967. The high energy flux
followed the same shape of the Forbush decrease seen in the
neutron monitor records, from which it can be deduced that
most of the high energy electrons are of galactic origin,.
whilst most of the low energy electrons are solar. Solar
electrons were observed on satellite detectors from the
class 3B flare (Meyer, 1969; Cline, 1969) lasting for some
days after the flare. The electron flux was still above
normal at the time of the first balloon flight (Cline, 1969;
Datlowe et al, 1969).

Similar effects have been seen in balloon flights by
Meyer and Vogt in 1960 and 1961. Observations on the IMP
series of satellites (Cline and McDonald, 1968) have revealed
several solar electron events associated with large solar
flares, and observations of very low energy electrons
(Anderson and Lin, 1966) have revealed electron fluxes

associated with many of the smaller flares.

The presence of solar electrons from solar flares is now a well established fact. During the period of activity described above, the solar electrons correlate well with the presence of X-ray emission and type IV radio emission on the 6th of July. The emissions occur during the initial phase of the flare before the maximum is reached and correspond to bremsstrahlung and synchrotron radiation of electrons in the sunspot regions.

Observations of Anderson and Lin (1966) show that a considerable anisotropy exists in the streams of low energy electrons coming from the sun, suggesting that the electrons travel directly along the field lines in interplanetary space, with very little scattering. Anderson (1969) also found that most prompt events occurred on the west limb of the sun, where field lines provide direct access to the earth. Those occurring on the east limb were usually associated with some type I radio noise coming from a large portion of the disc, where the electrons are stored before being released into space. The electrons cannot be stored in interplanetary regions, otherwise the anisotropy would not be observed, nor can they be stored in the sunspot region, because in that region their lifetime would be extremely short, due to energy losses by synchrotron radiation.

The solar corona is the only other region available for long term storage of electrons. The events of the 6th of July must have involved this storage mechanism to have been seen near the earth. The increase in both electron and proton fluxes occurring between the 13th and 14th, and not associated with any flare, but when the position of the sunspot group was W20-40 must be due to direct connection of the storage regions via the interplanetary field lines to the earth. This storage is still evident in the measurement at Kiruna on the 18th and 24th July. During the flight of the 18th, the sunspot group was on the east limb, and during the flight of the 24th, the group had gone on to the invisible side of the sun.

Models for electron storage have been proposed by Axford (1965) and Schatten, Ness and Wilcox (1968). The model of Axford suggests a storage system with a diffusing layer small compared with the radius of the sun, so that an east-west effect will still be present. The model of Schatten, Ness and Wilcox has a source surface $\sim 0.6\ R_o$ above the photosphere, and within it closed field lines. This surface is the beginning of the interplanetary field lines. Particles can diffuse within this surface, and then leak out of the surface and so be guided along the field lines to the earth.

Conclusions

The 1968 results of the low energy flux show consider-
able increases above the 1967 level. These increases are
well correlated with the intense solar activity before the
flights, and show enhanced fluxes for some days after the
solar activity. These effects are also seen on satellites
which were measuring electrons at the same time. These
observations are consistent with some sort of storage mech-
anism above the solar surface.

6.2 Modulation Effects

Three sets of measurements are available of the electron
flux at Kiruna between 1967 and 1968, during which time
the Mt. Washington neutron monitor changed by $\sim$ 3%. Of
these measurements, only the high electron channel can be
used in discussing the modulation, because of the presence
of solar electrons in the low energy channel. Any conclu-
sions drawn about the modulation can have little statistical
weight due to the small amount of relative modulation
between 1967 and 1968.

Not all the changes in the high energy channel are due
to modulation effects. During the first flight of 1968,
the high energy flux was depressed by a Forbush decrease,
and because of this, there cannot have been many solar

electrons in this channel.   So, when the neutron monitor
returned to normal, it is reasonable to assume that there
were no solar electrons in the high energy channel.   The
flights of 1967 and the second of 1968 can thus be compared
for modulation effects, whilst the two of 1968 can be com-
pared for effects of a Forbush decrease.

When comparing the flights for modulation effects, a
neutron monitor change of 3% corresponds to a measured
electron change of 12%.   Since this is less than three
standard deviations of the measurement accuracy, it can
only be used as an upper limit to the modulation.   This
upper limit is consistent with both the results of Rockstroh
and Webber (1969) and L'Heureux et al (1967).

The Forbush decrease before the 1968 flights reduced
the neutron monitor rate by ∼ 5%.   The corresponding
electron flux, seen later in the decrease was approximately
60% lower than the level measured after the decrease.
The ratio of electron flux decrease to neutron monitor
decrease measured on the 18th July is apparently much
greater than for the case of the long term modulation.

Two factors affect this ratio during a Forbush decrease.
First, the recovery rate of high rigidity particles is
quicker than that of low rigidity particles. .Analysis
of neutron monitor data (Kitamura and Kodama, 1959) shows

that high rigidity ($\sim$ 10-20 Gv) protons recover with an exponential rate with a characteristic time of approximately two to three days, whilst low rigidity protons ($\sim$ 1 Gv) recover with a characteristic time of 6-7 days. The second factor affecting the ratio is the size of the region which is producing the Forbush decrease. If this is of a similar order to the Larmor radius of the high rigidity protons, then it is possible that their attenuation in the decrease will not be so great. Both of these factors help to make the ratio of the electron decrease to the neutron monitor decrease larger than that expected on the basis of a mechanism similar to that producing the long term modulation.

The fact that a considerable decrease of the electron flux has been observed during the Forbush decrease stregthens the argument that the electron component has a large modulation, of similar size to the proton modulation, expecially if the same mechanism is producing the Forbush decrease. This large amount of modulation is consistent with the works of Ramaty and Lingenfelter (1968); Anand et al (1968a); and Webber (1967).

Conclusions

(i) An upper limit to the amount of modulation present
between 1967 and 1968 has been set at 12%, which is con-
sistent with the measurement of many other workers.
This amount of modulation is also consistent with a res-
idual and a rigidity dependant modulation.

(ii) A depression of the electron flux, observed at the
same time as a Forbush decrease, although of different
magnitude to the relative modulation effects, is not
inconsistent with the same mechanism being responsible
for both the long term and short term electron modulation.

6.3 The Primary Electron Flux

The exact value of the cut-off at Kiruna is of great
importance in the measurement of primary electrons.   The
cut-off due to the internal field alone is 500 Mv, but
with the effects mentioned in Section 1.3, a more realistic
value is ∼ 50 Mv.   The threshold for detection in the
low energy channel is 15 Mev, which in turn implies an
electron energy of ∼ 20 Mev at the top of the atmosphere.
It is possible that some overlap exists such that re-entrant
albedo electrons appear in the low energy channel.
Because of the change of cut-off rigidity due to the effects
of the magnetosphere at locations within 65°-70° geomagnetic

latitude, it should be possible to detect a diurnal varia-
tion in the electron fluxes, with a change taking place at
around 6 a.m. and 6 p.m. local time.   The only flight to
cover both of these times was the second one in 1968, but
during this flight, no significant changes were seen, and
the fluxes were enhanced due to solar electrons, making
it difficult to see such an effect.   The 1967 flight is
the only one in which the effect should be seen.   The
detector reached altitude at 1 a.m. and sent back inform-
ation until 8 a.m. L.T..   During this time, no significant
increase was seen.   From this can be drawn two alternatives.
Either, the transition from day to night conditions is so
slow that even at 8 a.m., the effects are not apparent, or
the reduction in cut-off value is not sufficient to exclude
completely all the re-entrant albedo electrons from the
measurements.   The second alternative cannot be ruled
out, since the location of Kiruna is only just with the
$65^{o}-70^{o}$ latitude region where these effects take place,
and also measurements of other workers at higher latitudes
have revealed cut-offs of $\sim$ 20 Mv..   So, it is reasonable
to expect the cut-off at Kiruna to be higher than this.

Using the response curves of the detector, and the
method outlined in Section 5.3, the differential fluxes
for the 1967 flight were calculated.   The energy limits

and mean energy for the channels have been corrected for

bremsstrahlung and ionisation losses in the few gm/cm^2

of atmosphere above the detector. The results are presented

in Fig. 6.2 together with measurements by other workers.

The low energy results between 10 and 200 Mev of Beuermann

et al (1969); and Rockstroh and Webber (1969); are taken

at night at Ft. Churchill. Those of Bleeker et al (1969)

were taken at Kiruna.

The high energy results are in good agreement with

the results of other workers, but the results of the low energy

channel are much too high to be consistent with other low

energy measurements. Because of the contamination of this

channel by re-entrant albedo, the measured flux is higher

than the primary flux alone. Comparison with the daytime

results of Beuermann, and Rockstroh and Webber give good

agreement with their measurement of re-entrant albedo. The

high energy flux is thus of primary origin, whilst the low

energy flux is comprised of primary and re-entrant electrons.

The measurement of the electron flux in the high

energy channel in 1967 is free from the effects of solar

activity and re-entrant albedo, and so is representative

of the flux of electrons reaching the earth from outside

the solar system.   The measurements of the modulation effects

suggest a change in the electron flux of similar magnitude

to the proton modulation.   Since the measurements of 1967

are taken near solar maximum, the electron flux at solar

minimum must be greater than that measured in 1967.   Any

additional residual modulation implies an even greater flux

outside the solar system.   Evidence of a residual modula-

tion (O'Gallagher, 1967) suggests that if the same amount

of residual modulation exists for electrons as for protons,

there is a considerable difference between the electron

flux at the earth and that outside the modulating region.

Comparison of the measured flux in 1967 and the other

measurements shown in Fig. 6.2 with the spectrum derived by

Ramaty and Lingenfelter (1966a) for the galactic secondary

flux shows that at high energies, where modulation effects

are small, the secondary flux is insufficient to explain

the observations.   At low energies, without the effects of

modulation, the two fluxes are comparable, but with the

effects of an electron modulation taken into account, the

secondary flux cannot account for all the observed electrons..

This fact is verified by the measurements of the positron

fraction by Hartman (1967), which show a fraction $\sim (30 \pm 10)\%$

of positrons in the range 200-500 Mev.   At these energies

the secondary flux is almost all positrons, so this figure

is an upper limit to the fraction of secondary electrons.
At higher energies, around 1-2 Gev, the fraction of posi-
trons is only $\sim$ 5%. At these energies approximately
half the secondaries will be positrons, so that the upper
limit to the secondary contribution at these energies is
$\sim$ 10%.

To explain the observed electron flux, an additonal
source of electrons is necessary, such as supernovae and
galactic nuclei outbursts. The amount of energy avail-
able from these sources is sufficient to account for the
measured flux if the electrons are contained within the
galaxy.

Conclusions

(i) The measurements at Kiruna should represent primary
electrons. However, because of the location of Kiruna,
the flux in the low energy channel is not solely primary,
and includes a large contribution from re-entrant albedo.
.The flux of electrons in the high energy channel is free
from re-entrant albedo contamination, and can therefore be
called primary.

The primary flux of electrons measured at Kiruna in
1967, in the range 250-800 Mev was:-

$$J = 24.4 \overset{+}{-} 3.0 \text{ p/m}^2 \text{ sec. ster.}$$

and the differential flux, at a mean energy of 330 Mev,

$$\frac{dJ}{dE} = (4.7 \overset{+}{-} 1.0) \times 10^{-2} \text{ p/m}^2 \text{ sec. ster. Mev.}$$

(ii) The primary electron flux is consistent with the production of the majority of the primary electrons in galactic sources such as supernovae and galactic nuclei, with confinement in the galaxy.   Only a small fraction of the observed flux is due to secondary production in collisions.
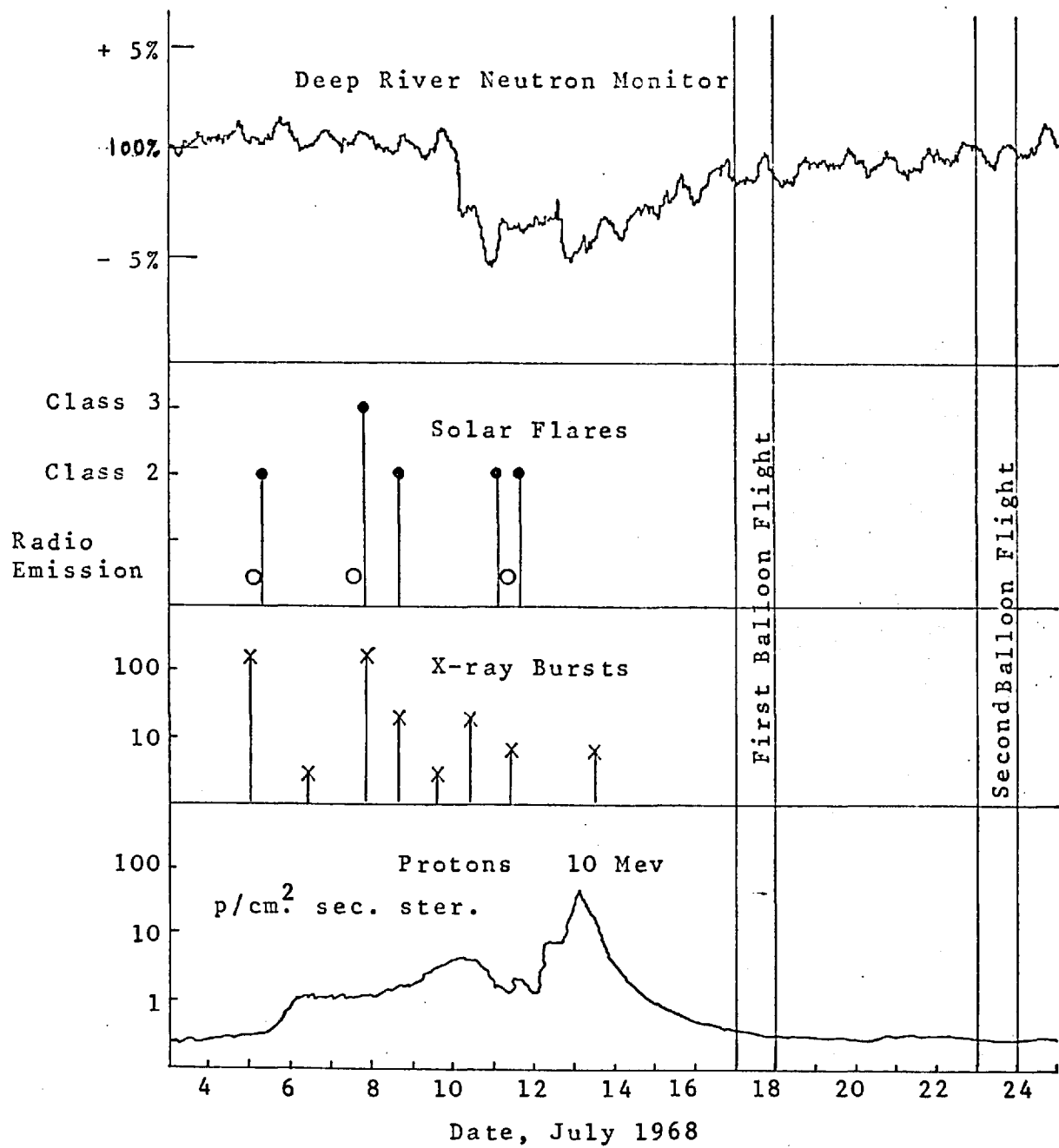
Fig. 6.1.   Solar Geophysical Data
            July 1968.

Electrons/m^2. sec. ster. Mev.

10^2

10^1

10^0

10^{-1}

10^{-2}

10^{-3}

10^{-4}

10^{-5}

10^{-6}

10^{-7}

10^{-8}

Present Experiment 1967

Bleeker et al (1967)

Beuermann et al (1969)

Anand et al (1968c)

Fanselow et al (1968)

Rockstroh and Webber (1969)

Fig. 6.2.   Electron Spectrum Measurements (1966-1968).

10^0 10^1 10^2 10^3 10^4 10^5 10^6 Electron Energy (Mev)
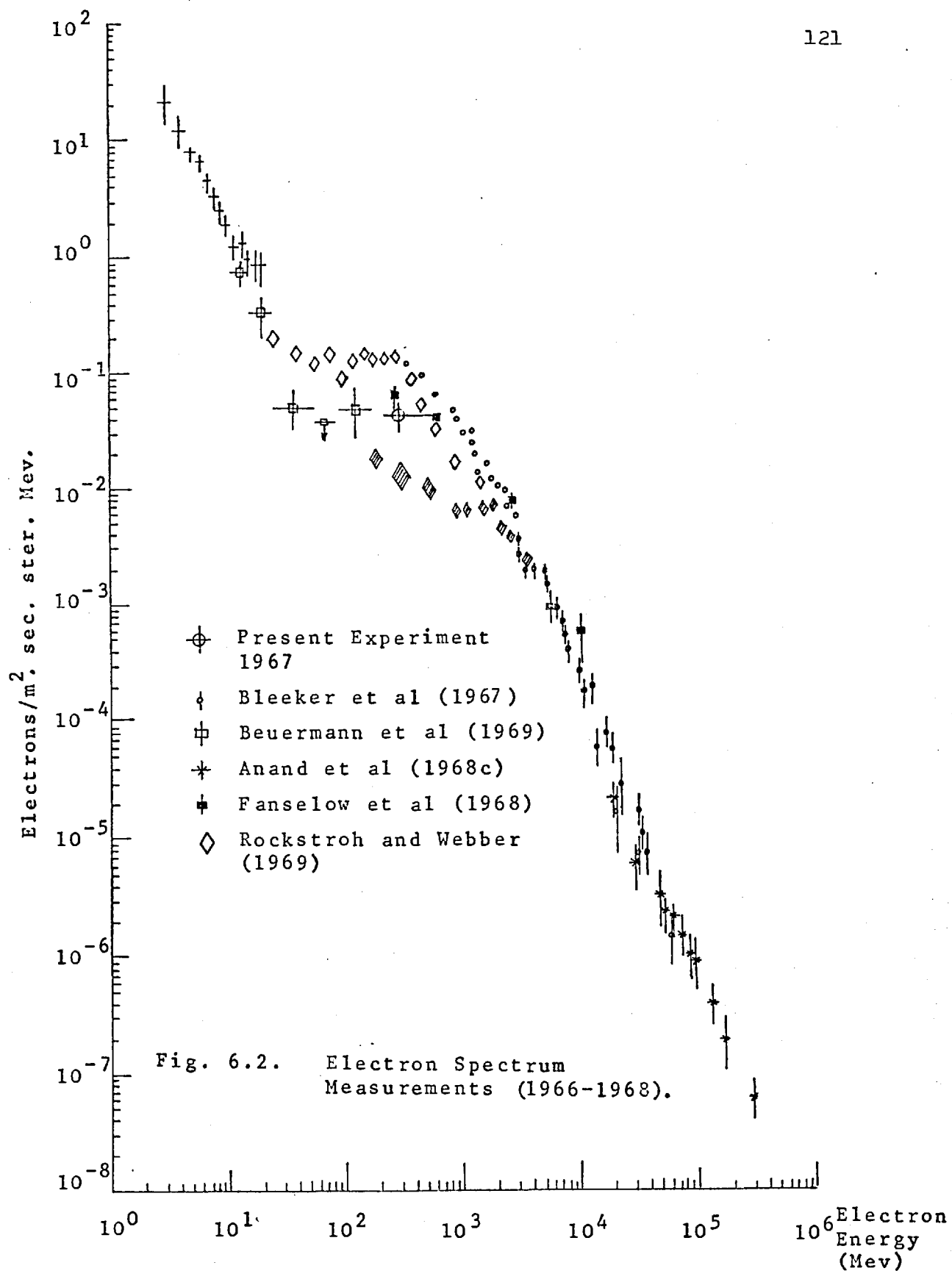
CHAPTER VII

COSMIC RAY ELECTRONS AND PHOTONS

7.1 Direct Acceleration Electron Sources

Direct acceleration sources include supernovae explo-
sions, galactic nuclei outbursts, radio galaxies and quasars.
The extragalactic sources have of course been postulated
for the extragalactic electron flux, of which no direct
measurement can be made. The galactic flux is accesible
in two ways, by radio noise measurements, and by measure-
ment of the electron flux on or near the earth. Because
of this it is the galactic sources, i.e. supernovae, which
have been studied most closely. It has been known for
some time from studies of radio noise from supernovae rem-
nants that their envelopes contain fluxes of relativistic
electrons, and in fact, all known supernovae are associated
with synchrotron radiation.

The processes involved in production of cosmic rays
in supernovae have been studied extensively (Colgate, 1967;
Ginzburg and Syrovatskii 1964, 1968). Special attention
has been paid to the electron component by the latter
authors. In attempting to explain the measured electron

flux by such discrete sources, both the energy available
to the electrons and their spectral shape must be explained.
Using the equipartition of cosmic ray, magnetic and turbu-
lent energy Ginzburg and Syrovatskii (1968), have produced
a model for electron production in supernovae which predicts
the spectral shape of the emitted electrons, with values
of the spectral index between 1.5 and 2.5, with the higher
value being applicable to young sources and the lower value
to the old sources.

From radio measurements of some of the more prominent
supernovae, it is found that the average value of the radio
spectral index is $\sim$ 0.5, corresponding to an electron
spectral index of 2.5.   In general, the type I supernovae,
such as the Crab, Kepler's and Brahe's supernovae have
values of the electron spectral index less than the values
for the type II supernovae.   Type I supernovae are those
which are due to old stars, whilst type II are due to young
stars.

Radio measurements can also give a measure of the
energy output of the supernovae.   Measurement of the radio
noise flux as a function of frequency gives the energy con-
tained in the electrons if the magnetic field is known.

Two assumptions are made by Ginzburg and Syrovatskii (1964) to find the magnetic field and hence the total electron energy density.. First, it is assumed that the electrons constitute 1% of the total cosmic ray energy density, and secondly, that equipartition of energy makes the cosmic ray energy equal to the total magnetic energy in the supernovae. The size and distance from the earth of the supernovae, and the radio flux measured at earth enables the total electron energy density to be found. The average value for the supernovae examined by Ginzburg and Syrovatskii was $\sim 10^{50}$ ergs, which is sufficient to explain the presence of cosmic ray electrons. Another point which fits in well with the observations is the fact that a direct source would accelerate only negative electrons. The observations of Fanselow et al (1968) suggest that the electrons are predominantly negative.

Whilst the supernovae sources can supply sufficient energy to explain the observations and give the same spectral form as observed at the earth or in the galaxy, it is by no means conclusive that this is the only source.

7.2 Secondary Electron Sources

The first mention of the possibility of electrons being produced by interactions of cosmic ray protons with the interstellar gas was made by Hayakawa (1952), and has since been elaborated by various authors (Hayakawa and Okuda, 1962; Ginzburg and Syrovatskii, 1964; Jones, 1963; Ramaty and Lingenfelter, 1966a). The basic processes considered are:

$$p + p \longrightarrow p + p + \pi^{\pm} + \pi^{o} ,$$
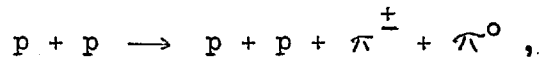
and the subsequent decay:

$$\pi^{\pm} \longrightarrow \mu^{\pm} + \nu , \quad \mu^{\pm} \longrightarrow e^{\pm} + 2\nu .$$
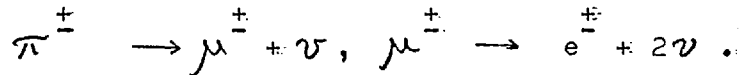
The earlier work of Hayakawa and Okuda used a power law cosmic ray spectrum, with index -2.5, extrapolated to low energies to allow somewhat for modulation, and considered only interactions between 1 and 100 Gev. Cosmic ray proton spectra at solar minimum were used by Jones, Ginzburg and Syrovatskii, and Ramaty and Lingenfelter, with the assumption that the solar minimum flux represents the galactic proton flux.

The most detailed work has been done by Ramaty and
Lingenfelter, who considered as well as p-p collisions,
p -α and α - p collisions, and as well as the $\pi^{\pm}$ decay,
the decay of the neutrons produced in these collisions,
thus:

$$p + p \longrightarrow p + n + \pi^+ + \pi^{\pm} + \pi^0$$

$$n \longrightarrow p^+ + e^- + \bar{\nu}$$
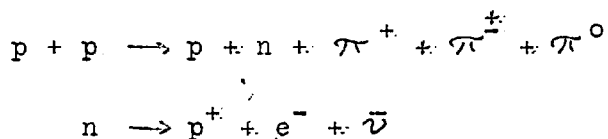
The threshold for the production of mesons is lowest
in the case of proton-helium collisions at 198 Mev.   The
threshold is 287 Mev in p - p collisions.   The neutron
threshold is 26 Mev in p - α collisions and 287 Mev in
p - p collisions.   At low energies around these thresholds,
the relative positive and negative production rates depends
critically upon the different mechanisms operating.

The interaction cross sections and multiplicities
derived from accelerator and cosmic ray studies are used
to cover the energy range under consideration, i.e. 100 Mev
to 1000 Gev, and to derive the pion and neutron production
spectra.   At low energies the neutron production is dominant.
Since this involves decay into -ve electrons, -ve electrons

will dominate. At energies $\sim$ 100 Mev, π^+ production is dominant so that positive electrons exceed the negative ones up to $\sim$ 500 Mev. At this energy both positive and negative production rates become comparable, since at around this energy and above, the positive and negative production rates become equal, and exceed the neutron production rate.

The electrons are produced from the decay in flight of π mesons and the neutrons. The μ-meson resulting from decay of the π-meson has essentially the same velocity as the parent π-meson, and decays into an electron, which has an isotropic distribution in the rest frame of the μ-meson. In the decay of the neutron, the electron has a maximum kinetic energy of 780 kev in the rest frame of the neutron. The production spectrum of the electrons from these sources is not the one observed in the galaxy, since the various energy losses acting upon the electrons change the form of the spectrum. The relevant loss mechanisms are ionisation, leakage from the galaxy, synchrotron radiation, inverse compton scattering and bremsstrahlung, and their effects on the electron spectrum are described in section 1.5. The ionisation loss depends upon the

density of the galactic medium, and for relativistic elect-rons is virtually independant of energy. Bremsstrahlung losses are proportional to the energy of the electron, and also the density of the galactic medium. Both inverse compton and synchrotron energy losses depend upon the square of the electron energy; inverse compton losses are also dependant upon the photon energy density in the galaxy, whilst the synchrotron losses depend upon the magnetic energy density. The equilibrium spectrum derived by Ramaty and Lingenfelter (1966a) for both positive and negative electrons is similar at high energies (> 1 Gev). Around 100 Mev the positive electrons exceed the negative ones by a factor of ∼ 10, and below ∼ 20 Mev the negative electrons become dominant.

The shape of the spectrum so derived depends upon the parameters assumed for the galaxy. Ramaty and Lingenfelter used 3-6 gm/cm^2 for the amount of matter traversed by the cosmic rays, with lifetimes of 1.5 - 6 x 10^{15} sec. and average halo hydrogen density of 0.015 - 0.03 atoms /cm^3. Their results agree reasonably well with the data at medium energies (∼ 500 Mev), and in fact the secondary electrons can more than explain the observations. At these energies,

however, the residual modulation, if it exists, makes the

flux at earth correspondingly less than predicted.   At

both higher and lower energies, the secondary electrons

fall off below the measurements.   A more sensitive test

for the fitting of the data is from the $e^+/e^+ + e^-$ ratio.

A value of $\sim$ 1 is predicted at low energies, where the

observations give a value of $\sim$ 0.3 (Fanselow et al, 1968).

The secondary source predicts a ratio of 0.5 at higher energies,

whereas measurements indicate a value of $\sim$ 5%.   Some other

source is necessary to explain all the electrons observed.

At high energies, an additional loss term was neglected by

Ramaty and Lingenfelter (1966a), namely the inverse compton

losses associated with the $3^\circ K$ radiation.   The increased

energy loss makes the predicted secondary flux at high

energies even smaller than calculated.

7.3 Production of Photons from π° Decay

As well as production of charged pions in p - p and

associated collisions, there is also production of π°'s.

At high energies the π°, π^+ and π^- have approximately

the same production rates and spectra, but differ at low

energies, where π^+ mesons have priority.   Neutral

mesons decay into two gamma rays, with a mean decay time

of $\sim 10^{-16}$ sec. In the π^{o} rest frame, the gamma rays

are emitted with an energy, W_{o} = 70 Mev, half the mesons

rest energy. In the lab. frame, the gamma rays can have

any energy between $W_{o}\sqrt{1-\beta}/1+\beta$ and $W_{o}\sqrt{1+\beta}/1-\beta$,

which bracket W_{o}. Because the π^{o}'s are produced with a

large variety of energies, including velocities near zero,

the resultant γ spectrum is peaked around 70 Mev.

Production of X-rays by the same mechanism is insig-

nificant, since in order to produce an X-ray, the photon

must be produced back along the direction of the parent

pion. To produce an X-ray of ~ 10 Kev requires a π

energy of ~ 400 Gev, at which energy the flux of π's is

so small as to make this production of X-rays unimportant.

The flux of gamma rays produced from π^{o} decay has

been calculated by various authors (Pollack and Fazio, 1965;

Ginzburg and Syrovatskii, 1965; Gould and Burbidge, 1965;

Garmire and Kraushaar 1965). In calulating the flux

measured at the earth, the total number of gamma rays

produced in an element of volume is first determined.

This depends upon the gas density in that volume. The

total number of gamma rays observed at the earth depends

131

upon the path length of observation, and the distribution
of gas along that path.   The gamma rays produced by this
mechanism will show a marked anisotropy because of the
variation of path length and gas intensity with position
in the sky.

The estimate of the gamma ray flux by Garmire and
Kraushaar is shown in Fig. 7.2, using a gas density-observation
length product of 1.5×10^{21} cm^{-2} for an average over the
whole of the sky.   Estimates of the integral flux have
been made by Ginzburg and Syrovatskii (1965), and Pollack
and Fazio (1965).   The first authors predict a flux of
3×10^{-4} p/cm^2 sec. ster. from the galactic centre.   Pollack
and Fazio predict a flux of 10^{-4} p/cm^2 sec. ster. from the
same region, above an energy of 50 Mev.

An offshoot of π decay mechanisms is the production
of positron-electron anihilation gamma rays.   When the π^+
decays, it eventually produces a positron, which loses
energy through ionisation and radiation, and anihilates
with a negative electron when its energy is zero or close
to zero.   The gamma radiation produced is a broad line
at 0.51 Mev.   Pollack and Fazio suggested that since this
process takes place in $\sim 10^9$ years, the relative intensity
of the line spectra and the π^o decay spectra should give

a measure of the gamma ray flux from 10^9 years ago.   As

pointed out by Ginzburg and Syrovatskii, leakage from the

galaxy affects such a measurement, since the leakage life-

time is more than an order of magnitude less than 10^9 years,

so that the 0.51 Mev line is controlled more by leakage

than the past history of the gamma ray flux.   A further

estimate (Stecker, 1969a) of the intensity of this radiation

using the increased energy losses of the positrons due to

inverse compton scattering with the $3^{\circ}K$ background radiation

shows that the 0.51 Mev line is virtually undetectable

against the background gamma ray flux.

7.4   Production of Photons from Bremsstrahlung

Both gamma rays and X-rays can be produced as brem-

sstrahlung, when an electron passing near another charged

particle (in the case of the galaxy, a hydrogen atom or

molecule) causes a photon to be emitted.   A similar effect

can take place with incident protons, but the probability

of this occurring is a factor of $(M_p/M_e)^2$ down on the electron

bremsstrahlung rate, so that despite a larger flux of protons

in for example the galaxy, the proton effect is negligible

compared with the electron effect.

The bremsstrahlung intensity is given by:

$$I_{brem} = \int_0^L dr \int_{E_\gamma}^\infty n(r) \, \sigma_r(E, E_\gamma) \, I_e(E, r) \, dE$$

where dr is an element along the observation path at r,
n(r) is the gas density, σ_r the cross section for brem-
sstrahlung and I_e the electron differential spectrum.
Since the cross section is inversely proportional to the
photon energy, the intensity becomes:

$$I_{brem} \sim N_H I_e(E)$$

So the intensity depends upon the total amount of gas in
the line of observation, and has a spectral slope identical
to that of the electron spectrum producing the radiation.
The intensity of radiation has been shown to be less than
the contributions from π^0 decay (Ginzburg and Syrovatskii,
1965; Garmire and Kraushaar, 1965), and the spectrum is
shown in Fig. 7.2.

In the X-ray region, the flux of photons produced by
bremsstrahlung is also less than that from π^0 decay
(Ginzburg and Syrovatskii).

7.5 Production of Photons from Inverse Compton Scattering

The inverse compton process is the collision of a
fast electron with a low energy photon, with subsequent
production of a high energy recoil photon.   In the case
of the galaxy, the electron component of the cosmic rays
provides the incident particles, whilst the starlight
photons or the 3°K radiation provide the low energy photons.
The intensity of the photons produced by inverse compton
scattering is given by:

$$I = \int_0^L dr \int_{E_\gamma}^\infty I_e(E,r)dE \int_0^\infty n_{ph}(\epsilon,r)$$

$$\times \; \sigma(E_\gamma, \epsilon, E)d\epsilon$$

where n_{ph} is the photon energy density at position r, σ
the cross section for the interaction, with the assumption
that the distribution of the recoil photons is isotropic.
The cross section is given by the Klein-Nishina formula,
which for low energies reduces to the Thomson cross section,

$$\sigma_T = \frac{8\pi}{3} \left(\frac{e^2}{mc^2} \right)^2$$

The factor in the brackets is the classical radius of the

electron.   This assumption is valid up to energies of

$\sim$ 50 Gev (Ginzburg and Syrovatskii).   A modified form of

the cross section has been used in flux estimations up to

10^{14} eV by Fazio, Stecker and Wright (1966).

If the spectrum of electrons is proportional to $E^{-\alpha}$,

then the radiation produced is proportional to $E^{-(\alpha +1)/2}$,

as well as to the energy density of the low energy photons.

Any change in slope of the electron spectrum produces a

corresponding change of slope in the compton spectrum.

Where energy degradation steepens or flattens the electron

spectrum by one power, the compton spectrum will steepen

or flatten by only one half power.   The energy of the

photons where this occurs corresponds to the electron energy

since the two are related by:

$$E_\gamma = \frac{4}{3} \epsilon \, \gamma^2$$

where ϵ is the mean energy of the ambient photons, γ

the ratio E/mc^2 for the electrons, and E_γ the energy of

the photons produced.   In the galaxy, if only starlight

existed, a 10 Mev electron would produce a 500 eV photon,

and a 10 Gev electron, a 500 Mev photon.   If the electron

interacts with photons of the 3°K radiation, the corresponding

photon energies would be $\sim \frac{1}{2}$ eV and 400 kev. The inverse

compton process thus produces photons with energies cover-

ing the X-ray and gamma ray regions, but the intensity of

the contributions from starlight interactions is small

compared with those from the 3°K radiation because of the

smaller starlight photon energy density.

The radiation so produced is proportional to the energy

density of the thermal photons in the observing region,

so one expects a more or less isotropic distribution from

inverse compton scattering, whereas with π° decay and

bremsstrahlung production an anisotropy is expected, related

to the interstellar gas density.

A further source of X and gamma rays could be from

inverse compton scattering with the 8.3°K radiation (Shivan-

andan, Houck and Harwit, 1968). The effects of such a

radiation have been discussed by Shen (1969); and Cowsik

and Yashpal (1969), but until further confirmation of the

measurement is made, no real conclusions can be drawn.

The flux of photons from the galaxy due to inverse

compton scattering is shown in Fig. 7.2, both for starlight

interactions and 3°K radiation interactions (Felten and

Morrison, 1966).

7.6 Production of Photons from Synchrotron Radiation

The production of X and gamma rays by synchrotron radiation comes from the interaction of energetic electrons with a magnetic field. The energy losses incurred in this process are proportional to E^2, E being the electron energy. In interstellar space, the synchrotron energy losses are roughly equal to the inverse compton losses, which are also proportional to E^2. The important difference is the typical photon energy for each process. In the case of inverse compton losses, the typical photon energy lies in the X-ray region for the galaxy, whilst the synchrotron process produces electromagnetic radiation in the radio region. In regions of space where the magnetic field is high, e.g. the crab nebula, synchrotron radiation appears in the optical band. It is possible that in regions where the field is even higher than this, that the process may be responsible for X-rays, but in the case of the background X and gamma radiation, the synchrotron process cannot compete with such processes as inverse compton and π^0 decay.

7.7. Distribution of Matter in the Galaxy and Beyond

(i) Galactic Gas

The main component of the galactic gas is hydrogen, which

exists in three forms: neutral (H1), ionized (H11), and molecular (H_2). The distribution is non-uniform, with the greatest density occurring in the spiral arms of the galaxy. Hydrogen contributes $\sim 90\%$ to the gas whilst helium contributes $\sim 10\%$. The distribution of neutral hydrogen is well known from studies of 21 cm line emission (Kerr, 1969). The disc containing the spiral arms is ~ 15 kpc in radius and ~ 300 pc thick. The gas density is highest within 150 pc of the centre of this disc, and is $\sim 10 \text{ cm}^{-3}$.between 3 and 8 kpc, then falling off to a negligible amount at 15 kpc. The mean density averaged over the disc is $\sim 0.7 \text{ cm}^{-3}$. Within the galactic halo, which is a sphere of radius similar to the disc, the gas density is $\sim 10^{-2} \text{ cm}^{-3}$ (Pollack and Fazio, 1963). In general, both the H1 and H11 have the same distribution with the density of H11 being approximately 10% of the density of H1..

The density and distribution of molecular hydrogen is at present uncertain. No radio emission line corresponding to the atomic 21 cm line exists for molecular hydrogen, and the spectral lines lie in the almost inaccesible infra-red and ultra-violet regions. Estimates of the quantity of molecular hydrogen have been made by

Gould, Gold and Salpeter (1963), who suggest that it may be anything between 1/10 and 10 times the total mass of the Hl and Hll.   Since the value of this ratio affects considerably the total amount of matter contained in the galactic gas, a more exact value is clearly necessary for any discussion on relative quantities of cosmic ray protons, electrons and photons, especially since so many production mechanisms depend upon the gas density.

Rocket measurements of ultra-violet spectra are at present the only direct way of observing the molecular hydrogen.   The results of Carruthers (1968) and Smith (1969) both suggest that the H_2 concentration is smaller than the Hl, and Hll, whereas Werner and Harwit (1968) suggest the opposite.   These measurements are taken looking at very limited areas of the sky, using the absorption spectra of the gas between selected stars and the earth.   Werner and Harwit have suggested that the small amounts of H_2 detected by Carruthers, and Smith may be in regions of the galaxy where ultra-violet radiation from nearby stars causes photo-- dissociation (Stecher and Williams, 1967).

Much of the evidence in favour of a large concentration of H_2 has been collected by Stecker (1969b), who considered as well as the results of Werner and Harwit, the distribution

of mass in the galaxy. From the distribution of matter

in the galaxy perpendicular to the galactic plane, the

observed mass is insufficient to explain the observed

distribution of stars and interstellar gas. This same

point has also been pointed out in a review by Varsavsky

(1966). An extra amount of matter, in the form of either

undetectable stars or invisible gas could explain the obser-

vations. Such an extra amount, in the form of molecular

hydrogen could exist with up to five times the known gas

density and still be consistent with the observed distrib-

ution of mass.

Even less is known of the extragalactic gas density

and composition. The measurements of 21 cm lines can give

a measure of the amount of H1 present. Typical values

quoted are $\sim 3.10^{-6}$ cm^{-3} (Penzias and Wilson, 1969) and

$\sim 10^{-5}$ cm^{-3} (Ginzburg and Syrovatskii, 1965).

(ii)   Thermal Photons

The starlight energy density in the galaxy is calculated

from the total light output averaged over the galactic halo.

With a galactic luminosity of 5×10^{43} ergs/sec. and a halo

diameter of 16 kpc, Felten and Morrison (1966) find the

energy density is 0.1 eV/cm^3. In a similar way Ginzburg

and Syrovatskii (1965) quote the values 0.2 eV/cm^3 for

the disc and 0.4 ev/cm^3 for the halo. The density
in the disc is somewhat lower because of interstellar
absorption.

The contribution of the black body radiation to the
photon energy density is:-

$$\rho = 4.75 \times 10^{-3} T^4 \quad ev/cm^3$$

where T is the black body temperature. For a $3^{\circ}K$ radi-
ation this is $\sim$ 0.4 ev/cm^3, and is almost completely
isotropic (Wilkinson and Partridge, 1967), and is assumed
to extend throughout the universe. The typical energy
of the starlight is $\sim$ 1 eV, whilst that of the $3^{\circ}K$ rad-
iation is $\sim 10^{-3}$ eV (i.e. microwave).

In extragalactic space the starlight energy density
is very small. Estimates from average luminosities of
galaxies yield a photon energy density from $\sim 2 \times 10^{-3}$
ev/cm^3 (Ginzburg and Syrovatskii) to $\sim 10^{-2}$ (Felten, 1966).

7.8 Discussion

The proton spectrum at the earth is well known, as
are the high energy galactic proton fluxes. The spectrum
of electrons at the earth is as yet somewhat uncertain:

the galactic flux is even more uncertain. The electron
flux at earth consists of a majority of negative electrons
with a small but detectable fraction of positrons. The
measurements of the charge ratio show that it is imposs-
ible that all the electrons are produced in collisions of
the primary cosmic ray flux with the interstellar gas.
The total flux of electrons at energies around 500 Mev
is less than predicted by the secondary source, yet the
charge ratio implies that there are more directly acceler-
ated electrons present than secondaries. In this energy
region, the solar modulation effects on protons are con-
siderable, so it is reasonable to assume that this is the
case for electrons (see section 1.6), and that a much
larger flux exists in the galaxy than near the earth. At
higher energies, where the effects of modulation are less
important, the flux of electrons predicted from secondary
source is less than the measured flux. This is in agree-
ment with the measurements of the charge ratio, which shows
that the secondaries cannot account for all the measured
electrons.

In order to calculate the true galactic electron flux,
Ramaty and Lingenfelter (1968) have fitted the measured
positron flux, derived from the cosmic ray electron spectrum

and the charge ratio measured by Hartman (1967) to the
expected positron flux from the secondary source, modu-
lated with functions similar to those obtained from proton
data.   The modulating function is::

$$\exp \left(\frac{-\eta}{f(R)\beta} \right) \quad \text{where } f(R) = R \text{ for } R > R_o$$

and

$$f(R) = R_o = \text{const. for } R < R_o.$$

This is a $1/R\beta$ function at high energies and a $1/\beta$
function at low energies.   With $\eta = 0.4$ Gv, and $R_o =$
0.5 or zero, reasonable fits to the data are obtained
Using this function, the spectrum of electrons in the galaxy
is obtained.   This is shown in Fig. 7.1.

Present measurements of solar modulation of electrons
are in dispute.   On the one hand, Rockstroh and Webber
(1969) and Bleeker et al (1969a) suggest a large amount of
modulation, whilst L'Heureux et al (1967) suggest little
or no modulation.   The results of Ramaty and Lingenfelter
favour a large modulation.

Further evidence on the galactic electron flux and the

relative modulation comes from the relation between the electrons and radio noise from the galaxy. It is now well established that the non-thermal radio noise in the galaxy is due to synchrotron radiation from electrons spiraling in the magnetic fields of the galaxy. Measurement of the intensity of this radio noise enable the electron flux in the galaxy to be derived as long as the magnetic field is known. Anand, Daniel and Stephens (1968b) have derived a value of the magnetic field in the galaxy using only the high energy electron flux measured at the earth, which they assume is unaffected by modulation. Comparison with radio noise measurements in selected directions gives values for the magnetic field of 6×10^{-6} gauss in the anticentre direction, and $\sim 10^{-5}$ gauss in the halo direction. Similar values have also been obtained using essentially the same method by Felten (1966) and by Okuda and Tanaka (1967).

In another paper, Anand, Daniel and Stephens (1968a) used these values of the magnetic field to derive the low energy electron spectrum from radio noise measurements. By comparing this electron spectrum with that measured at the earth, the modulating function was found. Their best fit to the data was a modulating function $\exp\left(\dfrac{-\eta}{R\beta}\right)$ between

0.5 and 5 Gev, with $\eta = 0.65$ Gv and below 0.5 Gev a
function $\exp\left(\dfrac{-\eta}{\beta}\right)$ with $\eta = 1.3$. The galactic flux
so derived is shown in Fig. 7.1.

In a similar manner, Webber (1968a) compared measure-
ments of electrons at the earth with detailed radio noise
measurements, taking into account interstellar absorption
at frequencies corresponding to low energy electrons,
and found a mean galactic magnetic field of 7×10^{-6} gauss
and a modulating function with $\eta = 0.75$ Gv gave the best
fit to the electron measurements. The interstellar
electron spectrum derived by demodulating the spectrum at
earth with Webber's function is shown in Fig. 7.1. There
is reasonable agreement between this and the spectrum of
Anand et al and of Ramaty and Lingenfelter, except at
energies $\sim$ 500 Mev and less where they differ. The mod-
ulating functions used in these calculations are similar
to the ones used for proton modulation.

The magnetic field and the thermal photons in the
galaxy provide important energy loss mechanisms for the
electrons. Both synchrotron and inverse compton energy
losses change the shape of the injection spectrum. Energy
losses proportional to E, such as leakage from the galaxy
cause no change in the spectral index of a power law

distribution of energy, whilst energy losses proportional
to E^2 (synchrotron and inverse compton) increase the
index by one.   The transition point where the index changes
by one is where the energy loss $\propto E$ is equal to the energy
loss $\propto E^2$.   Observations of the change of the index give
indications on the conditions existing in the galaxy.

Following the first few years of electron measurements,
only straight line power laws could be fitted to the data.
A spectral index of 2.4 in the range 0.6 - 3.5 Gev was
given by Felten (1966)..   The calculation of Felten and
Morrison predicted a steepening at 15 Gev due to synchro-
tron and inverse compton losses, considering only starlight,
and using a halo lifetime of 10^8 years.   With the addition
of the 3°K radiation this energy becomes 5 Gev.   The early
measurements of Daniel and Stephens (1965) extended the
range up to $\sim$ 50 Gev, with an index of 2.1, thus apparently
ruling out the steepening at a few Gev.   Since then,
increased statistics and the measurements of other workers
have established the shape of the electron spectrum from a
few Mev to $\sim$ 300 Gev, (Fig. 6.2).

The point where steepening occurs is when the leakage
lifetime is equal to the lifetime for energy losses due
to synchrotron radiation and inverse compton scattering.

Three possibilities exist for the absence of any steepening between a few Gev and a few hundred Gev. One, that the black body radiation does not exist: two, that there exists a second electron component at high energies, and three, that the electron leakage lifetime is much smaller than 10^8 years.

The presence of the $3°K$ radiation is now firmly established (Dautcourt and Wallis, 1968) so the first alternative can be rejected. The second alternative was put forward on the basis of a measured positron excess Daniel and Stephens (1966), but as yet has not been confirmed by any other measurements. The third alternative has been discussed by many authors. Both Cowsik et al (1966) and O'Connell (1966) have proposed a shorter lifetime, $\sim 10^6 - 10^7$ years for the electrons to explain the lack of steepening below 300 Gev. Ramaty and Lingenfelter (1966b) used a disc-halo model with a disc lifetime shorter than the halo lifetime. A similar explanation by Shen (1967) used a distribution of sources in the disc.

The two alternatives of the change of index occurring at 2 Gev and at $\sim$ 50 Gev have been discussed by Tanaka (1967). A knee at 2 Gev implies an injection spectrum with index 1.5, steepening to 2.5 to fit the high energy data. This

gives a storage time of 2.5×10^7 years if the electrons

are confined in the disc or 1.5×10^8 years if they are

confined in the halo. With confinement in the disc,

~ 40 gm/cm^2 of matter would be traversed with this life-

time, which is in contradiction with the lack of positrons

(Fanselow et al, 1968). Confinement in the halo is quite

compatible with ~ 5 gm/cm^2 of matter traversed if the halo

gas density is 10^{-2} atoms/cm^3.

A knee at 50 Gev gives a lifetime of 10^6 years with

confinement in the disc, and 5×10^6 years with confine-

ment in the halo. The halo lifetime implies a gas density

of ~ 0.5 atoms/cc if 3 gm/cm^2 of matter are traversed,

which is too high to be acceptable. The disc lifetime of

5×10^6 years gives 2 atoms/cm^3 in the disc, which is com-

patible with measurements of the gas density. Both the

halo model with knee at 2 Gev and the disc model with knee

at 50 Gev can fit the observed electron measurements.

Tanaka favoured the first alternative, but did not rule

out the second. The second alternative is in agreement

with the measurements of Anand, Daniel and Stephens (1968c)

The available evidence seems to favour a source with

a straight line power spectrum from a few Gev to a few

hundred Gev. Preservation of this index is easily achieved

with a short lifetime and confinement in the disc, and a
change of index occurring above ~ 300 Gev. Since the
source spectrum of all other components of cosmic rays
have indices around 2.5, an acceleration mechanism of
this kind for electrons is quite plausible.

Below a few Gev, where the spectrum begins to flatten,
the effects of solar modulation are becoming apparent, so
no conclusions can be drawn about a galactic flux. Any
knee may be just due to the effects of modulation. At
even lower energies, a knee due to energy losses independ-
ent of energy (e.g. ionisation) is likely to be obscured
by low energy solar protons, or interstellar knock-on
electrons, as well as the effects of solar modulation.

The effect of the inverse compton losses make it very
unlikely that the electrons are anything but galactic in
origin, since the universal $3^{\circ}K$ radiation would prevent
any flux outside the galaxy from existing for more than
~ 10^6 years. Any electrons produced in extragalactic
sources would be removed before they could reach the earth.
Furthermore, a universal electron flux would produce an
electron flux much larger than that observed at the earth.

The production of electrons from $\pi^{\pm}$ decay and gamma
rays from π° decay are related by a common collison source.

Despite this, their fluxes measured at the earth are not
related to the same interstellar parameters.   In the case
of the secondary electrons, the protons involved in the
collisions are supposed to have traversed a thickness of
~ 3 gm/cm^2 of interstellar matter (Ramaty and Lingenfelter,
1966a).   With containment in the halo, and a gas density
of $\sim 10^{-2}$ cm^{-3}, the protons have a lifetime of $\sim 10^8$ years.
If there exists substantially more material in the gas, in
the form of molecular hydrogen, which at present cannot
be detected, but which appear to the protons as target nuclei,
then with the same amount of matter traversed, the proton.
lifetime must be decreased.   An increase of gas density
of say 5 times would reduced the protons lifetime to 2 x 10^7
years.   Since the amount of matter traversed by the protons
has remained the same, so the flux of secondary electrons
must remain the same.

In the case of the π^0 decay, the flux of photons
measured at the earth is due to those collisions occurring
in the line of sight of the detector, and so is dependant
upon the length of the observation path, and the gas density
along that path.   In this case, a five fold increase in
gas density due to molecular hydrogen would produce a five
fold increase in the corresponding gamma ray flux.   The

gamma ray flux produced by π^o decay is shown in Fig. 7.2.
for the observable galactic gas (Garmire and Kraushaar,
1965).   Also shown are the measurements of the background
gamma ray flux (Sood, 1969, Kraushaar et al, 1965), and
an extrapolation of the X-ray measurements to gamma ray
energies.   It can be seen than an increase in gas density
and consequent increase in the π^o produced gamma rays
would make π^o decay a likely candidate for the observed
gamma rays.   The π^o photon spectrum flattens below
$\sim$ 1 Mev, and so cannot explain the X-ray measurements
even with an increased gas density.

If only the π^o decay process were producing gamma
rays, the shape of the gamma spectrum would be very useful
in determining the galactic gas density.   In the energy
range of interest, other processes are also producing gamma
rays of comparable intensity.   Both bremsstrahlung and
inverse compton processes produce gamma rays by interactions
of electrons.   The gamma rays from bremsstrahlung are due
to interactions with the galactic gas, but are of a lower
intensity than the gamma rays from π^o decay (Garmire and
Krausharr, 1965), as can be seen from Fig. 7.2.

The gamma rays produced from inverse compton scattering
are independant of the galactic gas density, since the

electrons from which they are produced are also indepen-
dant of the gas density..   The gamma ray spectrum from
inverse compton scattering reflects the shape of the
electron spectrum.   Where the electron spectral index
changes by one, the corresponding change in the gamma
ray spectral index is one half.   The energy of the gamma
ray produced from this process is related to both the
electron energy and the thermal photon energy.   For each
of the different types of thermal photons possible (e.g.
Starlight, 3^oK, 8.3^oK) there will be a separate gamma ray
spectrum extending over different ranges of gamma ray
energies for a given range of electron energies.   The
gamma ray energy is highest for starlight, and the spectral
break is highest in this case.   The spectra produced
by these sources are shown in Fig. 7.2.   Neither the flux
due to the 3^oK photons or the starlight photons can explain
the observed gamma ray flux.   The flux due to 8.3^oK photons
can explain the observed gamma rays (Shen, 1969;   Cowsik
and Yashpal, 1969;   O'Connell and Verma, 1969) and extra-
polation of this spectrum fits the observations of the
background X-ray flux.   However, the existence of the
8.3^oK radiation has only been measured by one type of
detector (Shivanandan, Houck and Harwit, 1968), and cannot

at present be taken as universal, so that despite the good fit to the gamma ray data, such a source cannot be firmly accepted.

The X-rays have been explained in terms of inverse compton photons (Felten and Morrison, 1966) assuming a metagalactic flux of 10^{-3} times the galactic electron flux. Such a flux predicts correctly both the shape and intensity of the observed background. However, the lifetime of the electrons makes it highly unlikely that such an electron flux can be universal. An alternative suggestion by Gould (1965), that leakage of electrons out of radio sources provides localized areas of X-ray emission, is more reasonable. With the resolution of the detectors available at present, these areas would appear as a diffuse background. This idea has been put forward by Clark et al (1968) and extended by Ogelmann (1969) to explain the observed flux of gamma rays. Extrapolation of all the X-ray sources up to gamma ray energies gives a large enough flux to explain the observed flux and still retain the accepted value of the galactic gas. The main evidence in favour of this model is the shape of the distribution of the predicted gamma rays, which is similar to the distribution observed by Sood (1969) and Clark et al (1968).

Conclusions

Reasonable estimates of the galactic electron flux between $\sim$ 5 and 100 Gev can now be made. This flux is due to both primary and secondary sources. Measurement of the positron component gives the fraction of secondary electrons. The interactions producing the positrons also produce gamma rays via the π^{o} decay process, which is related to the galactic gas density and distribution. Gamma rays are also produced with comparable intensity from inverse compton scattering with background photons in the galaxy. Neither of these processes can explain the observed gamma ray flux, but the π^{o} decay flux becomes comparable to the measured flux if an increased gas density is accepted. The X-rays can be explained in terms of unresolved discrete sources, or from inverse compton scattering with the background photons.
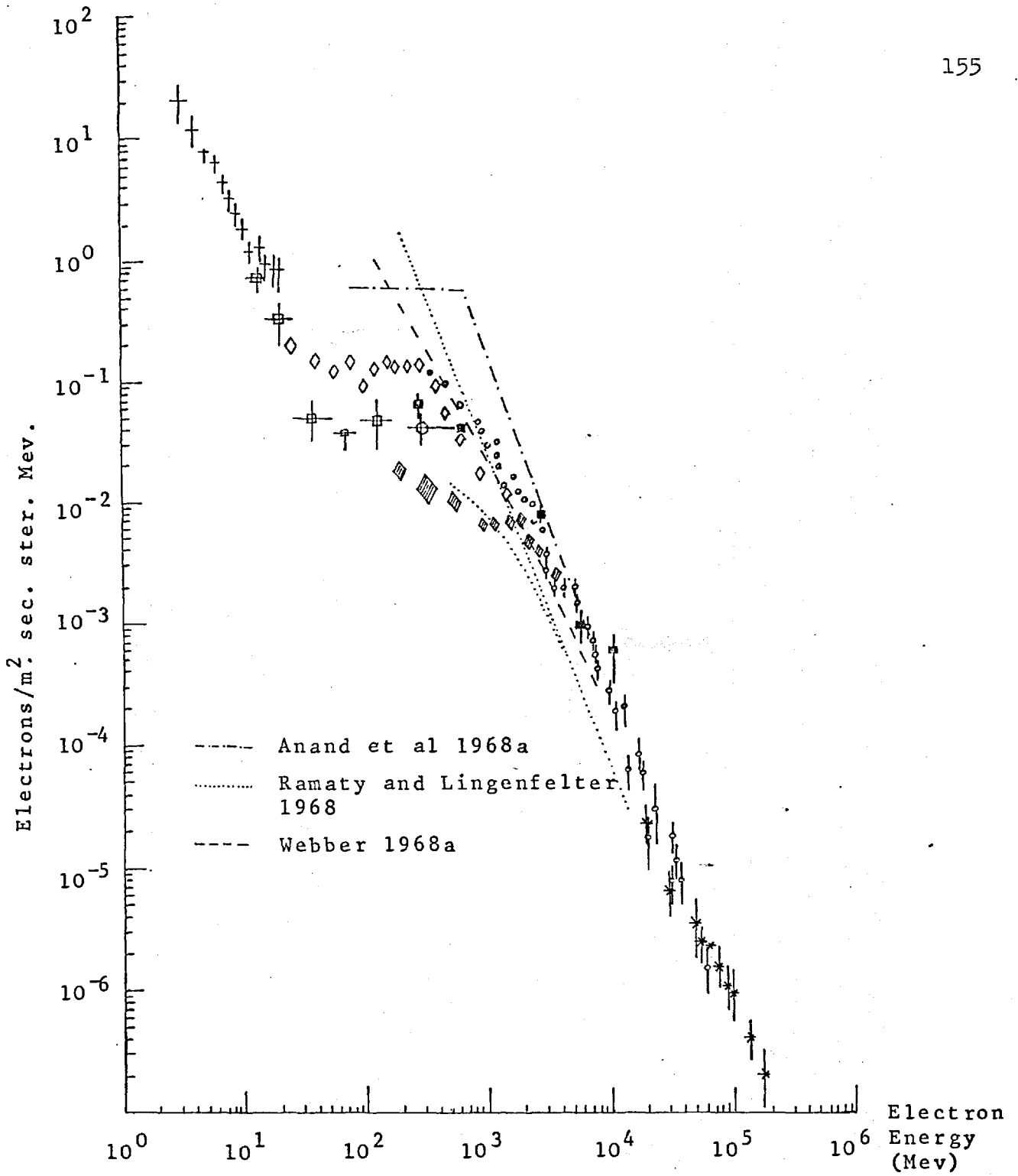
Fig. 7.1.   Measured Electron Flux (Fig. 6.2) and
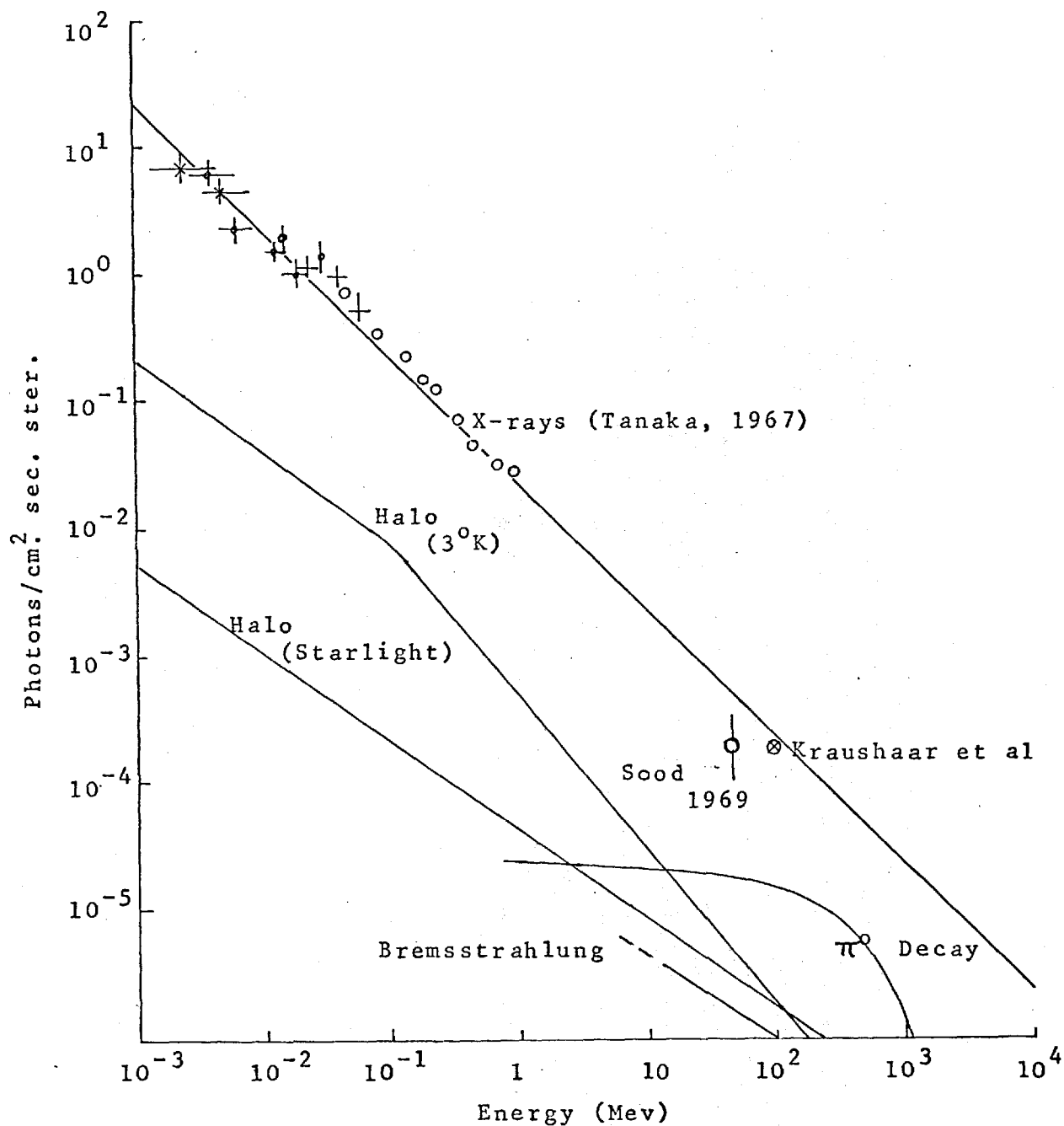   Predicted Flux in Galaxy.

Fig. 7.2.   X-ray and Gamma ray Measurements and
Theoretical Estimates.

REFERENCES

AGRINIER, B., Y. KOECHLIN, B. PARLIER, G. BOELLA, G. DEGLI
ANTONI, C. DILWORTH, L. SCARSI and G. SIRONI. Phys.
Rev. Letters, 13, 377, 1964.

ALVEN, H. and N. HERLOFSON. Phys. Rev., 78, 616, 1950.

ANAND, K. C., R. R. DANIEL and S. A. STEPHENS.
Nature, 217, 25, 1968a.
Proc. Ind. Acad. Sci., 67A, 267, 1968b.
Phys. Rev. Letters, 20, 764, 1968c.
Proc. Ind. Acad. Sci., 68A, 219, 1968d.

ANDERSON, K. A. Solar Physics, 6, 111, 1969.

ANDERSON, K. A. and R. P. LIN. Phys. Rev. Letters, 16,
1121, 1966.

AXFORD, W. I. Plan. & Sp. Sci., 13, 1301, 1965.

BALDWIN, J. E., Proc. Int. Conf. Cosmic Rays, Kyoto,
p173, 1961.

BEEDLE, R. E. and W. R. WEBBER. Proc. 10th Int. Conf.
Cosmic Rays, Calgary, p1014, 1967.

BEUERMANN, K. P., C. J. RICE, E. C. STONE and R. E. VOGT.
Phys. Rev. Letters, 22, 412, 1969.

BIRKS, J. B. Theory and Practice of Scintillation Counting,
Pergamon, 1964.

BLAND, C. J., G. DEGLI ANTONI, C. DILWORTH, D. MACCAGNI,
E. G. TANZI, Y. KOECHLIN, A. RAVIART and L. TREUGER.
Proc. 11th Int. Conf. Cosmic Rays, Budapest, 1969.

BLEEKER, J. A. M., J. J. BURGER, A. SCHEEPMAKER,
B. N. SWANENBURG and Y. TANAKA. Proc. 9th Int. Conf.
Cosmic Rays, London, p327, 1965.

BLEEKER, J. A. M., J. J. BURGER, A. J. M. DEERENBERG,
A. SCHEEPMAKER, B. N. SWANENBURG and Y. TANAKA.
Phys. Rev. Letters, 22, 1325, 1969a.

BLEEKER, J. A. M., J. J. BURGER, A. J. M. DEERENBERG,
    H. C. VAN de HULST, A. SCHEEPMAKER, B. N. SWANENBURG
    and Y. TANAKA. Proc. 11th Int. Conf. Cosmic Rays,
    Budapest, 1969b.

BURBIDGE, G. Review Article 10th Int. Conf. Cosmic Rays,
    Calgary, (unpublished).

CARRUTHERS, G. R. Ap. J., 151, 269, 1968.

CLARK, G. W., G. P. GARMIRE and W. L. KRAUSHAAR. Ap. J.,
    153, L 203, 1968.

CLINE, T. L., (private communication).

CLINE, T. L. and E. W. HONES. Proc. 10th Int. Conf.
    Cosmic Rays, Calgary, p527, 1967.

CLINE, T. L., G. H. LUDWIG and F. B. McDONALD. Phys. Rev.
    Letters, 13, 786, 1964.

CLINE, T. L. and F. B. McDONALD. NASA preprint X-611-68-154
    1968.

CLINE, T. L. and G. PORRECA. Proc. 11th Int. Conf. Cosmic
    Rays, Budapest, 1969.

COLEMAN, P. J. J.G.R., 71, 5509, 1966.

COLGATE, S. Proc. 10th Int. Conf. Cosmic Rays, Calgary,
    p476, 1967.

COWSIK, R., YASHPAL, S. N. TANDON and R. P. VERMA, Phys. Rev.
    Letters, 17, 1298, 1966.

COWSIK, R. and YASHPAL. Phys. Rev. Letters, 22, 550, 1969.

CRAWFORD, D. F. and H. MESSEL. Phys. Rev., 128, 2352, 1962.

CRITCHFIELD, C. L., E. P. NEY and S. OLEKSA. Phys. Rev.,
    85, 461, 1952.

DANIEL, R. R. and S. A. STEPHENS. Phys. Rev. Letters, 15,
    769, 1965.

DANIEL, R. R. and S. A. STEPHENS. Proc. Ind. Acad. Sci.,
    65A, 319, 1966.

DANJO, A., S. HAYAKAWA, F. MAKINO and Y. TANAKA. Proc.
    10th Int. Conf. Cosmic Rays, Calgary, p530, 1967.

DATLOWE, D., J. L'HEUREUX and P. MEYER. Proc. 11th Int.
    Conf. Cosmic Rays, Budapest, 1969.

DAUTCOURT, G. and G. WALLIS. Fortshr. Phys., 16, 545, 1968.

DE SHONG, J. A., R. H. HILDEBRAND and P. MEYER. Phys. Rev.
    Letters, 12, 1, 1964.

EARL, J. A. Phys. Rev. Letters, 6, 125, 1961.

ELLIOT, H. Solar Flares & Space Res., p356, 1969.

FAN, C. Y., G. GLOECKLER, J. A. SIMPSON and S. D. VERMA.
    EFINS Report, 67-66, 1967.

FANSELOW, J. L., R. C. HARTMAN, R. H. HILDEBRAND and P. MEYER.
    EFI Preprint, 1968.

FAZIO, G. G., F. W. STECKER and J. P. WRIGHT. Ap.J., 144,
    611, 1966.

FEENBERG, E. and H. PRIMAKOFF. Phys. Rev, 73, 449, 1948.

FELTEN, J. E. Ap.J., 145, 589, 1966.

FELTEN, J. E. and P. MORRISON. Ap.J., 146, 686, 1966.

FREIER, P. S. and C. J. WADDINGTON. J.G.R., 70, 5753, 1965.

GALL, R., J. JIMENEZ and L. CAMACHO. J.G.R., 73, 1593,
    1968.

GARMIRE, G. and W. L. KRAUSHAAR. Sp. Sci. Rev., 4, 123, 1965.

GINZBURG, V. L. and S. I. SYROVATSKII.
    Progress in Cosmic Rays, Vol IV, 1958, North Holland
    Publ. Co.
    The Origin of Cosmic Rays, Pergammon Press, 1964
    Sp. Sci., Reviews, 4, 267, 1965.
    Proc. 10th Int. Conf. Cosmic Rays, Calgary, (review article
        unpublished).
    Ap. & Sp. Sci. 1, 442, 1968.
GOULD, R. J. Phys. Rev. Letters, 15, 511, 1965.

GOULD, R. J. and G. BURBIDGE. Ann. D.'Astrophys., 28, 171, 1965.

GOULD, R. J., T. GOLD. and E. E. SALPETER. Ap. J., 138, 408, 1963.

HARTMAN, R. C. Ap.J., 150, 371, 1967.

HAYAKAWA, S. Prog, Theor. Phys. 8. 571, 1952. Proc. Int. Conf. Cosmic Rays, Kyoto, 181, 1961.

HAYAKAWA, S. and H. OKUDA. Prog. Theor. Phys. 28, 517, 1962.

HERISTCHI, D. Nucl. Inst. and Methods, 47, 39, 1967.

HOYLE, F. Phys. Rev. Letters, 15, 131, 1965.

HULTSIZER, R. I. and B. ROSSI. Phys. Rev., 73, 1402, 1948.

ISRAEL, M. M. and R. E. VOGT. Phys. Rev. Letters, 20, 1053. 1968. J.G.R., 74, 4714, 1969.

JELLEY, J. V. 'Cerenkov Radiation' Pergammon Press, 1958.

JOKIPII, J. R., J. L'HEUREUX and P. MEYER, J.G.R., 72, 4375, 1967.

JONES, F. C. J.G.R., 15, 4399, 1963.

KERR, F. J. Ann. Rev. Astron. Astrophys., p39, 1969.

KIEPENHEUER, K.O. Phys. Rev. 79, 738, 1950.

KITAMURA, M. and M. KODAMA. Proc. Int. Conf. Cosmic Rays, Moscow, IV, 202, 1960.

KRAUSHAAR, W., G. W. CLARK, G. GARMIRE, H. HELMKEN, P. HIGBIE and M. AGOGINO. Ap. J., 141, 845, 1965.

LEINBACK, H. Arkiv. for Geofysik., 3, 427, 1962.

L'HEUREUX, J. and P. MEYER. Phys. Rev. Letters, 15, 93, 1965.

L'HEUREUX, J., P. MEYER, S. D. VERMA and R. E. VOGT. Proc. 10th Int. Conf. Cosmic Rays, Calgary, p896, 1967.

LIN, R. P and K. A. ANDERSON. Solar Phys. I, 446, 1967.

LINNEY, A. D. and G. M. COURTIER. Pl. Sp. Sci., 14, 503, 1966.

MARSDEN, P. L., R. JAKEWAYS, J. B. CROWDEN, T. M. NAPIER and I. R. CALDER. Proc. 11th Int. Conf. Cosmic Rays, Budapest, 1969.

McDIARMID, I. B. and J. R. BURROWS. Canad. J. Phys., 42, 616, 1964.

MEYER, P., (private communication).

MEYER, P. and R. E. VOGT. Phys. Rev. Letters, 6, 193, 1961. Phys. Rev. Letters, 8, 387, 1962.

MICHEL, F. C. Pl. Sp. Sci., 13, 753, 1965.

NAGEL, H. Z.f. Physik, 186, 319, 1965.

NEELY, D. E. Univ. of Maryland, Tech. Report No. 845, 1968.

NESS, N. F. Proc. 9th Int. Conf. Cosmic Rays, London p14, 1965.

O'BRIEN, B. J. J.G.R., 68, 989, 1963.

O'CONNELL, R. F. Phys. Rev. Letters, 17, 1232, 1966.

O'CONNELL, R. F. and S. D. VERMA, Phys. Rev. Letters, 22, 1443, 1969.

O'GALLAGHER, J. J. Ap.J., 150, 675, 1967.

OGELMANN, M. B. Nature, 221, 753, 1969.

OKUDA, H. and Y. TANAKA. Proc. 10th Int. Conf. Cosmic Rays, Calgary, p642, 1967.

OKUDA, H. and Y. YAMAMOTO. Nagoya Univ., preprint 1965.

ORMES, J. F. and W. R. WEBBER. J.G.R. 73, 4247, 1968.

PARKER, E. N. Progress in Cosmic Ray Physics, Vol IX, 1967, North Holland Publ. Co.

PENZIAS, A. A. and R. W. WILSON. Ap.J., 142, 419, 1965. Ap. J. 156, 799, 1969.

PEROLA, G. C. and L. SCARSI.   IL Nuovo Cimento, 46, 718, 1966.

POLLACK, J. B. and G. G. FAZIO.   Ap. J., 141, 730, 1965.

RAMATY, R. and R. E. LINGENFELTER.   J.G.R., 71, 3687, 1966a.
    Phys. Rev. Letters, 17, 1230, 1966b.   Phys. Rev. Letters,
    20, 120, 1968.

REID, G. C. and H. H. SAUER.   J.G.R., 72, 197, 1967.

ROCKSTROH, H. J. and W. R. WEBBER.   J.G.R., 74, 5041, 1969.

ROSSI, B.   High Energy Particles, Prentice Hall, 1952

RUBTSOV, V. I. and V. I. ZATSEPIN.   Proc. 10th Int. Conf.
    Cosmic Rays, Calgary, p518, 1967.

SARI, J. W. and N. F. NESS.   Solar Physics, 8, 111, 1969.

SCHATTEN, K. H., N. F. NESS and J. M. WILCOX.   Solar Physics,
    5, 240, 1968.

SCHEIN, M., W. P. JESSE and E. O. WOLLAN.   Phys. Rev., 59,
    615, 1941.

SCHMOKER, J. W. and J. A. EARL.   Phys. Rev. 138, B300, 1965.

SCHWINGER, J.   Phys. Rev., 75, 1912, 1949.

SHAW, D. F.   High Energy & Nuclear Data Handbook, Rutherford
    Laboratory.

SHEN, C. S.   Phys. Rev. Letters, 19, 399, 1967.

SHEN, C. S.   Phys. Rev. Letters, 22, 568, 1969.

SHIVANANDAN, K., J. R. HOUCK and M. O. HARWIT.   Phys. Rev.
    Letters, 21, 1466, 1968.

SIMNETT, G. M. and F. B. McDONALD.   NASA preprint X-611-
    68-450, 1968.

SIRONI, G.   IL Nuovo Cimento, 39, 372, 1965.

SISCOE, G. L., L. DAVIS, P. J. COLEMAN, E. J. SMITH and
    D. E. JONES.   J.G.R., 73, 61, 1968.

SMITH, A. M.   Ap.J., 156, 93, 1969.

SOOD, R. K.   Ph.D. Thesis, 1969, Univ. of London.

STECHER, T. P. and D. A. WILLIAMS.   Ap.J., 149, L.29, 1967.

STECKER, F. W.   Ap. Sp. Sci., 3, 579, 1969a.   Nature, 222, 865, 1969b.

STONE, E. C.   J.G.R., 69, 3577, 1964.

TANAKA, Y.   Proc. 10th Int. Conf. Cosmic Rays, Calgary, p536, 1967.   I.A.U. Symposium, No. 31, Radio Astronomy and Galactic System, 455, 1967.

VAN ALLEN, J. A. and S. M. KRIMIGIS.   J.G.R., 70, 5737, 1965.

VARSAVSKY, C. M.   Sp. Sci. Rev., 5, 419, 1966.

VERMA, S. D.   J.G.R., 72, 915, 1967a.   Proc. Ind. Acad. Sci., 66A, 125, 1967b.

WEBBER, W. R.   J.G.R., 72, 5949, 1967.   Aust. J. Phys., 21, 845, 1968a.   J.G.R., 73, 4905, 1968b.

WEBBER, W. R. and C. CHOTKOWSKI.   J.G.R., 72, 2783, 1967.

WERNER, M. W. and M. HARWIT.   Ap. J., 154, 881, 1968.

WILKINSON, D. T. and R. B. PARTRIDGE.   Nature, 215, 719, 1967.

WILLIAMS, D. J. and G. D. MEAD.   J.G.R., 70, 3017, 1965.

WILSON, R. R.   Phys. Rev., 86, 261, 1952.

WOLTJER, L.   Ap.J., 133, 352, 1961.